

OREGON STATE UNIVERSITY
TRIGA® REACTOR.
LICENSE NO. R-106
DOCKET NO. 50-243

RESPONSE TO RAI REGARDING HEU/LEU
CONVERSION

REDACTED VERSION

SECURITY-RELATED INFORMATION REMOVED

REDACTED TEXT AND FIGURES BLACKED OUT OR DENOTED BY BRACKETS



Radiation Center
Oregon State University, 100 Radiation Center, Corvallis, Oregon 97331-5903
T 541-737-2341 | F 541-737-0480 | http://ne.oregonstate.edu/facilities/radiation_center

June 20, 2008

Mr. Alexander Adams
U. S. Nuclear Regulatory Commission
Research and Test Reactors Branch A
Office of Nuclear Reactor Regulation
Mail Stop O12-G13
One White Flint North
11545 Rockville Pike
Rockville, MD 20852-2738

Reference: Oregon State University TRIGA Reactor (OSTR)
Docket No. 50-243, License No. R-106
Request for Additional Information (RAI) Regarding Amendment Request for
Reactor Conversion, Oregon State University TRIGA Reactor (TAC NO.
MD7360) dated April 22, 2008

Subject: Oregon State University Response to RAI Regarding Conversion Amendment,
Oregon State University TRIGA Reactor dated April 22, 2008

Mr. Adams:

In a letter dated April 22, 2008, you requested that Oregon State University (OSU) provide additional information related to an amendment request, submitted on November 6, 2007, as supplemented, for conversion of the OSTR. Answers to the RAI can be found in the Attachment 1. Attachment 2 contains commercial proprietary information and should be withheld from public disclosure per 10 CFR 2.390. Attachment 3 contains reference 14 as requested per RAI question 55.

I declare under penalty of perjury that the foregoing is true and correct.

Executed on: 6/20/08

Sincerely,

Steve Reese
Director

Enclosure

cc: Document Control, NRC Rich Holdren, OSU
Craig Bassett, NRC Todd Palmer, OSU
John Cassady, OSU Todd Keller, OSU (w/o Enclosure)

A020
NRR

Attachment 1

Oregon State University

Responses to NRC RAI Letter of April 22, 2008

- 1. Section 1.1. Your application states that the aluminum clad graphite reflector elements will be replaced with stainless steel clad graphite elements and that the annular reflector assembly may be replaced with a new annular reflector. Are these changes being made as part of the conversion? If so, please provide justification.**

The replacement of the reflector elements will be part of the conversion. Many of the current aluminum clad reflector elements exhibit characteristics of concentric swelling which prevents them from passing through the grid plate. If these elements were not permanently removed from the core, the proposed (and necessary) fuel movements and core configurations would be precluded. Replacement of the aluminum with stainless steel clad should significantly reduce the likelihood of this phenomenon reoccurring. The new reflector elements will be functionally identical to the old units. Replacing reflector elements having 20 mil aluminum cladding with elements having 20 mil stainless steel cladding will not significantly affect core neutronics.

The potential replacement of the annular reflector is not part of the conversion project.

- 2. Section 4.2. Please provide engineering diagrams and specifications for the fuel. Please describe the quality assurance process for production of the fuel. Are there any quality assurance tests that Oregon State will apply upon receipt of the fuel? If yes, please briefly describe.**

The engineering diagrams and specifications for the fuel are proprietary information owned by TRIGA International. OSU has been provided with electronic versions of fuel element drawings, but this information is considered proprietary by the manufacturer. OSU will receive "as built" drawings of the fuel when the fuel is delivered. Attachment 2 contains engineering drawings for the fuel.

Close communication between Oregon State University TRIGA Reactor, General Atomics, and the Idaho National Laboratory has been maintained throughout the development of the safety analysis report and the reactor component design process. This communication ensures that the appropriate technical and functional requirements from the reactor safety basis are carried forward through the design and fabrication of the new reactor components. OSTR has ensured that the drawings and fabrication specifications indicate the dimensions and other design parameters that must be met for each item to be in compliance with the reactor's safety basis. These documents are used to definitively communicate each component's requirements to OSTR personnel, INL procurement personnel, General Atomic personnel, and the QA Engineers from each organization. OSTR then relies on the well established QA processes at the INL to ensure that the final product meets the requirements per the drawings and specifications.

The INL has a Quality Assurance Program that meets or exceeds the requirements for procuring items and services as established by the DOE. The INL has audited CERCA as

required to ensure that their QA program meets or exceeds the requirements of NQA-1. These requirements are contained in 10 CFR 830 Subpart A, *Quality Assurance Requirements*, DOE Order 414.1C, *Quality Assurance*, and NQA-1-2000, *Quality Assurance Requirements for Nuclear Facility Applications*. These requirements establish the methods that the INL, and their suppliers, must use to procure material and fabricate items. More specifically, the process requirements relevant to the procurement of safety related items for the OSTR are:

- Items and services shall be procured to meet established requirements and perform as specified. [DOE Order 414.1C, Attachment 2, 3.g. (1)] [10 CFR 830.122 (g) (1)]
- Prospective suppliers shall be evaluated and selected on the basis of specified criteria. [DOE Order 414.1C, Attachment 2, 3.g. (2)] [10 CFR 830.122 (g) (2)]
- Process shall be established and implemented to assure that approved suppliers continue to provide acceptable items and services. [DOE Order 414.1C, Attachment 2, 3.g. (3)] [10 CFR 830.122 (g) (3)]

To complete the process, source inspections of the items will be performed by qualified INL Inspectors before being released to the OSTR. After delivery, receipt inspections of the items will be performed by OSTR personnel. Receipt inspection consists of measuring and recording:

- Fuel element serial number
- Highest radiation reading on contact and at one foot
- Gross surface contamination level
- Fuel standard length, deviation of fuel element length from the standard and the temperature of the element at the time that the length was measured
- Fuel element transverse bow
- Inspect the fuel element for any visible indications of damage including scratches, dents and discoloration

When fuel production has been completed, the manufacturer will provide isotopic composition for all major constituents for every fuel meat. The manufacturer will also provide detailed trace element analysis of a representative sample for the fuel meats.

3. Section 4.2.1. Please add a discussion of ZrH_x composition in the section on fuel.

In the OSTR LEU fuel, the value of x is nominally 1.6. As discussed in the answer to question #56, the fuel element average range of acceptance for the hydrogen to zirconium atom ratio in the LEU fuel is 1.57 to 1.65. An exhaustive review of $ZrH_{1.6}$ characteristics was provided in the license renewal application of November 6, 2004, from which this amendment is based.

4. **Section 4.2.1. Please specify the composition of the inner region of the fuel rod.**

The center region of the fuel rod will contain a rod composed of zirconium metal.

5. **Section 4.5.1, Figure 4-3. The figure might be better interpreted by having arrows on Figure 4-2 showing the sectioning. The figure does not appear to be at the core midplane as stated. Please clarify.**

This figure is a vertical cross section of the MCNP5 model taken at core midplane as can be seen from the display aspect of the central thimble. The axis of the vertical section in Figure 4-3 is coincident with the red arrow in Figure 4-2 labeled "Transient Rod". This orientation was selected in order to maximize relevant details displayed in Figure 4-3. We will consider adding section arrows to Figure 4-2.

6. **Section 4.5.1, Figure 4-10 and Section 4.5.2, Figure 4-16. Why doesn't the calculated BOL excess reactivity equal \$7.10 as quoted on page 15 for the HEU core and \$5.48 as quoted on page 29 for the LEU core?**

The \$7.10 and \$5.48 values for excess reactivity were calculated assuming cold, clean conditions with no experiments in the core. Figures 4-10 and 4-16 calculate excess reactivity at various times in core life assuming 1.1 MW_{th} operating power. The calculated power defect from 0.0 to 1.0 MW_{th} is calculated to be \$2.05 for the HEU core and \$2.16 for the LEU core. The \$2.05 value is in agreement with observed values for the HEU core. The calculated cold, clean BOL excess reactivity values are 3.41 %ΔK/K (HEU core, Figure 4-10) and 2.29 %ΔK/K (LEU core, Figure 4-16). These values are consistent with the values at 1.1 MW_{th} operating power if the power defect is taken into account.

$$\$7.10 - \left(\frac{1.1}{1.0}\right) * \$2.05 = \$4.85 \approx \$4.87 = 0.0341/0.0070$$

$$\$5.48 - \left(\frac{1.1}{1.0}\right) * \$2.16 = \$3.10 \approx \$3.05 = 0.0229/0.0075$$

7. **Section 4.5.1, Figures 4-6 to 4-9. It would help in interpreting these figures, and Table 4-5, if experimental errors were shown (assuming they are large enough to be visible).**

In the answer to question 11 (below), accuracy of control rod reactivity measurement is estimated to be within approximately 5%. Uncertainty in the true value of Beta-effective could add another 5% to this estimated value for a total estimated uncertainty of \$0.03, or ~10% per measurement. We will consider adding \$0.03 error bars to the measured data entries. Note that the fourth entry on Figure 4-8, corresponding to 36% withdrawal of the regulating rod was mis-entered. This will be corrected.

8. **Section 4.5.1. Was the segmentation of the fuel rods for the depletion analysis done for each rod individually or for an average rod?**

The segmentation was done for each rod individually.

9. **Section 4.5.1. The HEU core is analyzed assuming operation at constant power. Have any calculations been done with the actual operating history to see what the effect of this assumption is on key parameters? If so, what was the impact?**

Operation of the reactor over the course of its operating history typically involved several power changes over a single eight hour operating shift. Core configuration (ICIT/CLICIT/NORMAL) is also changed frequently. The core has also undergone eight major fuel element reconfigurations since 1976. The effort required to duplicate the power history since 1976 was considered highly impractical and was not modeled.

Analysis of the MSNR [1] indicates that long term fuel depletion can be accurately simulated using long time steps even for reactors with highly variable operating cycles.

Calculation of OSTR key parameters was done under cold (50°C), clean (no xenon) conditions at BOL, MOL and EOL. MOL and EOL calculations included all significant depletion byproducts except xenon. The presence of xenon in the reactor would harden the neutron spectrum which could affect core parameters. Calculations could have included xenon, but this is typically not done. Xenon concentration changes rapidly, thus making accurate measurements of such parameters difficult unless the core is operating with either no xenon (i.e., zero power physics testing on a cold, clean core) or equilibrium xenon. Steady state physics testing of the OSTR is done with reactor power between 15W and 1000W, or essentially zero power.

10. **Section 4.5.1. Were any data (like excess reactivity or control rod worth) available at other than BOL to use to benchmark the neutronic model for the HEU core? If so, why weren't they used?**

The HEU FLIP core that was loaded in 1976 and served as the HEU modeling basis was only operated for a short duration before the core was significantly reconfigured. As such, the available plant data beyond the BOL benchmark is inconsistent with the HEU modeling basis and unsuitable for direct comparison with the model. The overall features of the HEU depletion curve are in accord with those experienced during actual operation of the facility. The ability of the HEU neutronic model to accurately predict measured BOL data, combined with its ability to properly account for the gross features of the burnup profile for the HEU core, give us confidence in the validity of the modeling technique.

11. **Section 4.5.1, Figure 4-9 and Table 4-5. Why does the calculated transient rod worth deviate from the measurement for the HEU core at BOL while the other three control rods showed much closer agreement between calculated and measured worth?**

A review of the rod calibrations performed on the HEU BOL core shows that the reactor period (and hence reactivity) measurements were based upon observing an increase in reactor power by a factor of 1.5. The time for the increase was measured with a stopwatch and the power trace was recorded on a chart recorder. Given the crude nature of this procedure, it is likely that either the recorded time or the actual power levels had associated errors. As an example, consider the calibration of a rod using a power increase by a factor of 1.5 from 40 percent to 60 percent of a measurement

scale. Here the time of the power increase is taken to be 8.0 seconds with a Beta-effective of 0.0070 and a prompt-neutron lifetime of 18.7 μ sec. To estimate uncertainty of this method using a timed power increase to calculate period and determine the associated reactivity, consider two hypothetical measurements. If the final power in one case is 59% while that in the second is 61%, a calculated reactivity difference of \$0.0115 results. Likewise, an error in timing from 7.9 seconds to 8.1 seconds results in a calculated reactivity difference of \$0.0035. If one assumes an error of \$0.015 for each rod pull, this corresponds to an error of ~5% for each measurement. The transient rod calibration (measured and simulated) consisted of a total of eight individual measurements. The MCNP5 error in total rod worth is ~5.5%. The measurement error in total rod worth, assuming eight measurements each with an uncertainty of 5% is ~14.1%. The difference between the MCNP5 calculated and the measured HEU BOL value for the transient rod worth is 26.6%.

The MCNP5 calculation of the transient rod worth used the rod positions from the HEU BOL testing data, hence the discrepancy between the predicted and measured values cannot be attributed to systematic error (e.g. rod shadowing effects) between the two methods.

12. **Section 4.5.1. Differences in bulk pool temperature appear in the SAR. On Page 19, Section 4.5.1, Depletion analysis was conducted at 50 degrees C. On Page 24, Section 4.5.1, RELAP analysis was conducted at 49 degrees C. On Page 19, Section 4.5.2, Depletion analysis was conducted at 50 degrees C. On Page 39, Section 4.7, T/H analysis was conducted at 49 degrees C. On Page 39, Section 4.7, OSU TS limit pool temperature to maximum of 49 degrees C. How do these differences in temperature impact the results of the calculations?**

For consistency, all of these calculations should have been performed using the same core inlet temperature of 49°C which is the pool temperature Technical Specification limit. It is considered impractical to repeat the calculations. Given that numerous conservative assumptions were made during the course of the analysis, and the results indicate that there is a large margin to CHF under allowed operating conditions, it is considered unlikely that this one degree temperature inconsistency would have any significant impact on the results of the calculations.

13. **Section 4.5.1, page 18. Please elaborate on the aspects of the evaluation techniques that contribute to the discrepancy between the measured and calculated shutdown margin for the HEU BOL core when the regulating rod is fully withdrawn. How does the calculated shutdown margin compare with the measured value for the other control rods?**

The discrepancy is due to the difference by which core excess was calculated and how it is actually measured. For the calculated MCNP5 model, one rod is completely withdrawn while the remaining three are completely inserted into the core. This calculation method allows determination of the shutdown margin exactly as defined. However, this method cannot be used to actually measure shutdown margin because reactivity cannot be directly measured by the period method when the core is significantly subcritical. To measure core excess, the reactor is brought to 15 W with three rods at a specified withdrawal height, and the fourth rod withdrawn to criticality. The reactivity value of the three rods at their reference height is known from their calibration curves. The value of the fourth rod at its critical height is also determined from its calibration curve. The three rods are typically 50% withdrawn which creates

shadowing and rod worth effects that can't be otherwise accounted for. The inherent difference between the two methods was not calculated. The shutdown margin for rods other than the most reactive rod was not calculated because, by definition, the shutdown margin requires that the highest worth rod is fully withdrawn from the core.

14. Section 4.5.1, Table 4-7 and Section 4.5.2, Table 4-14. Please justify the use of two points to extrapolate to zero boron concentration in the algorithm for calculating neutron lifetime.

In the conversion SAR we use the equation

$$l_p = \frac{1}{N_{B-10} \sigma_{a0} v_0} \frac{k_{ref} - k_p}{k_p}$$

to calculate prompt neutron lifetime. A more accurate statement is

$$l_p = \lim_{N_{B-10} \rightarrow 0} \frac{1}{N_{B-10} \sigma_{a0} v_0} \frac{k_{ref} - k_p}{k_p}$$

Since $\frac{k_{ref} - k_p}{k_p}$ varies as a function of N_{B-10} , the expression for l_p tends to some finite value as $N_{B-10} \rightarrow 0$. Thus for appropriately small values of N_{B-10} , a linear extrapolation is justified. This theory is explained in greater detail in the RERTR Bretscher report [2].

Two boron concentration data points were used for the calculations. Data points for boron concentration were selected to be sufficiently large that MCNP5 calculations with sufficient histories could be collected to ensure that the errors in the calculated k_{eff} values for the two points did not lead to unnecessary uncertainty in the value of l_p . Data points for boron concentration were selected to be sufficiently small that reactor parameters would not be significantly perturbed.

15. Section 4.5.1, page 24. The prompt neutron lifetime is usually written as l_p in the SAR but on page 24 it appears that the symbol Λ is used. Please confirm.

Due to an oversight on our part, this symbol was not explicitly defined in the text. The mean generation time (Λ) is frequently used in point reactor kinetics equations and is defined as:

$$\Lambda(t) = \frac{l_p}{k(t)}$$

16. **Section 4.5.1. A measurement was done for the reactivity worth of an irradiation facility placed in the B-1 grid position. Have you calculated this worth and if so, what is the value?**

An MCNP calculation of the reactivity worth of this facility was not performed. This calculation would have essentially been a repetition of the void worth calculation using slightly different volumes.

17. **Section 4.5.1 and 4.5.2. The void coefficients and moderator coefficients are assumed to have been calculated at BOL. Are there any changes to the differences from HEU to LEU if MOL or EOL is considered?**

The reported values of void and moderator coefficients are at BOL. The complete range of calculated results are shown in the following table:

	HEU		LEU	
	Void Coef (\$/%)	Mod coef (¢/°C)	Void Coef (\$/%)	Mod coef (¢/°C)
BOL	-0.86	-0.57	-0.96	-0.72
MOL	-0.80	-0.47	-0.98	-0.55
EOL	-0.61	-0.42	-0.91	-0.65

18. **Section 4.5.1 and 4.5.2. On pages 23 and 36 it says a reactivity loss was observed. This implies a measurement although the text is referring to a calculation. Please clarify.**

The use of the word "observed" was not appropriate and should be replaced with "calculated" in each of these cases.

19. **4.5.2, page 33. Does the shutdown margin requirement take into account the reactivity added by irradiation facilities and experiments in place and the total worth of all non-secured experiments in their most reactive state and the core in the reference condition? Is the most reactive control rod fully-withdrawn?**

The actual shutdown margin, as measured during reactor operation, will take into account all factors required by the technical specification, including reactivity due to irradiation facilities and experiments. The shutdown margins calculated in section 4.5.2 assumed a "cold, clean" core with the highest worth rod stuck out of the core, but did not attempt to account for reactivity due to experiments or facilities. These calculations indicate that the LEU core, as initially loaded, will experience relatively small reactivity changes over core life (as compared to the HEU core). We anticipate the necessity to manage shut down margin and excess reactivity of the core by adding or removing fuel elements as needed during core lifetime. We will also manage core inventory as required to account for reactivity changes due to experiments.

20. Section 4.7.2, Table 4-21. The analysis for the HEU core uses 84 fuel rods in the core although it appears from Figure 4-4 and Table 4-1 that there should be 85 rods present with control rods withdrawn. Please explain the difference.

There are two typographical errors. The value for the number of HEU elements described on pages 24 and 55 should be 85.

Table 4-21 contains incorrect values for the HEU core hot rod peak factors. The numbers in the table are based on 84 instead of 85 fuel elements. Note that the values in this table are provided for reference and to allow comparison between cores. They are not used as input to any calculations.

The column in Table 4-21 labeled 'Hot Rod Fuel Radial Peak Factor' also needs to be updated. The numbers in the table were calculated using total power in annular volumes. The more customary method involves comparison of power density throughout the fuel element. The updated table is shown below (new values are highlighted) and will be incorporated into the conversion SAR. The discussion of the radial peak factor on page 49 will also be updated. The few instances in the text where peaking factors are explicitly listed will also be updated.

Table 4-21, Hot Rod Power Summary

Hot Channel Power Summary						
	Hot Rod Location	Hot Rod Thermal Power [kW]*	Hot Rod Peak Factor $[P_{max}/P_{avg}]$	Hot Rod Fuel Axial Peak Factor $[P_{max}/P_{avg}]$	Hot Rod Fuel Radial Peak Factor $[P_{max}/P_{avg}]$	Effective Peak Factor
HEU-BOL NORMAL Core	B3	18.02	1.393	1.236	1.498	2.579
HEU-MOL NORMAL Core	B6	18.37	1.420	1.209	1.074	1.844
HEU-EOL NORMAL Core	B6	16.48	1.273	1.234	1.280	2.011
LEU-BOL ICIT Core	B6	18.47	1.477	1.221	1.562	2.817
LEU-BOL CLICIT Core	B3	17.03	1.362	1.221	1.536	2.554
LEU-BOL NORMAL Core	B3	17.77	1.422	1.219	1.538	2.666
LEU-MOL ICIT Core	B6	18.52	1.482	1.225	1.434	2.603
LEU-MOL CLICIT Core	B3	17.03	1.363	1.225	1.406	2.348
LEU-MOL NORMAL Core	B3	17.80	1.424	1.222	1.409	2.452
LEU-EOL ICIT Core	B6	17.61	1.409	1.181	1.304	2.170
LEU-EOL CLICIT Core	C7	16.35	1.308	1.212	1.275	2.021
LEU-EOL NORMAL Core	B3	17.02	1.362	1.178	1.267	2.033

* Hot channel thermal power corresponds to core power of 1.1 MW_{th}.

Additional discussion of the radial peak factor calculations is found on page 57-58, and in figure 4-32. Figure 4-32 will be updated as shown, and the discussion of the radial peak factor calculations will be corrected.

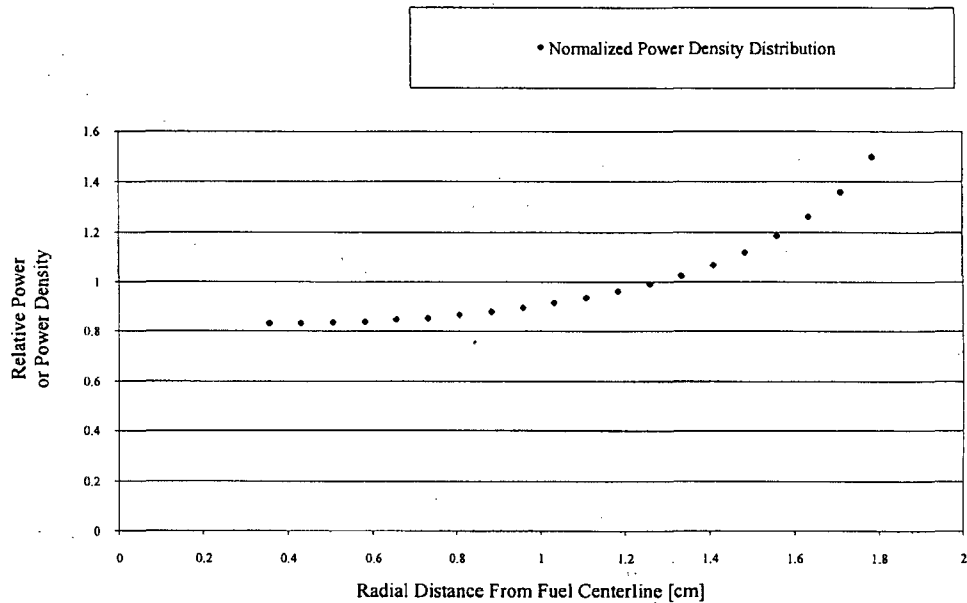


Figure 4-32, Radial Power Profile and Radial Power Density Profile vs. Distance from Fuel Centerline for the Hot Rod in the OSU HEU BOL NORMAL Core.

21. Section 4.7.2, Table 4-21. What is the effect on power peaking of replacing a burnt fuel rod (e.g., an IFE) with a fresh fuel rod? What controls are in place with respect to loading new fuel? Provide a calculation to indicate the change in the peaking factor when fresh fuel is placed in an EOL core at the worst location.

Due to the presence of erbium, fresh fuel acts as a poison with respect to reactivity when replacing a partially burned fuel rod. As a fuel rod is burned, the erbium is consumed faster than the U-235 so the ratio of erbium to U-235 number densities is higher in fresh fuel than in burned fuel.

MCNP calculations were run in order to quantify the effect of inserting fresh fuel into a MOL or EOL core. The ICIT core configuration has the highest effective peak factor at all stages of core life, so this core was selected for analysis. Five separate MCNP calculations were performed using the LEU MOL ICIT core. For each run, one of the B-ring fuel elements was replaced with a fresh fuel element. Five similar MCNP runs were also performed using the LEU EOL ICIT core configuration.

Table 21-1, Power per Element (Swapped Element) shows the effect of inserting fresh fuel on the power generated in the swapped element. The 'reference' column shows power in the element prior to replacement with fresh fuel. The 'fresh' column shows power in the element after replacement. Note that for the ICIT core, the B-1 position does not contain fuel.

Table 21-1, Power per Element (Swapped Element)

Position	LEU MOL ICIT		LEU EOL ICIT	
	reference (kW)	fresh (kW)	reference (kW)	fresh (kW)
B2	18.08	16.94	17.28	15.06
B3	17.79	16.84	16.91	15.00
B4	17.19	16.12	16.52	14.40
B5	17.39	16.49	16.64	14.50
B6	18.52	17.47	17.61	15.44

Although power in the swapped element is reduced, power in other elements increases to maintain overall core power at 1100kW. The peak power, and hence the effective peak factor is actually higher in each perturbed core than in the original core. The highest power seen in the perturbed LEU MOL ICIT core is 19.55 kW. The highest power seen in the perturbed LEU EOL ICIT core is 19.88 kW. The peak power seen in each perturbed core is shown in table 21-2, Power per Element (Peak Element). It can be seen from Table 21-2 that replacing any B-ring fuel element in the LEU MOL ICIT or LEU EOL ICIT core results in an increase in the maximum power generated in a single rod over the base (unperturbed) case.

Table 21-1, Power per Element (Peak Element)

Swapped Element	LEU MOL ICIT		LEU EOL ICIT	
	Peak Position	Peak Power (kW)	Peak Position	Peak Power (kW)
None	B6	18.52	B6	17.61
B2	B6	19.35	B6	19.73
B3	B6	19.55	B6	19.88
B4	B6	19.32	B6	19.84
B5	B6	19.42	B6	19.56
B6	B2	18.95	B3	19.31

Thermal hydraulic analysis of the hot channel was based on the assumption that the hot channel is triangular (or hexagonal), and is bordered on all three sides by a fuel rod generating power equal to the hottest rod in the core under analysis. In actuality, flow channels in the hottest regions of the core (inside the D-ring) are either approximately square or triangular, and are bordered by elements of differing powers. If we calculate the average power level in each flow channel inside the D-ring, we find that the power in the theoretical hot channel, which was assumed to be bounding, is slightly lower than the hottest channel in the perturbed core. The theoretical hot channel analyzed in the conversion SAR assumes a power of 18.52 kW in each neighboring fuel element (as seen in the LEU MOL ICIT core). The highest average in any perturbed core flow channel is 18.79 kW which occurs in the square channel bordered by positions B2, B3, C3 and C4. This is an increase of 1.5% over the previous bounding limit, and is unlikely to significantly impact MDNBR or maximum pulse temperature. The average power level in the hottest channel of each core is shown in Table 21-3, Hot Channel Average Power. It should be noted that with the exception of the LEU EOL ICIT channel bordered by B3/C4/C5, each of these hot channels is actually a square channel, but is only heated by three adjacent elements, and thus the true mathematical average power of the four surrounding structures is actually significantly less than the mathematical average power of the three adjacent heated structures. If this phenomenon is taken into account for all heated channels in each perturbed core, then the average power of each subchannel is less than 18.52 kW in all cases.

Table 21-3, Hot Channel Average Power

LEU MOL ICIT Core			
Swapped Element	Hot Channel		
	Bordered by	Heated by	Avg. Power (kW)
None	B6	B6	18.52
B2	B1/B6/C11/C12	B6/C11/C12	17.96
B3	B1/B6/C11/C12	B6/C11/C12	18.08
B4	B2/B3/C3/C4	B2/B3/C3	18.27
B5	B2/B3/C3/C4	B2/B3/C3	18.27
B6	B2/B3/C3/C4	B2/B3/C3	18.40
LEU EOL ICIT Core			
Swapped Element	Hot Channel		
	Bordered by	Heated by	Avg. Power (kW)
None	B6	B6	17.61
B2	B3/C4/C5	B3/C5	18.36
B3	B1/B6/C11/C12	B6/C11/C12	18.35
B4	B2/B3/C3/C4	B2/B3/C3	18.79
B5	B2/B3/C3/C4	B2/B3/C3	18.78
B6	B2/B3/C3/C4	B2/B3/C3	18.73

Since DNBR is generally considered to be a local phenomenon strongly dependent on heat flux, it is appropriate to examine the impact of peak power in any single rod. As shown above, the highest powered element in any perturbed core is 19.88 kW (LEU EOL ICIT core, B6 position with the B3 element replaced with fresh fuel). In section 4.7.9, LEU End of Life ICIT Core Analysis, we conclude that under our conservative assumptions, MDNBR in the hot channel will reach a value of 2.0 at approximately 20.0 kW hot channel steady state power. A steady state fuel element power of 19.88 kW is thus acceptable. Additionally, in the LEU MOL ICIT core, the maximum perturbed core element power of 19.55 kW is below the 19.85 kW power that would produce a MDNBR ratio of 2.0 in that core.

Increased power peaking will also affect pulse analysis. In the MOL ICIT core, the highest power element increases from 18.52 to 19.55 kW, or an increase of 6 percent with a commensurate 6 percent increase in the hot channel peak factor. In the EOL ICIT core, the highest power element increases from 17.61 to 19.88 kW, or an increase of 13 percent. The hot channel peak factor is used for the pulse analysis. All pulse analyses were performed on un-perturbed cores. Due to a combination of prompt temperature coefficient and peaking factors, the LEU MOL ICIT core is the most limiting core in terms of pulse behavior. As stated in the answer to question #41, the assumption that the pulsing reactor maintains the same power profile as the steady state reactor is conservative. Thus even though the hot channel peak factor in the perturbed LEU MOL ICIT core is 6 percent greater than in the un-perturbed core (13 percent greater than in the un-perturbed LEU EOL ICIT core), the conservative analyses performed on the LEU ICIT cores would still produce fuel temperatures below the safety limit.

All in-core fuel movements are controlled under the 10 CFR 50.59 process. In-core movement of fuel is approved in advance by the Reactor Operations Committee.

22. Section 4.7.2. RELAP5 had a fundamental error in the point kinetics model that has recently been fixed. Which version of the code was used for the analysis in the SAR? Please verify that your model is giving results consistent with the transient (e.g., by checking results as a function of time step or with another stand-alone point kinetics model).

Version 2.4.2 was used for all OSU conversion SAR calculations. This version included the point kinetics error. Investigation showed that this error had little impact on the predicted maximum temperature during a reactor pulse. The maximum temperatures predicted by version RELAP5 version 2.4.2 are higher than the those predicted by other methods and thus are conservative.

To verify that this error did not significantly effect calculation results, a point reactor kinetics model was developed from basic principles. This model incorporated six delayed neutron precursor groups, a prompt negative fuel temperature coefficient and adiabatic conditions in the fuel. The basic equations used to model the core are:

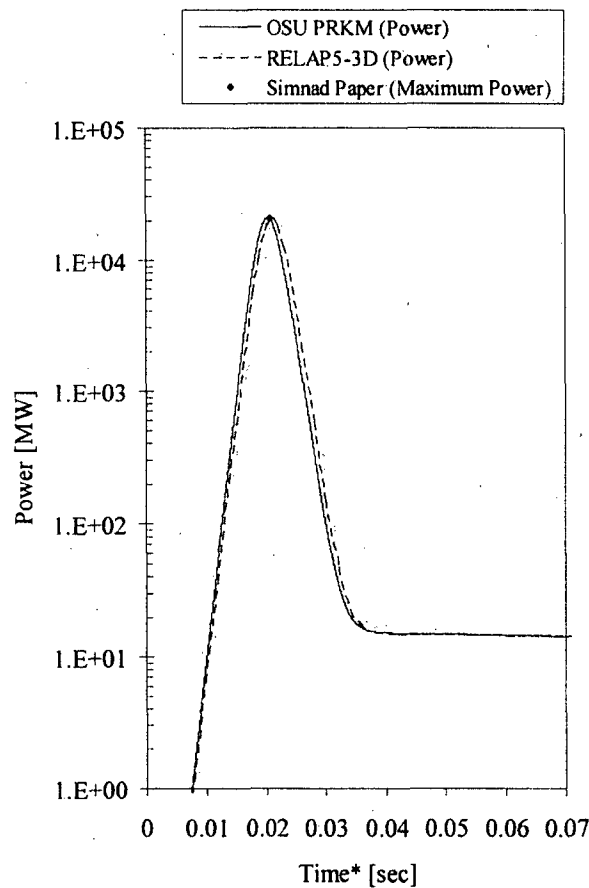
$$\frac{d}{dt}P(t) = \left(\frac{\rho(t) - \beta}{\Lambda} \right) P(t) + \sum_{i=1}^6 \lambda_i C_i(t)$$

$$\frac{d}{dt}C_i(t) = -\lambda_i C_i(t) + \frac{\beta_i}{\Lambda} P(t), \quad i = 1 \dots 6$$

$$\text{and } \int_{\rho_0}^{\rho} d\rho = \int_{T_0}^T \alpha(T') dT'$$

where all symbols are defined as usual. A benchmark problem originally published by General Atomics [3] was run using RELAP and the point reactor kinetics model. A comparison of results is shown below. Predicted values were in reasonably good agreement with the most conservative (i.e. highest) peak temperature being predicted by the RELAP model.

Pulse Results Summary			
	GA Paper	RELAP5-3D	OSU PRKM
Maximum Power [MW]	20000	20606	21058
Time of Maximum Power [sec]	~0.0207	0.02108	0.02032
Pulse FWHM	~0.00351	0.00464	0.00454
Peak Adiabatic Fuel Temp. [°C]	1000	1083.1	880.665
Average Adiabatic Core Temp [°C]	500	492.032	473.249
Core Energy Release After 0.1 sec [MJ]	106	109.47	108.24



23. **Section 4.7.2. Please provide Reference 14 in order to justify the pressure loss coefficients used in the RELAP5 analyses.**

Reference 14 can be found in Attachment 3.

24. **Section 4.7.2. Please provide analytical justification for ignoring cross flow between neighboring flow channels.**

One, two, and eight channel RELAP5-3D models were individually analyzed against the BOL core. Cross flow was incorporated in the two and eight channel models through junctions connected at each individual axial nodal location between adjacent subchannels. The axial and radial fuel temperature distributions were assumed to be identical in each model.

Figure 24-1 provides a quantitative comparison of the bulk coolant temperature distribution found in the one, two and eight channel models. This comparison provides evidence that with an increase in the number of subchannels there is an expected corresponding decrease in exit bulk coolant temperature.

The coolant equilibrium quality and subchannel mass flux as a function of axial position are presented in Figure 24-2. These properties, along with system pressure, are the

primary parameters for CHF. With an increase in the number of subchannels the mass flux is perturbed greater due to cross flow in the lower axial portion of the core. The equilibrium quality for the single, two, and eight channel models remain similar through the majority of the axial length of the core. As a result of the increased mass flux in the eight channel model near the exit of the subchannel, less energy is deposited into the fluid producing lower equilibrium quality values for the eight channel model relative to the two and one channel models.

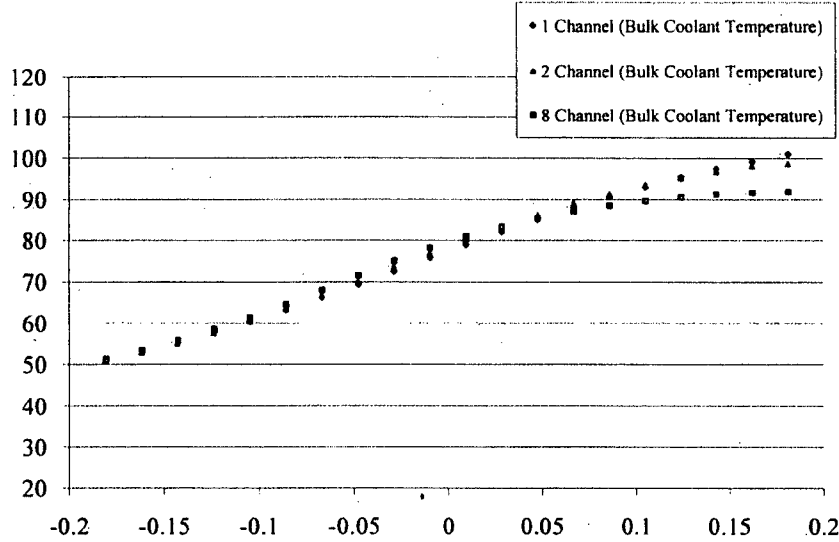


Figure 24-1: Axial Bulk Coolant Temperature Distribution for 1, 2, & 8 Channel Model (HEU Beginning of Life Normal Core)

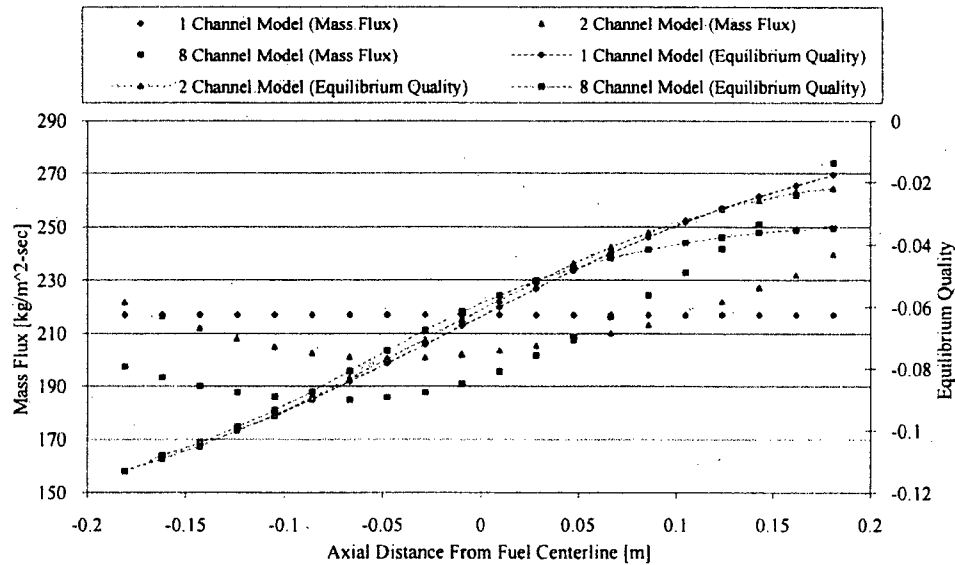


Figure 24-2: Mass Flux and Equilibrium Quality Distribution for 1, 2, & 8 Channel Model (HEU Beginning of Life Normal Core)

Figure 24-3 presents the CHF determined using the 2006 Groeneveld AECL look-up tables and Bernath correlation for the one, two, and eight channel models. Small

differences in the CHF values for the different models compared can be accounted for by the observations made above. The exit CHF value for the eight channel model is larger than for the two channel model, which is larger than the one channel model. This is due to a decrease in equilibrium quality near the exit of the subchannel. Although there are small deviations in the CHF axial distributions it is important to note that the minimum critical heat flux ratio (MCHFR) differs by only 0.3% on average for the look-up tables and 0.6 % for the Bernath correlation. This is well within the error margin associated with each CHF method of calculation.

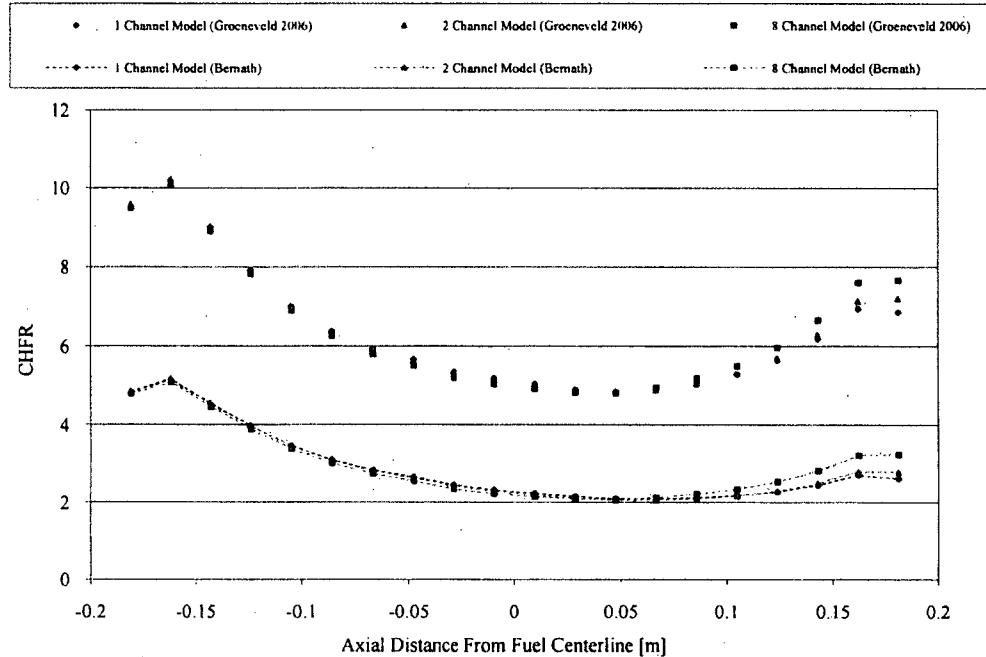


Figure 24-3: Axial CHF Distribution for 1, 2, & 8 Channel Model
(HEU Beginning of Life Normal Core)

Based on a conservative method for safety analysis, the single channel model provides critical heat flux results using the 2006 Groeneveld look-up tables within ~1.0 % of those produced from the eight channel model. The single channel model produced the most conservative results relative to the two and eight channel models.

25. Section 4.7.2, Figure 4-24. Should the bottom of the end fitting align with the top of the grid plate (to be consistent with Eq. 4.5) or the bottom (as shown in Fig. 4-24)?

Figure 4-24 of the conversion SAR is not an accurate, "to scale", quantitative representation of axial node positions. The bottom of node 02 (lower unheated node, labeled 'lower reflector' in Figure 4-24) should align with the top of the lower gridplate. Similarly, the upper end of node 23 (upper unheated node, labeled 'upper reflector' in Figure 4-24) should align with the bottom of the tri-flute. We will consider replacing Figure 4-24 with a more accurate diagram.

26. **Section 4.7.2, Table 4-20. Could the coordinate for the Outer Gap (Node Number 23 in Table 4-20) be in error? In reference to Figure 4-26, the value listed in Table 4-20 (0.01785-0.01786 m) implies the clad is actually closing in on the fuel and there is practically no gap.**

The Outer Gap nodal coordinate value in Table 4-20 (Node 23) is stated to vary from 0.01785-0.01786 meters (0.70285-0.70305 inches). Because gap thickness more accurately varies on the order of microns, not enough significant figures were taken into consideration. The correct dimensions used for Node 23 are 0.01785239-0.01785747 meters (0.70285-0.70305 inches).

27. **Section 4.7.2. Was the transient rod also removed for the calculation of the rod power distribution in the core?**

Yes, all rods were fully withdrawn for the calculation of power distribution in the core.

28. **Sections 4.5.8, 4.7.3, and 4.8.3. Does the peak power density (maximum local heat flux) at steady-state occur in the fuel element (rod) with the maximum rod power?**

It is assumed that all rods in the core have approximately the same axial heat distribution shape, and thus the maximum powered rod would produce the maximum local heat flux. Although minor variations in axial power shape occur throughout the core, we made the conservative assumption that the hot channel is bordered on all sides by a fuel rod having the same characteristics as the hot rod. In reality, the hot channel will likely be bordered by the hot rod, and two other rods of lower power. Thus even in the unlikely event that the maximum heat flux does not occur in the hot rod, the conditions in the hot channel are still expected to bound conditions at all other points in the core. Note: there are no sections 4.5.8 or 4.8.3 in the OSU Conversion SAR.

29. **Section 4.7.2 Table 4-21. What is the significance of the Effective Peak Factor (EPF) in relation to the peak fuel temperature and the minimum DNBR? It does not appear that the EPF has a direct relation to the heat flux at the clad surface.**

The primary purpose of the effective peak factors presented in Table 4-21 is to identify the core configuration and lifetime which produces the most limiting maximum fuel temperature during steady state and pulse operation. DNBR does not have a direct association with the effective peak factor. DNBR is a measure of the predicted conditions required to create departure from nucleate boiling to the heat flux measured locally. Since the locally measured heat flux used when calculating axial DNBR distribution is taken from the outer cladding in contact with the bulk coolant, the radial peak factor has no impact on this value. Consider two examples: if the hot channel peak factor was a value of 1.5, the axial peak factor was 1.5, and the radial peak factor was 2.0, the associated effective peak factor would be 4.5. In contrast, if the hot channel peak factor was 1.73, the axial peak factor was 1.73, and the radial peak factor was 1.5, the associated effective peak factor would still be ~4.5. Although the effective peak

factors for both cases are equivalent, the latter scenario produces more limiting DNBR values because of its greater axial and hot channel peak factors.

Note that none of the peak factors listed in Table 4-21 of the CA SAR are used as input parameters for RELAP steady state calculations. Radial and axial power profiles are entered as power density distribution vectors, and channel power is varied as needed for analysis. For pulse calculations, the 'Hot Rod Peak Factor' is used as an input parameter. We have verified that the correct value for this parameter was used in all pulse calculations.

30. **Section 4.7.2. Please correct the citation for Reference 18, the 2006 CHF Look-up table.**

The correct citation is: [18] Groeneveld, D.C., et al., *The 2006 CHF look-up table*. Nuclear Engineering and Design, 2007: p. 1-24.

31. **Section 4.7.2. Please provide reference(s) for the correction factors, the K's, and explain their specific adaptation for the OSTR geometry and operating conditions. Are there additional correction factors that go with the most recent (2006) Look-up table?**

In 1986 Groeneveld et al. developed a critical heat flux (CHF) prediction method by compiling the world's CHF data for water and relating it to a corresponding mass flux, equilibrium quality, and pressure. By interpolating in the Groeneveld look-up tables using these parameters one can acquire a predicted CHF value. This value corresponds to a tube of diameter 0.008 meters uniformly heated on the inner surface. In order to adapt this CHF prediction for systems other than the geometry described above, six correction factors have been added to the interpolated CHF value. These correction factors allow for the adaption of a single 8 millimeter cylinder to be broadened to incorporate phenomena such as a change in hydraulic diameter (K_1), rod bundle effects (K_2) such as cross flux and additional surface friction, grid plate spacer dependency (K_3), Axial heated position to include phase change dependence (K_4), Axial flux distribution factor (K_5) to account for non-uniform axial heat distributions, vertical/horizontal orientation factor (K_6) to account for gravitational effects associated with flow regimes.

During the OSTR core conversion analysis three of the six correction factors were used (K_1 , K_2 , and K_4). All other correction factors were assumed to be equal to or very close to 1.0 such that their impact on the final CHF is insignificant. K_3 was neglected because the OSTR has an upper and lower grid plate only, no grid spacers are found in the axially heated region of interest, therefore K_3 is equal to 1.0. K_5 was neglected because it is only applied under conditions in which the equilibrium quality is greater than zero. All departure from nucleate boiling circumstances for the OSTR occur in negative equilibrium quality values. Therefore the K_5 factor is not applicable under OSTR operating conditions and is assumed to be equal to 1.0. K_6 corrects for flow direction only if the flow direction opposes the gravitational buoyancy directions (i.e. forced downward convection). Because the OSTR operates under natural circulation where the primary coolant velocity is in the positive vertical direction (upward vertical direction) K_6 is not a valid correction factor to apply under the OSTR's operational conditions and is therefore assumed to be equal to 1.0.

Three correction factors apply to the OSTR under operational conditions; K_1 corrects for the change in hydraulic diameter from 0.008 meters and an inner heater surface to a 0.001301 meter hydraulic diameter with an outer heated surface (i.e. external flow). K_2 predicts the correct trend of equilibrium quality, and must be taken into consideration because the OSTR operates under low flow, upward vertical conditions in which the equilibrium quality has a significant impact on the final CHF prediction value. K_4 significantly affects the final CHF prediction value because it predicts the phase change effects from liquid to vapor in the subchannel as a function of axial position. By incorporating K_4 , the CHF prediction value incorporates the additional buoyancy and velocity effects due to subchannel vapor, which has potential to increase the predicted CHF value.

All of the descriptions provided for the Groeneveld correction factors are presented in the original 1986 AECL-UO paper [4]. An investigation by Argonne National Laboratory further supported the correction factors used during the steady state analysis for the OSTR under operational conditions [5].

32. Section 4.7.2. Why did the thermal analysis not use the Groeneveld Look-up table built into RELAP5-3D?

Six different methods for calculating critical heat flux with reference to the core conversion study are considered. In order to quantitatively compare the relationship of these correlations, the HEU Beginning of Life NORMAL core was chosen for analysis.

RELAP5-3D internally calculates the critical heat flux with reference to the 1986 AECL Groeneveld look-up tables. All other correlations were calculated externally using the thermal hydraulic properties resulting from the RELAP5-3D model. In order to verify that these external calculations were being completed in the correct manner, the critical heat flux was calculated externally with reference to the 1986 AECL Groeneveld look-up tables. The result of this comparison is shown in Figure 32-132-1. The external calculations produced values that deviated from those conducted in RELAP5-3D by ~1.0% on the conservative side. The deviation was potentially caused by round off error. Qualitatively, this deviation was estimated to be within an acceptable margin. The axial CHFR distribution for the RELAP5-3D internally calculated values as well as all external calculated values are presented in Figure 32-1.

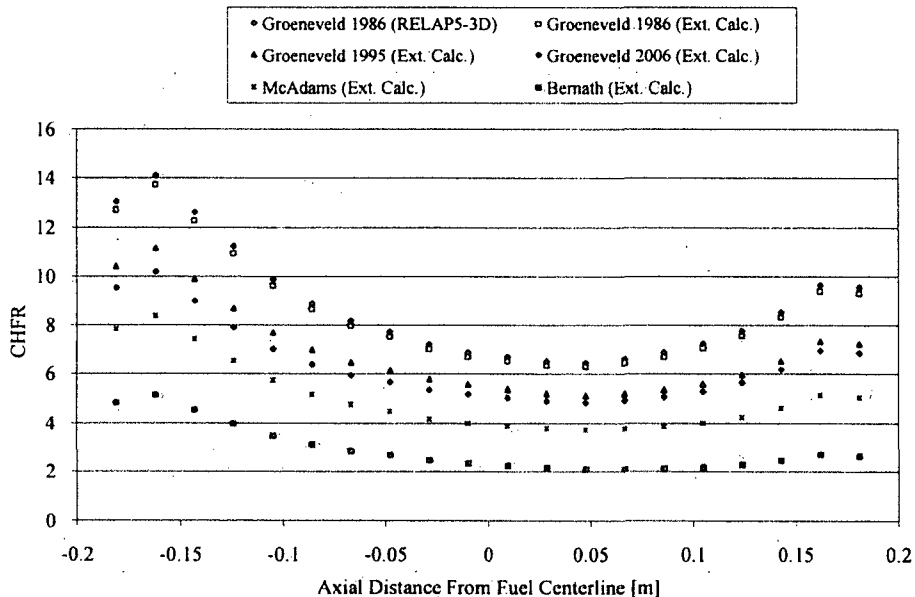


Figure 32-1: Axial CHF Distribution, Correlation Comparison
(HEU Beginning of Life Normal Core using the single channel model)

As presented in Figure 32-1, the 1986 AECL Groeneveld look-up tables produce the least conservative CHF distribution values, followed by the 1995 and 2006 Tables. The McAdams correlation and Bernath correlation, produce the most conservative CHF distribution values. Based on the results presented in Figure 32-132-1, the 2006 Groeneveld look-up tables and the Bernath correlation were used in the final version of the core conversion project. They were chosen for the following reasons:

Bernath -

- It is traditionally used as a supplement in research reactor SARs with respect to the RERTR program including the recent submission of the Washington State University Research Reactor [6].
- The correlation produces the most limiting CHF values over all other correlations considered during this study.

2006 AECL Groeneveld look-up Tables -

- The correlation is the most current method for calculating CHF values over all others considered during this study.

33. **Section 4.7.2, Table 4-18.** In accordance with the subchannel shown in Figure 4-23, a consistent definition for the heated diameter should be the heated perimeter divided by pi. That is the definition adopted by Bernath for his CHF correlation. In the conversion SAR, what was the heated diameter used in the Bernath correlation?

All CHF correlations considered during the analysis use the heat flux of the outer cladding at a given nodal location. Because of this the outer cladding serves as both the wetted diameter as defined in section 4.7.2 and the heated diameter for the Bernath correlation ($D_H = D_{outer\ clad} = 3.724E-02$ meters). Table 4-18 contains an error in the

physical heated diameter. The correct value of 3.724E-02 meters was used in all calculations.

For clarity, we will replace Figure 4-23 with the following Figure:

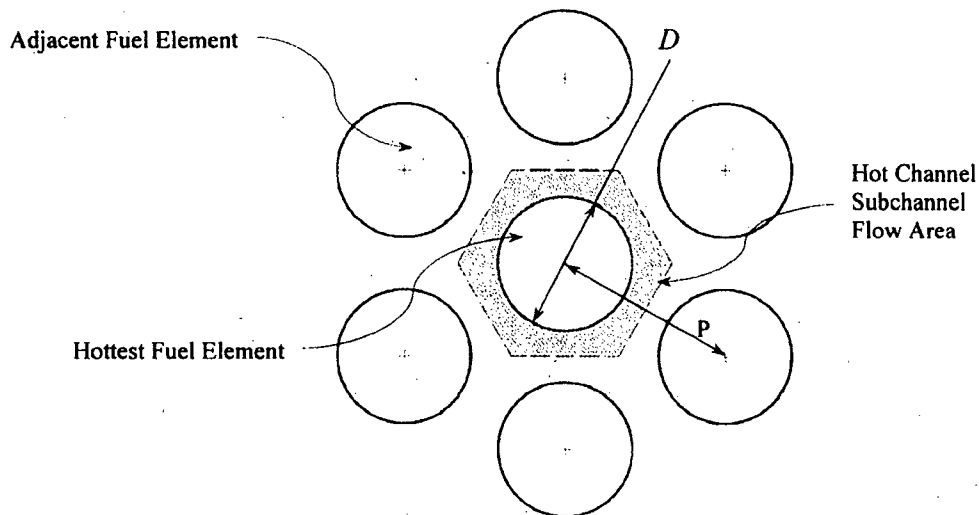


Figure 4-23, Hexagonal Array Axial Average Unit Subchannel Dimension

34. Section 4.7.4, Figure 4-30. Are there any contributors to the change in axial power profile with burnup other than burnup (e.g., control rod movement)?

Axial power distribution is affected by burnup, control rod movement and the presence of experiments in the core. Axial power distribution could also be affected by such changes as flooding of the reflector or rotating rack. Note that the OSTR core is physically small in size with a high degree of leakage and relatively large neutron mean free path. As a result the flux in the core is closely coupled and physical changes in the core will have a relatively small affect on flux distribution and hence power distribution. None of these effects, other than burnup, were explicitly modeled.

Previous analysis by GA for the Washington State University LEU core calculated axial peaking factors with all rods partially withdrawn of 1.27 for the BOL, cold critical core and 1.29 for the BOL, hot critical core [7]. The OSU LEU BOL cores have axial peaking factors with all rods fully withdrawn of 1.22 for each of the three core configurations. These cores are not identical, but these results indicate that partially withdrawn control rods cause only a slight (~4%) increase in axial peaking factors. Note that with rods partially inserted, the power in the fuel rods close to the control rod will be suppressed, so even though the axial peak factor is slightly increased, power in nearby fuel elements will be suppressed, potentially reducing the hot rod peak factor and the net effective peak factor.

35. **Section 4.7.4. The text stated that there are 84 FLIP fuel elements in the initial HEU core including the three control rod fuel followers. However Figures 4-27,4-28, and 4-29 indicate that there are 85 fuel elements. What is the correct number of fuel elements assumed in the RELAP5-3D model of the OSTR?**

This is a typographical error. The correct number of fuel elements was 85. We have verified that all RELAP calculations used the correct number of fuel elements.

36. **Section 4.7.4 and Table 4-21. What is the number of HEU fuel elements assumed in calculating the hot rod peak factors for the HEU core in Table 4-21?**

The total number of fuel elements in the HEU core analysis was 85. Please note the updates to Table 4-21 discussed in question #21.

37. **Section 4.7.4. Are changes in gap properties (e.g., gap size, oxidation at the fuel boundary, gas composition) over time taken into account when calculating fuel temperatures? Also is a gap of 0.1 mills assumed for the LEU cores?**

The gap properties were held constant over time for this analysis. For gap thickness, a sensitivity study looking at the affect of increasing gap thickness from 0.05 mil to 0.40 mil in 0.05 mil increments on radial fuel temperature was conducted. Calculated values of fuel temperature for a gap value of 0.10 mil were found to be just above that measured in the Instrumented Fuel Element at BOL, accounting for differences in element location and thermal couple position within the element.

The only gap thermal model used was that listed as the "gap" thermal model listed in the material properties table of RELAP5-3D. This model was chosen because it incorporates fission product build up in fuel elements. This will produce a larger thermal resistance compared with air and is conservative over the lifetime of the fuel.

Oxidization was not considered in the thermal analysis for OSTR fuel elements. All LEU core calculations assume a gap thickness of 0.10 mils.

38. **Section 4.7.5. What reactivity feedback mechanisms other than Doppler are included in the RELAP5 model?**

During the pulse analysis the only feedback mechanism incorporated into the RELAP5-3D model is the prompt negative fuel temperature coefficient associated with fission heating. Because the pulse transients occur on such short timescales and the thermal resistance in the fuel, gap, and clad are very large, the heat flux at the outer clad surface does not change until several seconds after the pulse initiates. To verify these assertions, two RELAP5-3D cases were considered. The first case involved only fuel feedback. The second case involved both fuel and moderator feedback. The results are shown in Figure 38-1.

The reactivity is identical for the case with and without moderator feedback. This is because there is not enough heat that is transferred into the moderator to affect its

temperature or density within the extremely short time frame. Note that this calculation did not account for moderator heating due to gamma heating. This is believed to be conservative since higher moderator temperatures would result in stronger negative reactivity feedback and hence smaller pulses.

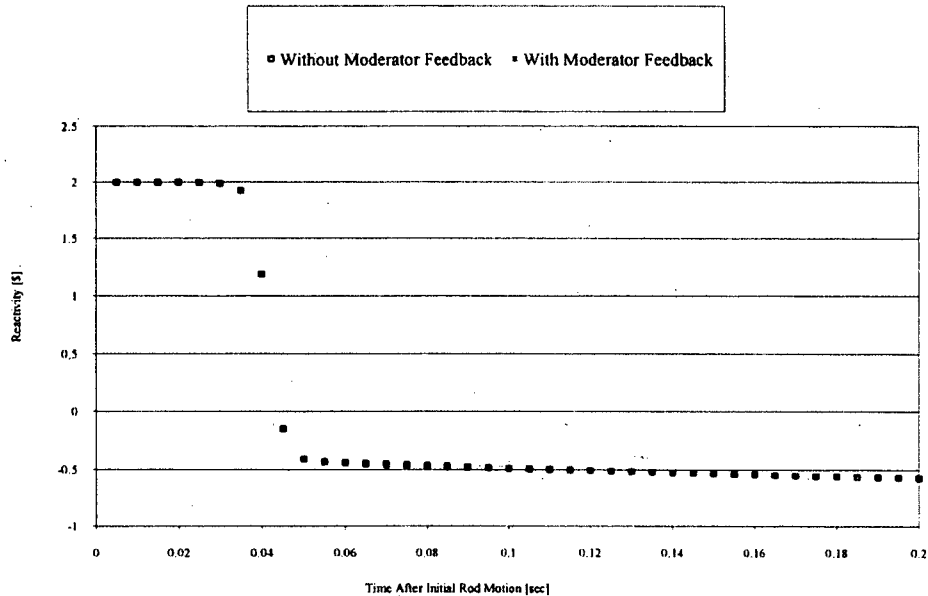


Figure 38-1: Transient Reactivity Comparison (\$2.00 Insertion)
(HEU Beginning of Life Normal Core)

39. Section 4.7.5. Were core average thermal-hydraulic parameters (e.g. hydraulic diameter and heated diameter) used in the representation of the average channel?

The two channel model was implemented for the pulse analysis of core conversion project only. In the case of the HEU and LEU cores, all fuel elements have the same geometry, therefore the heated perimeter is equal to the product of the number of fuel elements incorporated in a given subchannel times the heated perimeter of a single fuel element. A similar statement can be made with reference to the heated surface area of the average core relative to the hot channel. The average core hydraulic diameter was scaled as the product of the number of fuel elements in the subchannel times the hydraulic diameter of the hot channel. However, because time scales of less than 0.5 seconds are considered during the pulse analysis, the channel flow area associated with the average core has no impact on the maximum fuel temperature solution.

40. Section 4.7.5. How were core-average properties (e.g. coolant temperature and fuel temperature) determined for use in calculating reactivity feedbacks?

A two channel model was developed in order to study pulse transients in the OSTR for different core configurations and reactivity insertions. Figure 40-1 presents the schematic of the two channel model constructed for this quantitative comparison. The

models were based on 85 fuel elements for the HEU core and 88 fuel elements for the LEU core which includes all fuel followed control rods and the instrumented fuel element. A relation for the two channel model is presented below assuming the number of fuel elements found in the HEU core.

The pulse transient simulated by RELAP5-3D implements the point reactor kinetics model that has been built into the code. The following parameters defined in the model are the dominant factors in the outcome of the point reactor kinetics solution:

- Volumetric Heat Capacity $\rho C_p(T)$
- Effective Delayed Neutron Fraction / Mean Neutron Generation β/Λ
- Prompt Fuel Temperature Coefficient $\alpha(T)$

Because the parameters listed above were obtained for this study as core average parameters it is paramount that they be represented in the model as such. In order to correctly insert a given reactivity (ρ), into the RELAP5-3D model it must be done such that it is distributed through all fuel elements in the core.

The purpose of this study is to model time varying conditions in the hot rod of the core so that the most limiting conditions may be observed. Referring to Figure 40-1 volume 102, as the core average solution is produced from the point reactor kinetics model, the heat generation information is then passed to the hot rod (volume 101). The hot rod is a single separate channel which includes radial, axial, and hot channel peak factors. The solution in the hot channel (i.e. heat generation and removal) is then produced for a given time step as a result of the thermal power solution that was produced from the point reactor kinetics solution in the average core.

As a result of this, since a total of 85 fuel elements are found in the OSTR HEU core, 85 heat structure elements must be included in the RELAP5-3D model. 84 heat structure elements are included in the core average volume (volume 102) which produce a core average solution for a given reactivity insertion, and a single separated heat structure (volume 101) is used to determine hot rod temporal conditions.

The pulse analysis conducted as a part of the core conversion project was done using an explicit numerical scheme to solve the point reactor kinetics model incorporated into RELAP5-3D. Because the prompt fuel temperature coefficient is a temperature dependant property of the fuel, it must be explicitly solved along with the point reactor kinetics equations, this is done in RELAP5-3D by volume weighting the average temperature in fuel portion of the heat structure. After volume weighting the average temperature, RELAP5-3D then linearly interpolates on the prompt fuel temperature coefficient and moves into the next time step solving the point reactor kinetics equations. It is important to acknowledge that the volume weighted average temperature is only considered within the fuel portion of the fuel element, this is the only region where prompt fuel temperature coefficient is found.

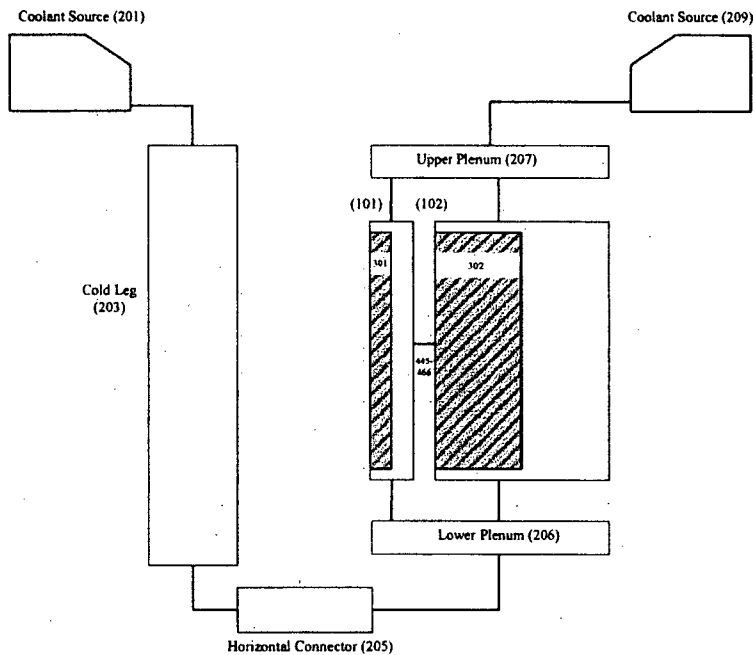


Figure 40-1: Two Channel RELAP5-3D Model Schematic

41. **Section 4.7.5. Does the pulsing of the transient rod result in a change in the location of the hot rod in the B Ring?**

The point reactor assumption is an oversimplification. Since the hotter rods experience stronger negative feedback, the overall power profile during a pulse tends to be flatter than the steady state power profile. As a result, the assumption that the pulsing reactor maintains the same power shape as the steady state reactor is conservative. The calculations required to answer this question are considered to be beyond the scope of the analysis and have not been performed.

42. **Section 4.7.5. In order to better understand the comparison of the measured temperature with the IFE reading it is necessary to know the location of the IFE. Please provide.**

As shown in SAR Figure 4-4, the IFE was located in position B-1 in the HEU BOL core.

43. **Section 4.7.7. Figure 4-59. Where are the locations of the parameters plotted in Figure 4-59?**

Each parameter is taken at a different elevation in the hot subchannel. The fuel centerline temperature is shown at the axial nodal location which produces the maximum fuel centerline temperature (fuel axial center). The outer cladding

temperature is shown at the axial location which produces the maximum outer cladding temperature (slightly above the axial fuel centerline). The bulk coolant temperature is shown at the location which produces the maximum bulk coolant temperature (highest vertical subchannel node). Coolant mass flux is shown as the mass flux which corresponds to the maximum bulk coolant temperature (highest vertical subchannel node). Each location was selected to show the most limiting value of the associated parameter. This information will be added to the text.

44. **Figure 4-61. It appears that the data for the outer cladding temperature and the bulk coolant temperature are reversed. Please comment.**

Bulk coolant and clad temperatures have been reversed in this figure. This will be corrected.

45. **Section 4.7.8. Please verify that reference to BOL instead of MOL in several places in this section is a typographical error.**

There was a typographical error in the last sentence and the last paragraph not as clear as it could have been. The final paragraph in section 4.7.8 should be replaced with the following:

The steady state results shown above are for the LEU ICIT MOL core configuration. The ICIT core was analyzed because it has the highest predicted hot rod thermal power and effective peaking factor for each of the core configurations and burn up time periods. Figure 4-65 shows that the MDNBR in the hot channel will reach a value of 2.00 at approximately 19.85 kW hot channel steady state power using the Bernath correlation and significantly higher yet using the Groeneveld 2006 correlation. Additionally, the value of 19.85 kW is larger than the predicted hot channel steady state power of 18.52 kW. Shown in Figure 4-67, the LEU ICIT MOL has a MDNBR of 2.06 at 1.1 MW_{th} steady state using the Bernath Correlation. Again this number would be significantly higher using the Groeneveld 2006 correlation. Taken together, the LEU MOL ICIT core is predicted to operate at a power well below that required for departure from nucleate boiling.

46. **Section 4.7.9. Please verify that reference to BOL and Middle of Life instead of EOL in several places in this section is a typographical error.**

There were two typographical error in this section. The first and final paragraphs in section 4.7.9 should be replaced with the following, respectively:

The results for the LEU End of Life ICIT core analysis are presented in this section. Hot rod temperature profiles are shown in Figures 4-60, 4-71, and 4-73. The hot channel peak factors used in this analysis are shown in Table 4-21. The hot channel power summary of parameters and results are given in Tables 4-28 and 4-29.

The steady state results shown above are for the LEU ICIT EOL core configuration. The ICIT core was analyzed because it has the highest predicted hot rod thermal power and effective peaking factor for each of the core configurations and burn up time periods.

Figure 4-70 shows that the MDNBR in the hot channel will reach a value of 2.00 at approximately 20.00 kW hot channel steady state power using the Bernath correlation are significantly higher yet using the Groeneveld 2006 correlation. Additionally, the value of 20.00 kW is larger than the predicted hot channel steady state power of 17.61 kW. Shown in Figure 4-72, the LEU ICIT EOL has a MDNBR of 2.20 at 1.1 MW_{th} steady state using the Bernath Correlation. Again this number would be significantly higher using the Groeneveld 2006 correlation. Taken together, the LEU EOL ICIT core is predicted to operate at a power well below that required for departure from nucleate boiling.

47. **Figure 4-74.** The figure is missing labels for the two vertical axes.

This is correct. The left side axis should be labeled "Power(W)" and the right side axis should be labeled "Energy (J)" This will be corrected.

48. **Section 4.7.10, Figure 4-80.** Please note that the legend is incomplete in the pdf version.

Please refer to the figure below for the temperature contour during time of peak fuel temperature for the LEU MOL ICIT core, including a complete legend.

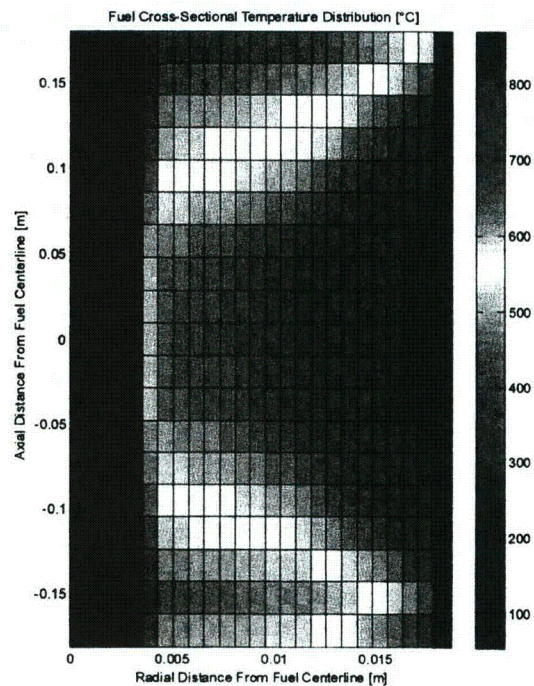


Figure 4-80: LEU MOL ICIT, Fuel Temperature Distribution at Time of Prompt Max Fuel Temperature (\$2.00 Pulse)

- 49. Sections 12.2 and 12.4. Do you want the changes to procedures and to the emergency plan to be made as part of the conversion order or do you plan to follow your technical specification (TS) requirements for procedures changes and 10 CFR 50.54(q) for emergency plan changes. If you want to make these changes as part of the conversion order please submit the changes.**

All changes to the emergency plan, if necessary, will be made following our Technical Specification requirements and 10 CFR 50.54(q).

- 50. Section 12.5. If you plan to make any changes to the physical security plan as part of the conversion order, please submit the changes.**

All changes to the physical security plan, if necessary, will be made following our Technical Specification requirements and 10 CFR 50.54(p).

- 51. Section 13.2.1. Explain the differences in FLIP reactor room air activity without water between the license renewal SAR and the conversion SAR.**

The cumulative fission yields used to calculate the room air activities for the license renewal were taken from The Chart of the Nuclides, General Electric Co and KAPL, Inc, 1996. The cumulative fission yields used to calculate the room air activities for the conversion SAR were taken from the Evaluated Nuclear Data File (ENDF), specifically ENDF/B-VI. The ENDF/B-VI data file information was used because it was thought to contain the most current and up-to-date data on cumulative fission yields.

- 52. Section 13.2.2. How much reactivity is inserted by the flooding of a beam port?**

This calculation has not been performed. Measurements taken on the HEU core indicate that replacing a single reflector element in the G-ring with water (i.e. removal of a reflector element) results in a reactivity increase of about \$0.01. Although beam ports are larger than reflector elements, they are generally further away from the core center, so flooding of a beam port is expected to result in a reactivity change of the same magnitude.

- 53. Have the consequences of pulsing the reactor from full power operation been considered? If yes, what are the results; if no, why not?**

The core configuration containing the largest effective peak factor value is the LEU Middle of Life ICIT Core. As a result of this the LEU Middle of Life ICIT Core was chosen to compare pulse characteristics for a scenario in which the OSTR is at steady state at its interlock power of 1.0kW_{th} and then pulsed to the maximum reactivity insertion for the LEU core of \$2.15. A second case is considered where the OSTR operates at maximum licensed steady state power of $1.1\text{ MW}_{\text{th}}$ and is then pulsed with \$2.15 reactivity insertion.

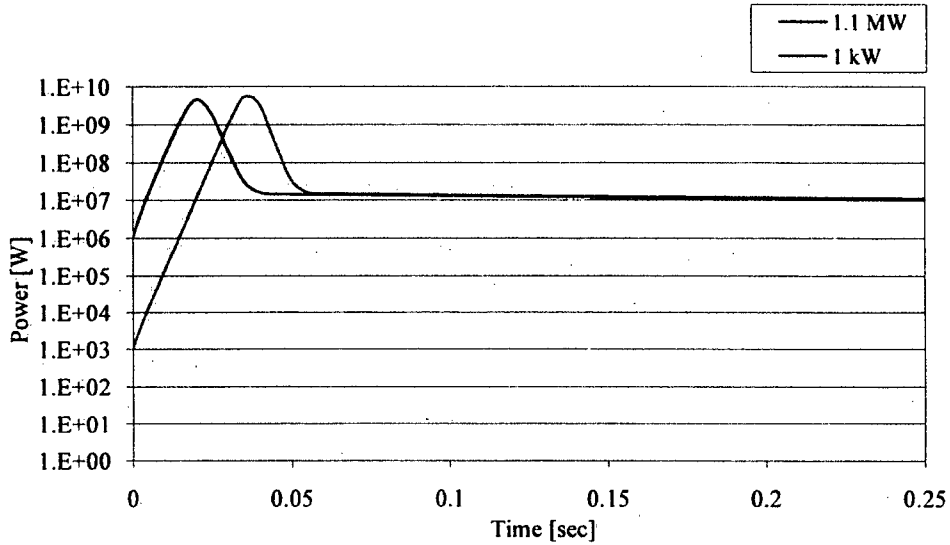


Figure 53-1: Pulse Power Trace Comparison for given initial Conditions (\$2.15 Insertion) (LEU-Middle of Life ICIT Core Configuration)

As shown in Figure 53-1, the pulse power trace for an initial steady state core at 1.1 MW_{th} has a total core peak power value of 4504 MW_{th} which produces a maximum prompt fuel temperature of 900.1 °C, while for the case where the core is initially at 1.0 kW_{th} steady state the total core peak power reaches a value of 5198 MW_{th} and produces a maximum prompt fuel temperature of 939.2 °C. A summary of the pulse comparison results are presented in Table 53-1.

Table 53-1: Pulse Initial Conditions Sensitivity Study (LEU-Middle of Life ICIT Core Configuration)

LEU-EOL ICIT Core Configuration/Initial Conditions Sensitivity Study		
Initial Steady State Power [kW]	1.0	1.1E3
Reactivity Insertion [\$]	2.15	2.15
Peak Total Core Power [MW _{th}]	5198	4504
Time of Peak Total Core Power [sec]	0.045	0.03
Prompt Peak Fuel Temperature [°C]	939.2	900.1
Time of Prompt Peak Fuel Temperature [sec]	0.05	0.035

As a result of this comparison it is demonstrated that although the initial steady state power is much greater for the case where the reactor is pulsed from 1.1 MW_{th} it results in a lower maximum prompt fuel temperature than that of the lower initial steady state power. This is due to the temperature dependant prompt fuel temperature coefficient that is inherent to the OSTR.

54. Section 13.2.3. What is the maximum calculated temperature for the OSTR LOCA and the acceptance criterion?

The content of this answer was kindly provided by TRIGA® International.

The strength of the fuel element clad is a function of its temperature. The stress imposed on the clad is a function of the fuel temperature as well as the hydrogen-to-zirconium ratio, the fuel burnup, and the free gas volume within the element. The analysis of the stress imposed on the clad and strength of the clad uses the following assumptions:

- 1) The fuel and clad are the same temperature.
- 2) The hydrogen-to-zirconium ratio is 1.7 for standard fuel (8.5 wt%) and 1.6 for FLIP fuel and 30/20 fuel.
- 3) A space one-eighth inch high within the clad represents the free volume within the element.
- 4) The reactor contains fuel that has undergone burnup equivalent to 77 MW-days for FLIP fuel and 54 MW-days for LEU 30/20 fuel.
- 5) Maximum operating temperature of the fuel is 600°C.

The fuel element internal pressure P is given by:

$$P = P_h + P_{fp} + P_{air}$$

Where:

- P_h is the hydrogen pressure;
- P_{fp} is the pressure exerted by volatile fission products; and
- P_{air} is the pressure exerted by trapped air.

For the hydrogen-to-zirconium ratios greater than about 1.58, the equilibrium hydrogen pressure can be approximated by:

$$P_h = \exp \left(1.76 + 10.3014 x \frac{19740.37}{T_k} \right)$$

Where:

- x is the ratio of hydrogen atoms to zirconium atoms, and
- T_k is the fuel temperature (K).

The pressure exerted by the fission product gasses is given by:

$$P_{fp} = f \frac{n}{E} \frac{RT_k}{V} E$$

Where:

- f is the fission product release fraction;
- $\frac{n}{E}$ is the number of moles of gas evolved per unit of energy produced (mol/MW-day);
- R is the gas constant (8.206×10^{-2} L-atm/mol-K);
- V is the free volume occupied by the gasses (L); and
- E is the total energy produced in the element (MW-days)

The fission product release fraction is given by:

$$f = 1.5 \times 10^{-5} + 3.6 \times 10^{-3} \exp\left(\frac{-1.34 \times 10^4}{T_o}\right)$$

Where:

T_o is the maximum fuel temperature in the element during normal operation (K).

The fission product gas production rate $\frac{n}{E}$, varies slightly with power density. The value 1.19×10^{-3} mol/MW-day is accurate to within a few percent over the range from a few kilowatts per element to well over 40kW per element. The free volume occupied by the gases is assumed to be a space of one-eighth inch (0.3175cm) high at the top of the fuel so that

$$V = 0.3175 \pi \cdot r_i^2$$

Where:

r_i is the inside radius of the clad (1.745cm).

For standard TRIGA fuel, the maximum burnup is about 4.5MW-days per element, but the TRIGA-FLIP fuel is capable of burnup to about 77 MW-days per element. The LEU 30/20 fuel has been tested to 50% burnup so its capability is slightly less than FLIP fuel at 54 MW-days per element. As the fission product gas pressure is proportional to the energy released, assume that the FLIP fuel in the reactor has undergone maximum burn-up.

Finally, the air trapped within the fuel element clad will exert pressure

$$P_{air} = \frac{RT_k}{24}$$

where it is assumed that the initial specific volume of the air is 22.4 L/mol. Actually, the air forms oxides and nitrides with the zirconium, so that after relatively short operation the air is no longer present in the free volume inside the fuel element clad. The results of the stress imposed on the clad for standard and FLIP fuel due to its lower maximum burnup capability. These results confirm the conclusion of NUREG-1282 that the LEU 30/20 fuel has a safety limit of 950°C when the clad temperature equals the fuel temperature.

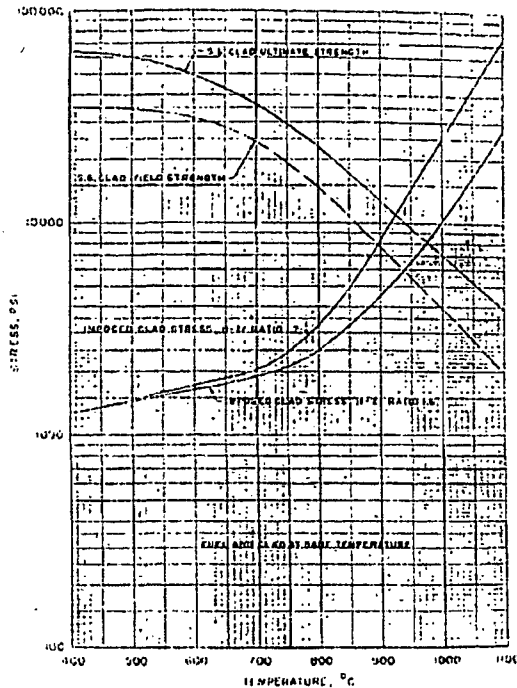


Figure 54-1: Strength and Applied Stress as a Function of Temperature for 1.7 and 1.6 H-Zr TRIGA Fuel

The maximum fuel cladding temperature after a loss of pool water depends on the fuel rod power and the time delay between reactor shutdown and uncovering of the core. For the case of no delay, a value of 21 kW/element is reported to prevent fuel temperatures from exceeding 900°C (Foushee, 1972). The analysis developed a two dimensional transient-heat transport computer code model TAC2D for calculating the maximum fuel temperatures after the loss of pool water for various delay times. During the loss of pool water, the low water level alarm occurs when the water is 18ft above the top of the core. The time between the actuation of the pool level alarm and the uncovering of the fuel for a catastrophic failure of an eight-inch beam tube is assumed to be 15 minutes (900 sec.) Figure 54-2 presents a curve of maximum fuel cladding temperature versus fuel rod power density using a 15 minute delay. The results show that standard 8.5% fuel can remain below 900°C at a power density of 22.3kW/element. The results also show that a FLIP of LEU (30/20) fuel element can remain below 950°C at a power density 23.5kW/element. This power density is above the maximum power density of 18.52 kW/element for the OSU LEU MOL ICIT core operating at 1.1 MW.

Additional delay time is likely since the most likely initiator of a beam tube rupture is the dropping of a large heavy object from above the reactor pool. Such activity is not anticipated for several hours after reactor shutdown.

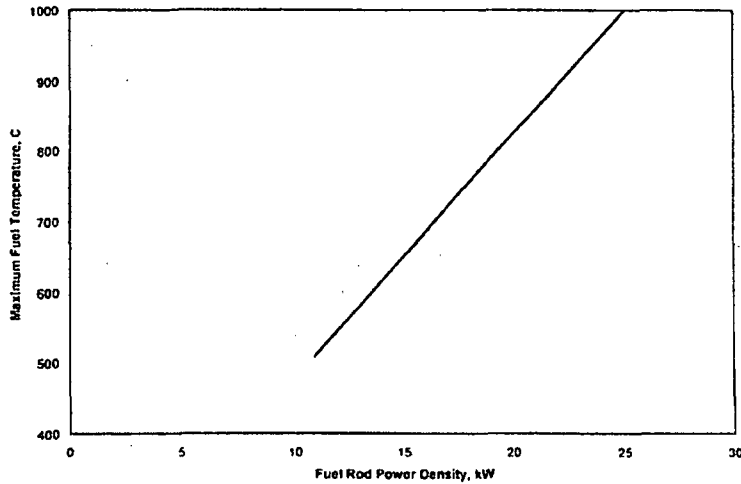


Figure 54-2: Maximum Fuel Rod Temperature for Loss of Coolant 15 Minutes After Shutdown

If the reactor operates for seventy MW-hours or less per week, power generation per element values approximately 20% higher are sufficient to meet the safety limits. Thus, 26.7 kW/elements for standard and 28.2 kW/element for FLIP and LEU 30/20 fuel are adequate power densities. A comparison of decay heat generation versus time following loss of coolant for infinite reactor operations and 70MW-hours per week cycle operations are in Figure 54-3.

Even though the probability of a loss-of-coolant accident is extremely remote, calculations have been performed to evaluate the radiological hazards. The radiation dose rates are given in Table 54-1 and are based on the assumption that the reactor has been operating for a very long time at a power level of 1MW prior to the loss of pool water. The times listed in the table are after shutdown of the reactor from full power. The first location is directly on top of the reactor at the bridge level which is 23.5 feet above the top of the actual fueled portion of the core. The second location is at the pool room floor level at the freight door at the east end of the pool room. This second location is shielded from direct radiation from the core but subjected to scattered radiation from the ceiling of the pool room. The ceiling is assumed to be thick concrete yielding the maximum possible reflected radiation dose which is a conservative assumption since the actual roof structure would yield much less scattered radiation.

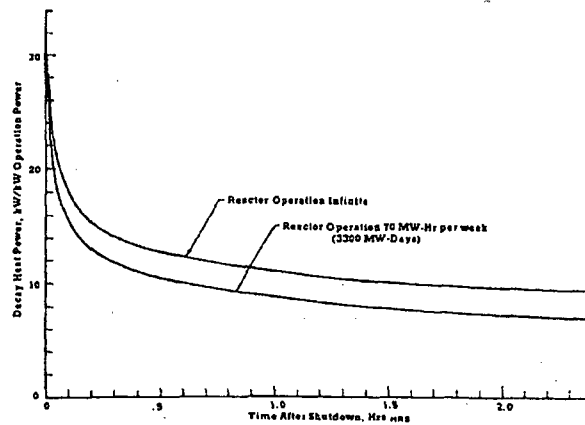


Figure 54-3: Decay Heat Power Generation Following Loss of Coolant for Infinite Reactor Operations and Periodic Reactor Operations

Table 54-1
Calculated Radiation Exposure Rates in a Loss-of-Pool-Water Accident

Time After Shutdown	Reduction Factor Due to Decay	Direct Radiation (rem/hr)	Scattered Radiation (rem/hr)
10 sec	1	7350	0.25
1 hr	2.70	2720	0.093
1 day	8.67	848	0.025
1 week	18.84	396	0.015
1 month	72.20	102	0.0035

The data given in Table 54-1 was calculated assuming that the bare unshielded core is a cylindrical source of 1MeV photons with a uniform source distribution. The dimensions of the cylinder were taken equal to the active core lattice which has an equivalent radius of 29.1 cm, height of 38.1 cm, and a volume of $5.75 \times 10^4 \text{ cm}^3$. The source strength as a function of time was determined from Perkins and King's data on fission product decay. No accounting was made for sources other than fission product decay gammas or for attenuation through the fuel rod end pieces, core support structure, or bridge deck plate. It is assumed that no buildup occurs in the core. The sum total effect of these assumptions is a conservative (overestimation) of the dose rates.

Foushee, F.C., "TRIGA Four-rod Cluster Loss-of-Coolant Accident Analysis," Gulf General Atomics, E-117-196, October, 1972

Perkins, J.F., and King, R.W., "Energy Release from the Decay of Fission Products," Nuclear Science and Engineering, Vol. 3, p. 726, 1968.

55. **Section 14. Please identify and specifically justify the changes that were made to the TSs.**

Please replace Section 14 with the following:

1) Delete the following from the Basis in section 2.2:

MCNP based analysis performed in 2007 shows that the peak power in the B ring occurs at position B-3, and is approximately 4% higher than the power in the B-4 IFE position. The IFE is calibrated annually. Experience has shown that true temperature differs from indicated temperature by no more than 5%.

Axial flux measurements made in the In-Core Irradiation Tube (ICIT) core configuration indicate that the difference between peak axial flux and the minimum flux at any of the three thermocouple elevations is no more than 18%.

Typical fuel temperatures observed at full power are approximately 350°C. The analysis in section 13.2.2.2.1 shows that an uncontrolled withdrawal of a control rod at an initial power level of 1 MW would result in a trip signal being initiated within 0.28 seconds resulting from a reactivity insertion of \$0.15. For an uncontrolled withdrawal of a control rod at an initial power level of 100 W, the trip signal would be initiated in 5.06 seconds resulting from a reactivity insertion of \$1.06. Because fuel temperature lags behind power and the power is so low, each of these scenarios would result in high power trips before the fuel temperature trip is reached. This is confirmed by our experience of observed instrument behavior after a pulse. For the loss of coolant accidents described in section 13.2.3, the primary water temperature would trip the reactor or the low level alarm would annunciate and alert the operator long before enough water is lost to initiate a high fuel element temperature trip. Regardless, section 13.2.3.2.2.1 clearly shows that natural convective air cooling of the fuel will keep the maximum fuel temperature well below the SL even after an instantaneous complete loss of primary water at 1.5MW or below.

The thermocouple is located 0.300 inches from the fuel centerline. The maximum temperature of fuel in the fuel element is expected to occur at 0.125 inches from the centerline where the fuel meat to central zirconium pin interface is located. If it is assumed that pool temperature is 30°C, there is no temperature drop across the clad, and temperature at the TC is 350°C, then using a quadratic (conservative) curve fit, the temperature distribution within the fuel meat is calculated to be: $T(r) = 411 - 677r^2$. At the inner radius of the fuel, temperature is calculated to be: $T(0.125) = 400^\circ\text{C}$. Under the same assumptions, but with a thermocouple reading of 510, the temperature distribution within the fuel meat is calculated to be: $T(r) = 601 - 1016r^2$. At the inner radius of the fuel, temperature is calculated to be: $T(0.125) = 586^\circ\text{C}$.

Basis for this change: This information has been replaced with that derived directly from the RELAP-3D model. The new model provides explicitly the temperature at the depth of the thermal couple within the hottest fuel element (see the following change to the Basis of section 2.2). This estimation of the profile is no longer needed.

2) Change the Basis in section 2.2 from:

During steady state operation, temperatures were calculated for the beginning-of-life normal core. Linear extrapolation of temperature and power indicates that an IFE power of 23.2 kW will produce an indicated power of 510°C in the IFE at the midplane thermocouple location. The highest ratio of maximum to minimum power for elements in the B-ring was found to be 1.036, so if the IFE is generating 23.2 kW, the maximum power in any B-ring element would be limited to $23.1 \times 1.036 = 24.03$ kW. For a power of 24.03 kW, the maximum temperature anywhere in the hot channel fuel element will be 588°C. This is well below the Safety Limit.

to:

During steady state operation, maximum temperatures are predicted to occur in the LEU MOL ICIT core. Linear extrapolation of temperature and power from Table 4-27 of section 4.7.8 indicates that an IFE power of 23.1 kW will produce an indicated power of 510°C in the IFE at the midplane thermocouple location. Of the nine LEU cores analyzed in the SAR, the highest ratio of maximum to minimum power for elements in the B-ring is 1.121, so if the IFE is generating 23.1 kW, the maximum power in any B-ring element would be limited to $23.1 \times 1.121 = 25.9$ kW. Figures 4-59, 4-64 and 4-69 indicate that at 25.9 kW, the maximum temperature anywhere in the hot channel fuel element will be less than 600°C.

Additional analysis has shown that if a B-ring element in the LEU MOL ICIT or LEU EOL ICIT core is replaced with fresh fuel, the highest ratio of maximum to minimum power in the B-ring is 1.378. In these cores, if the IFE is generating 23.1 kW, the maximum power in any B-ring element would be limited to $23.1 \times 1.378 = 31.8$ kW. Figures 4-59, 4-64 and 4-69 indicate that at 31.8 kW, the maximum temperature anywhere in the hot channel fuel element will be less than 700°C.

Basis for this change: This data comes directly from the RELAP-3D and MCNP5 models and represents the best available information relating the maximum fuel temperature and the temperature in the IFE.

3) Change the Specification in section 3.1.4 from:

“...such that the reactivity insertion shall not exceed \$2.55.”

to:

“...such that the maximum fuel element temperature shall not exceed 830°C.”

Basis for this change: TRIGA® International is proposing that 830°C as a maximum pulse temperature limit. This limit should be based on temperature not reactivity.

4) Change the Basis in section 3.1.4 from:

The fuel temperature rise during a pulse transient has been estimated conservatively by adiabatic models. These models accurately predict pulse characteristics for several core configurations and should be accepted with

confidence, relying also on information concerning prompt neutron lifetime and prompt temperature coefficient of reactivity. These parameters have been established for these cores by calculations and have been confirmed in part by measurements at existing facilities. In addition, the calculations rely on flux profiles and corresponding power densities which have been calculated (SAR 13.2.2.2.1).

to:

The basis for the temperature limit given can be found in GA-C26017, *Pulsing Temperature Limit for TRIGA® LEU Fuel*. The fuel temperature rise during a pulse transient has been estimated by RELAP-5-3D using non-adiabatic models. The core analyzed had the highest accumulative peaking factor for any core configuration, was analyzed at the middle of life because that presents the highest core reactivity during the fuel lifetime and looked at the rod with the predicted maximum temperature in that core. These models predict pulse characteristics for operation of operational cores and should be accepted with confidence, relying also on information concerning prompt neutron lifetime and prompt temperature coefficient of reactivity. The reactivity value calculated to produce a temperature of 830°C is \$2.33. Therefore limiting reactivity insertions to a maximum of \$2.30 will ensure that fuel temperature will not exceed 830°C.

Basis for this change: TRIGA® International is proposing that 830°C as a maximum pulse temperature limit. The basis should be redefined to specifically identify the relevant GA document but also identify the reactivity corresponding to 830°C. It also needs to be clear that the reactivity value is derived from the newly created RELAP-3D model.

5) Change the function of the Transient Rod Cylinder Position in Table 3 of the Specification in section 3.2.3 from:

Prevent pulse insertion of reactivity greater than \$2.55.

to:

Prevent pulse insertion of reactivity greater than that which would produce a maximum fuel element temperature of 830°C.

Basis for this change: TRIGA® International is proposing that 830°C as a maximum pulse temperature limit. This limit should be based on temperature not reactivity.

6) Change the following part of the Basis in section 3.2.3 from:

1 kW Pulse Interlock: The 1-kW permissive interlock is designed to prevent pulsing when wide range log power is above 1-kW. SAR 13.2.2.2.1 shows that the peak temperature reached during an end-of-life core will be 1,150°C for an initial fuel temperature of 20°C. The methodology clearly shows that if the initial temperature was higher, the resulting peak temperature must be lower. However, there has not been analysis or experiment to look at the relationship between heat generated within the fuel at power (i.e., > 1-kW) and heat generated on the surface of the fuel during a pulse. Therefore, this interlock prevents the reactor from pulsing at power levels which produce measurably significant increases in fuel temperature.

Shim, Safety and Regulating Rod Drive Circuit: The single rod withdrawal interlock prevents the operator from removing multiple control rods simultaneously such that reactivity insertions from control rod manipulation is done in a controlled manner. The analysis in SAR 13.2.2.2.2 and 13.2.2.2.3 show that the reactivity insertion due to the removal rate of the most reactive rod or all the control rods simultaneously is still well below the reactivity insertion design limit of \$2.59.

Shim, Safety and Regulating Rod Drive Circuit: In pulse mode, it is necessary to limit the reactivity inserted to less than the design limit of \$2.59 at the end of core life analyzed in SAR 13.2.2.2.1. This interlock ensures that all pulse reactivity is due to only the transient rod while in pulse mode. Otherwise, any control rod removal in pulse mode would add to the inserted reactivity of the transient rod and create an opportunity for exceeding the reactivity insertion limit.

Transient Rod Cylinder Position Interlock: For the transient rod cylinder interlock, SAR 13.2.2.2.1 shows that the designed limiting reactivity insertion for the fuel is \$2.59 at the end of core life. This interlock limits transient rod reactivity insertions below this value. Furthermore, this interlock is designed such that if the electrical (i.e., limit switch) portion fails, a mechanical (i.e., metal bracket) will still keep the reactivity insertion below the criterion.

to:

1 kW Pulse Interlock: The 1-kW permissive interlock is designed to prevent pulsing when wide range log power is above 1-kW. Analysis of pulsing at full power shows that if the initial temperature was higher, the resulting peak temperature will be lower. However, there has not been an experiment to look at the relationship between heat generated within the fuel at power (i.e., > 1-kW) and heat generated on the surface of the fuel during a pulse. Therefore, this interlock prevents the reactor from pulsing at power levels which produce measurably significant increases in fuel temperature.

Shim, Safety and Regulating Rod Drive Circuit: The single rod withdrawal interlock prevents the operator from removing multiple control rods simultaneously such that reactivity insertions from control rod manipulation are done in a controlled manner. The analysis in SAR 13.2.2.2.2 and 13.2.2.2.3 show that the reactivity insertion due to the removal rate of the most reactive rod or

all the control rods simultaneously is still well below the reactivity which would produce a fuel element temperature of 830°C.

Shim, Safety and Regulating Rod Drive Circuit: In pulse mode, it is necessary to limit the reactivity below that which would produce a fuel element temperature of 830°C. This interlock ensures that all pulse reactivity is due to only the transient rod while in pulse mode. Otherwise, any control rod removal in pulse mode would add to the inserted reactivity of the transient rod and create an opportunity for exceeding the reactivity insertion limit.

Transient Rod Cylinder Position Interlock: The transient rod cylinder interlock shall limit reactivity insertions below that which would produce a fuel element temperature of 830°C. This interlock limits transient rod reactivity insertions below this value. Furthermore, this interlock is designed such that if the electrical (i.e., limit switch) portion fails, a mechanical (i.e., metal bracket) will still keep the reactivity insertion below the criterion.

Basis for this change: These changes address references in the Basis of this section to pulse limits. TRIGA® International is proposing that 830°C as a maximum pulse temperature limit. This limit should be based on temperature not reactivity.

7) Change the Specification 3.8.1.b from:

The sum of the absolute values of the reactivity worths of all experiments shall be less than \$2.55.

to:

The sum of the absolute values of the reactivity worths of all experiments shall be less than that which would produce a fuel element temperature of 830°C.

Basis for this change: TRIGA® International is proposing that 830°C as a maximum pulse temperature limit. This limit should be based on temperature not reactivity.

8) Change the Basis in section 3.8.1 from:

The reactivity limit of \$0.50 for movable experiments is designed to prevent an inadvertent pulse from occurring and maintain a value below the shutdown margin. Movable experiments are by their very nature experiments in a position where it is possible for a sample to be inserted or removed from the core while critical. That being said, Section 13.2.2.2.1 clearly shows that this value is still below the analyzed design limit of \$2.59 for end of life fuel.

The reactivity worth limit of \$2.55 for all experiments is designed to prevent an inadvertent pulse from exceeding the design limit of \$2.59 for end of life fuel. This limit applies to movable, unsecured and secured experiments. Regardless of any other administrative or physical requirements, this limit has been shown in Section 13.2.2.2.1 to protect the reactor during the fuel's entire lifetime.

to:

The reactivity limit of $\beta 0.50$ for movable experiments is designed to prevent an inadvertent pulse from occurring and maintain a value below the shutdown margin. Movable experiments are by their very nature experiments in a position where it is possible for a sample to be inserted or removed from the core while critical. That being said, the value is clearly less than the limit on pulsing.

The reactivity worth limit for all experiments is designed to prevent an inadvertent pulse from exceeding the recommended limit on pulsing. This limit applies to movable, unsecured and secured experiments. A maximum reactivity insertion of $\beta 2.30$ will ensure that fuel temperature will not exceed 830°C .

Basis for this change: TRIGA[®] International is proposing that 830°C as a maximum pulse temperature limit. This limit should be based on temperature not reactivity.

9) Change the Specification 5.3.3.1 from:

Uranium content: maximum of 9 wt% enriched to a nominal 70% ^{235}U ;

to:

Uranium content: nominal 30 wt% enriched to a nominal 20% in ^{235}U ;

Basis for this change: This specifically describes a fuel element having characteristics of LEU fuel.

10) Change the Specification 5.3.3.3 from:

11)

Natural erbium content (homogeneously distributed): between 1.1 and 1.6 wt%;

to:

Natural erbium content (homogeneously distributed): nominal 1.1 wt%;

Basis for this change: This specifically describes a fuel element having characteristics of LEU fuel.

56. Section 14.2.1. Please confirm that the ratio of hydrogen to zirconium will not change so that the limiting temperature remains the same upon conversion.

The existing specification for the FLIP fuel is given by Technical Specification 5.1.a.2 "Hydrogen-to-zirconium atom ratio (in the ZrH_x): between 1.5 and 1.65." The fuel element average range of acceptance for the hydrogen to zirconium atom ratio in the LEU fuel is 1.57 to 1.65.

57. **Section 14.5.3.1 (b).** It appears that you are proposing that this TS be changed from a "shall" statement to a "may" statement. Please explain why this change is needed as part of the conversion process or request this change as part of your license renewal application.

This was a typographical error. Section 14.5.3.1 (b) should continue to be a "shall" statement.

58. **Section 15.2.** Your proposed changes to license condition 2.b(2) do not contain authority to possess the AGN core. If you desire to remove this part of the license condition an application should be made by the normal license amendment process. If not, please propose changes to your proposed license condition as appropriate. Your proposed license conditions after conversion will not allow receipt, possession or use of any HEU. Will you need to possess any HEU (e.g., fission chambers and flux foils) after conversion? If so, please propose and justify appropriate license conditions. Your proposed license condition contains the authority to possess, but not separate, such special nuclear material as may be produced by the operation of the facility. Does this part of your proposed license condition duplicate license condition 2.b(4)? If so, is it needed?

The removal of the AGN core from the license was an oversight and not intended. The AGN core is addressed in the response to RAI Question 59 below.

To address the possession of HEU for purposes such as fission chambers and to keep license condition 2.b.(4) as it is, the following amended license condition 2.b.(2) is proposed:

Pursuant to the Act and 10 CFR Part 70, "Domestic Licensing of Special Nuclear Material," to receive, possess, and use: (1) up to 16.30 kilograms of contained uranium-235 of enrichment of less than 20 percent in the form of non-power reactor TRIGA[®] fuel; and (2) up to 100 grams of contained uranium-235 of any enrichment in the form of fission chambers, flux foils and fueled experiments, all used in connection with operation of the facility;

59. **Section 15.2.** Your proposed license condition 2.b(5) for possession of the HEU fuel until it is removed from the facility allows receipt of uranium-235. Please confirm that no additional HEU will be received and that the HEU possessed under this license condition will not be used. Please amend your proposed license condition.

No additional HEU will be received. To address these concerns, we propose the following language for section 2.b.(5):

Pursuant to the Act and 10 CFR Part 70, "Domestic Licensing of Special Nuclear Material," to possess, but not use: (1) up to 12.83 kilograms of contained uranium-235 at equal to or greater than 20 percent enrichment in the form of non-power reactor TRIGA[®] fuel until this fuel is removed from the facility; and (2) up to 660 grams of contained uranium-235 of enrichment of less than 20 percent contained in the control rods and core from the AGN-201 reactor, License No. R-51, Docket No. 50-106, until this fuel is removed from the facility;

60. Appendix A. Describe in greater detail startup tests planned for pulsed operation.

Pulse mode operation tests shall consist of, at a minimum, a sequence of pulses starting at about \$1.10 and proceeding in \$0.10 increments until the maximum pulse reactivity insertion limit is reached. Peak power, temperature and integrated power data shall be recorded from console instruments. Graphs of peak temperature vs. prompt reactivity, integrated power vs. prompt reactivity and peak power vs. (prompt reactivity)² shall be constructed. These graphs are expected to show a linear dependence, although some departure from linearity at higher reactivity insertions may be observed due to the fact that longer rod ejection times are experienced during larger reactivity insertions.

61. Appendix B. What action is taken if an acceptance criterion for a startup test is not met?

If an acceptance criterion is not met, reactor operation shall be suspended. Reactor operation may be continued once the Reactor Administrator and Reactor Supervisor agree on and implement (as appropriate) modifications to the reactor re-start procedure.

Addendum.

During the RAI response period, it was determined that calculations of the fuel prompt temperature feedback coefficient (α_f) had been performed with inconsistent cross section libraries. Low temperature (i.e. 300K) calculations used cross section from the 1997 ENDF library while all higher temperature calculations used 1993 ENDF library data. For consistency, all calculations should have used 1993 data (the 1997 library contained uranium cross section information for only 300K). Calculations based entirely on 1993 ENDF data result in a different value for α_f , as shown in Figure A-1, Fuel prompt temperature coefficient. Data in Figure A-1 is for the LEU MOL core. Use of consistent cross section libraries results in increasing the magnitude of the lowest temperature point. This raises the magnitude of the linear best fit line for the temperature coefficient at low temperatures and decreases the slope of the best fit line.

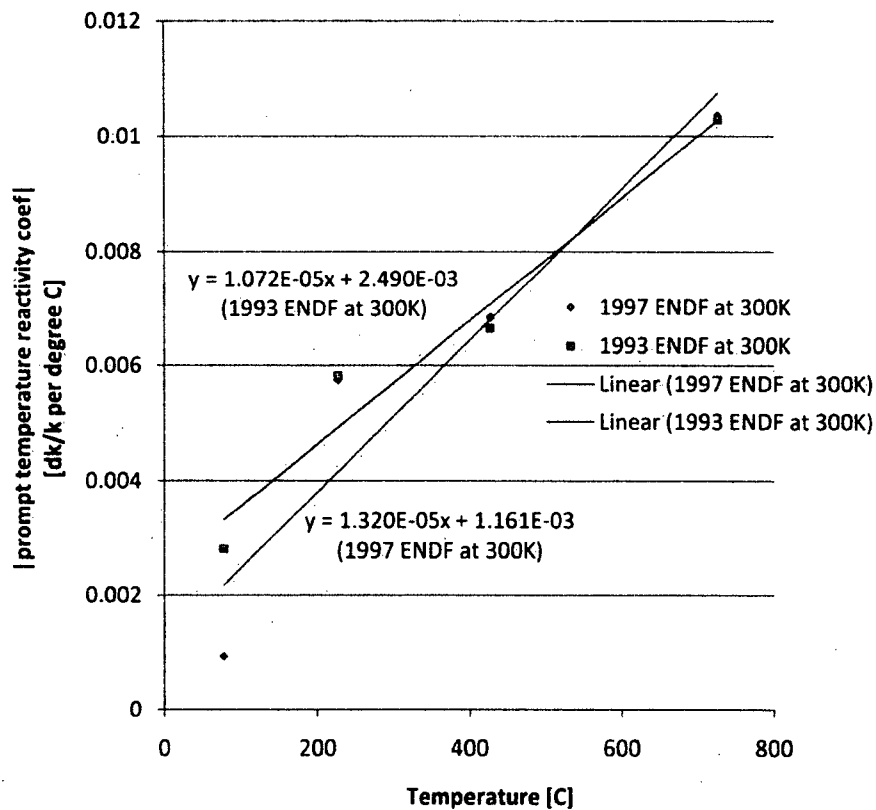


Figure A-1, Fuel prompt temperature coefficient

It is reasonable to expect that the low temperature data points for α_f for each core (BOL, MOL, EOL) would be similarly affected, and thus the LEU MOL ICIT core would remain the core with the most limiting pulse behavior. The increased magnitude of the best fit line results in smaller pulses for a given reactivity in the region that the OSTR operates.

One other change was identified. In CA SAR calculations, the average temperature of the fuel included the temperature of the gap and the clad. When using fuel temperature to determine the magnitude of temperature coefficient feedback, it is more accurate to consider the temperature of fuel only. An average including only the volume of the fuel tends to result in a higher spatially averaged fuel temperature which causes stronger prompt temperature feedback, thus resulting in smaller pulses for a given reactivity.

Pulse calculations were re-performed for the LEU MOL ICIT core with both of these issues corrected. Proper calculation of α_f and proper fuel temperature averaging both tend to result in smaller pulses for a given reactivity insertion. LEU ICIT core analysis results are given in section 4.7.10. Table 4-31 will be replaced as shown. Figures 4-78 through 4-80 will also be replaced with updated calculation results (new figures shown). The summary paragraph on page 96 will also be updated to reflect a new pulse reactivity insertion limit of \$2.30 which corresponds to a maximum temperature of 819°C.

Table 4-31 (Old) Summary of LEU MOL ICIT Pulse Behavior

LEU-MOL-ICIT Core Configuration Pulse Results Summary					
Reactivity Insertion [β]	1.50	1.75	2.00	2.25	2.50
Peak Total Core Power [MW]	1393	2636	4460	7276	10017
Prompt Peak Fuel Temperature [$^{\circ}$ C]	591	743	870	982	1082
Max. Thermocouple Temperature [$^{\circ}$ C]	490	608	707	794	872

Table 4-31 (New) Summary of LEU MOL ICIT Pulse Behavior

LEU-MOL-ICIT Core Configuration Pulse Results Summary					
Reactivity Insertion [β]	1.50	1.75	2.00	2.25	2.50
Peak Total Core Power [MW]	875	1910	3316	5087	7270
Prompt Peak Fuel Temperature [$^{\circ}$ C]	448	582	697	800	894
Max. Thermocouple Temperature [$^{\circ}$ C]	375	480	574	657	724

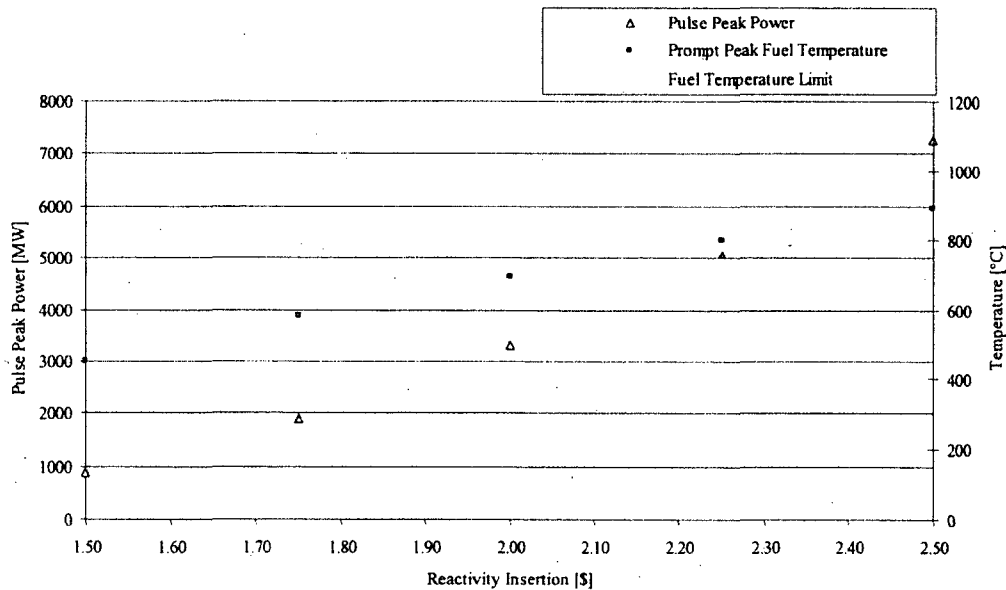


Figure 4-78, Pulse Summary (LEU MOL ICIT Core)

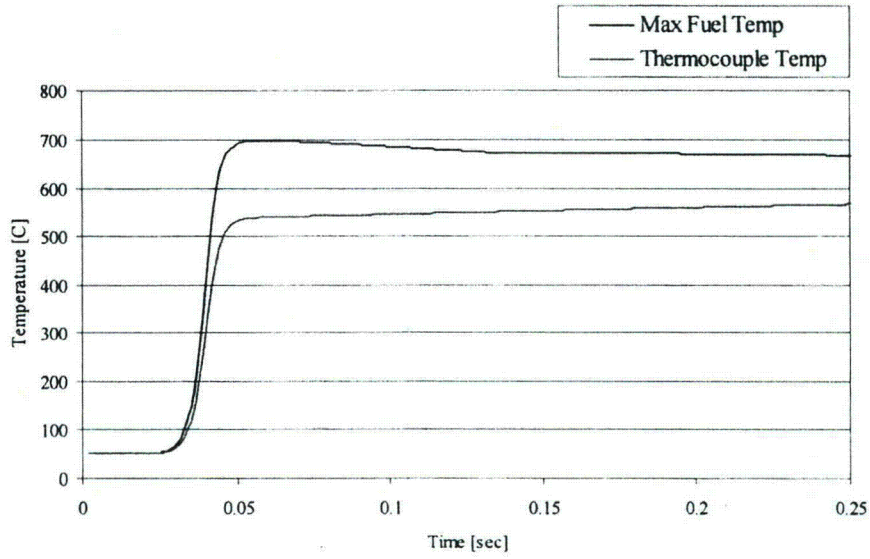


Figure 4-79 LEU MOL ICIT, Hot Channel Fuel Temperature (\$2.00 Pulse)

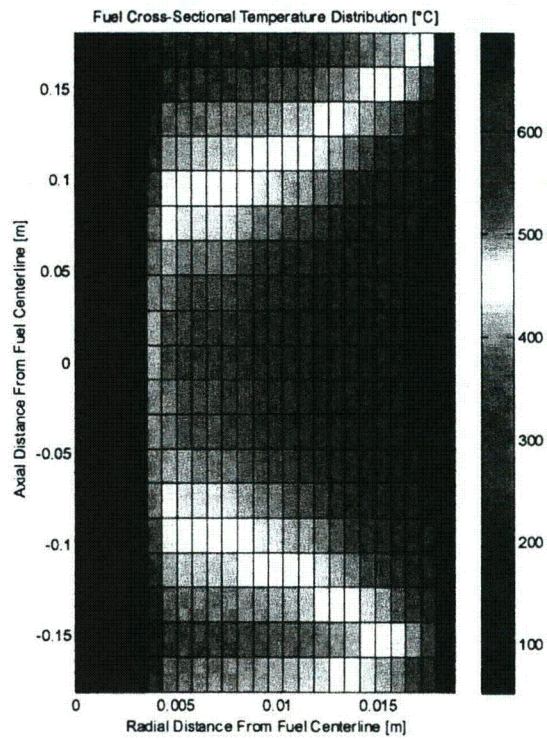


Figure 4-80 LEU MOL ICIT, Fuel Temperature Distribution at Time of Prompt Maximum Fuel Temperature (\$2.00 Pulse)

References

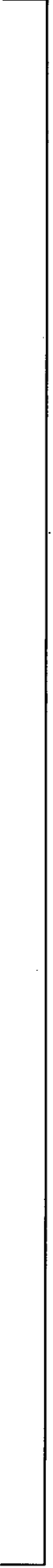
1. J.R. Liaw and J.E. Matos, "MNSR Flux Performance and Core Lifetime Analysis with HEU and LEU Fuels", 2007 International Meeting on Reduced Enrichment for Research and Test Reactors, Prague, Czech Republic, 23-27 September 2007.
2. Bretscher, M., " β_{eff}/l_p for Water Reflected Fresh Critical Cores of the Oak Ridge Research Reactor Reflected by Water," RERTR Program, Argonne National Laboratory, July 31, 1986.
3. Simnad, M., F. Foushee, and G. West, *Fuel Elements For Pulsed TRIGA Research Reactors*. 1975, General Atomics: Sandiego, CA.
4. Groeneveld, D.C., S.C.Cheng, and T. Doan, 1986 AECL-UO Critical Heat Flux Lookup Table. *Heat Transfer Engineering*, 1986. 7(1-2): p. 46-62.
5. Earl E. Feldman, *Fundamental Approach to TRIGA Steady-State Thermal-Hydraulic CHF Analysis*, ANL/RERTR/TM-07-01, December 2007.
6. INC., G.A.E.S., *Safety Analysis for the HEU to LEU Core Conversion of the Washington State University Reactor*, N.R. Commission, Editor. 2007, General Atomics: TRIGA Reactors Division of General Atomics-ESI. p. 1-112.
7. General Atomics Electronics Systems, Inc., "Safety Analysis for the HEU to LEU Conversion of the Washington State University Reactor", Report TRD 070.01002 RGE 001 Rev. N/C, Table 18, August 2007.

Attachment 2

Contains Proprietary Information

Withhold from public disclosure per 10 CFR 2.390

FACTS



Attachment 3

Reference 14

GA-C26016

**TRIGA REACTOR THERMAL-HYDRAULICS
STUDY STAT-RELAPS COMPARISON**

**Prepared Under
Contract DE-AC07-05ID14517**

**By Project Staff
A.R. Veca**

**GENERAL ATOMIC PROJECT 39293
DATE PUBLISHED: MARCH 2008**



TABLE OF CONTENTS

1.	INTRODUCTION.....	1
2.	CONCLUSIONS AND RECOMMENDATIONS	3
2.1	Conclusions.....	3
2.2	Recommendations	6
3.	SUMMARY OF FINDINGS	7
4.	BRIEF DESCRIPTION OF TRIGA REACTOR THERMAL HYDRAULICS.....	8
5.	DISCUSSION OF TASK 1: DEFINE REACTOR PHYSICAL DATA FOR THE TRIGA REACTOR TYPES THAT UTILIZE NATURAL CONVECTION COOLING	10
5.1	Overall Reactor Core Configurations and Geometries.....	10
5.2	Coolant Flow Area Configurations	10
5.3	Coolant Flow Inlet and Outlet Pressure Loss Coefficients	11
5.4	Axial Power Profiles	12
5.5	Reactor Pool Geometry.....	13
6.	DISCUSSION OF TASK 2: DETERMINE AVAILABLE EXPERIMENTAL DATA	14
7.	DISCUSSION OF TASK 3: COMPARE THERMAL-HYDRAULIC CORRELATIONS ..	16
7.1	Momentum Equation Formulation	16
7.2	Wall Friction Factor Correlations.....	17
7.3	Wall Heat Transfer Convective Correlations	18
7.4	Wall Heat Transfer Flow Boiling Correlations	19
7.5	Critical Heat Flux Correlations	20
8.	DISCUSSION OF TASK 4: PERFORM CALCULATIONS AND COMPARE RESULTS	22
8.1	STAT and RELAP Analyses Configurations	22
8.2	STAT and RELAP Thermal Hydraulics General Results	22
8.3	STAT and RELAP Thermal Hydraulics Off-Nominal Rod Results	23
8.4	STAT and RELAP Hot Rod Flow Rate versus Reactor Power	24
8.5	STAT and RELAP Hot Rod Flow Rate versus Inlet/Outlet Loss Coefficient	25
8.6	STAT and RELAP Hot Rod Maximum Wall Temperature versus Hot Rod Flow Rate.....	25
8.7	STAT and RELAP CHF versus Reactor Power.....	26
8.8	STAT and RELAP Hot Rod CHF versus Inlet/Outlet Loss Coefficient	29
8.9	STAT and RELAP Hot Rod CHF versus Hot Rod Flow Rate	29
9.	REFERENCES.....	30
	APPENDIX A: EVALUATION OF INLET/OUTLET LOSS COEFFICIENTS.....	A-1

LIST OF FIGURES

Figure 1a. WSU Core Configuration	35
Figure 1b. TAMU Core Configuration	36
Figure 1c. OSU Top Grid Plate Showing the Core Configuration	37
Figure 1d. MNRC (UC Davis) Bottom Grid Plate Showing the Core Configuration	38
Figure 2a. TAMU and WSU Rods and End Fittings	39
Figure 2b. OSU Rod and End Fittings	40
Figure 2c. MNRC Rod and End Fittings	41
Figure 3. Reactor Rod Axial Peaking Factors	42
Figure 4. TAMU Core Configuration Showing Measured Outlet Temperature Locations	43
Figure 5. Flow Rate Comparison	44
Figure 5. Flow Rate Comparison (Continued)	45
Figure 6. Bernath and McAdams Critical Heat Fluxes vs. Channel Velocity	46
Figure 7. Hot Rod Flow Rate vs. Reactor Power	47
Figure 8. Hot Rod Flow Rate vs. Inlet + Outlet Loss Coefficients	48
Figure 9. Max. Clad Temperature vs. Rod Flow Rate	49
Figure 10. Hot Rod CHF vs. Reactor Power	50
Figure 11. CHF vs. Inlet/Outlet Loss Coefficients	51
Figure 12. CHF vs. Rod Flow Rate	52

LIST OF TABLES

Table 1. TRIGA Reactor Core Physical Data	31
Table 1-A. TRIGA Reactor Core Physical Data – Metric Units	32
Table 2. STAT-RELAP Comparison Results	33
Table 2-A. STAT-RELAP Comparison Results – Metric Units	34
Table 3. Comparison of Bernath and Groeneveld 2006 CHF Predictions	35

1. INTRODUCTION

There are 40 TRIGA research reactors worldwide currently operating. Some of these reactors operate with highly enriched uranium fuel (HEU). As part of the Global Threat Reduction Initiative (GTRI), several TRIGA reactors in the United States are being converted from HEU to LEU. A review of the thermal hydraulic analysis methods used for TRIGA reactors has been recommended (Ref. 1) along with the HEU to LEU conversion program. This document is a response to that recommended review.

The steady state thermal performance and evaluation of the critical heat flux ratio (CHFR) of TRIGA reactors has been historically performed using the General Atomics STAT computer program. Reference 1 recommends comparing the TRIGA thermal hydraulic performance and the CHFR evaluation as predicted by STAT to the later developed RELAP code.

To accomplish this comparison, Reference 1 recommends that four specific tasks be addressed.

Task 1: Define Reactor Physical Data for the TRIGA Reactor Types That Utilize Natural Convection Cooling

Generate physical data needed to develop STAT and RELAP input models for the following TRIGA reactors that generally represent the total collection of TRIGA reactors:

- Washington State University (WSU)/University of Wisconsin (UWRR) – TRIGA conversions utilizing fuel in the form of uniformly pitched 4-rod clusters, 1 MW power
- Texas A&M (TAMU) – TRIGA conversion utilizing fuel in the form of non-uniformly pitched 4-rod clusters, 1 MW power
- Oregon State University (OSU) – single rods arranged in a mostly irregular regular circular lattice, 1 MW power
- UC Davis (McClellan Nuclear Research Center - MNRC) – single fuel rods arranged in a hexagonal lattice, 2 MW power.

Task 2: Determine Available Experimental Data for Bench Marking STAT and RELAP Calculations

The following TRIGA reactors have been suggested to ascertain if core outlet measurements exist and to secure these data:

- Torrey Pines – circular lattice
- TAMU – TRIGA conversion, square lattice
- OSU – standard TRIGA configuration, circular lattice
- MNRC (UC-Davis) – hexagonal lattice
- Pennsylvania State University
- Morocco

Task 3: Comparison of STAT and RELAP Thermal-Hydraulic Correlations

Task 4: Comparison of STAT and RELAP Predicted Reactor Thermal-Hydraulic Performance

Throughout the report, the phrase "thermal hydraulics" refers to the core flow (continuity), buoyancy and friction (momentum) and thermal behavior (energy). The fuel rod temperatures are not addressed. The critical heat transfer (CHF) calculation is not part of thermal hydraulics calculation. It follows the thermal hydraulic calculation and uses some of the thermal hydraulics results. Discussions of the CHF generally follow the thermal hydraulics discussions.

2. CONCLUSIONS AND RECOMMENDATIONS

2.1 Conclusions

The STAT code was developed in the mid-1960's specifically for TRIGA thermal hydraulic analyses. The code has simple, but developed from first principles, formulations for the steady state continuity, momentum, and energy equations. It also employs simple correlations for wall friction and wall heat transfer correlations. The code has built-in the Bernath and McAdams critical heat flux (CHF) correlations. STAT has been used for TRIGA analyses for over 35 years, and it seems to adequately predict conservative steady state performance.

RELAP has been an industry standard code for the analysis of power reactors. Its development and improvements have occurred over at least 25 years. The code performs steady state and transient reactor neutronics, thermal hydraulics and fuel rod thermal analysis. It allows for very general modeling – multiple rod and channel configurations and heat structures for rod thermal performance. The code has sophisticated single and two phase flow modeling both in its continuity, momentum and energy formulations, as well as for wall and interfacial friction and heat transfer correlations. The RELAP5 versions of the code have built-in the Groeneveld 1986 look-up table critical heat flux correlation.

RELAP has had considerable comparison with experimental data at high forced convection flow rates and reactor powers and pressures commensurate with commercial power reactors. Comparison with reactor performance data at TRIGA steady state conditions has been lacking.

Much of the current study is the comparison of STAT and RELAP results for four selected reactors: WSU, OSU, TAMU and MNRC (UC-Davis). The selection of these four reactors covers other TRIGA reactors identified for conversion.

Table 2* summarizes the results for the STAT and RELAP cases run for the four selected reactors. These results and all of the results presented are typical of the reactors studied. The following input parameters for each reactor are typical. These input parameters could easily change value for a specific reactor's current or future operation. The reported results could be different for those operational results.

Number of fuel rods

Radial and axial peaking factors and rod power axial shapes

Specific hot rod selected

Inlet/outlet form loss coefficients

Inlet temperature [taken here as 86°F (30°C)].

The main objective of the report is a STAT-RELAP comparison.

*Tables and figures are located at the end of the main body of the report (page 31).

For a given set of reactor conditions, STAT predicts channel flow rates lower than RELAP. The average of the flow differences for all of the computer runs is 12% at design power and 18% at 1.5 times design power. The WSU, OSU and TAMU reactors show slightly smaller flow rate differences between STAT and RELAP, and MNRC shows slightly larger flow rate differences.

Limited measurements of core outlet temperatures were made at the TAMU reactor. Temperature measurements were made at four locations and for reactor powers of 0.25, 0.50, 0.75, and 1.0 MW. Extracting channel flow rates from the data depended on DIFF3D calculations for the four rod powers surrounding each flow channel, the measured inlet temperature of 84°F and the assumption that the flow rate could be calculated from $Q=m*cp*\Delta T$. (At design power only the 2 MW MNRC reactor hot rod had a non-zero outlet void fraction equal to 0.0012. The heat for this net vaporization is 1.3% of the total hot rod heat.) Figure 5* shows the comparison for the four rod locations. A comparison between "measured" and STAT and RELAP predicted channel flow rates for the first three sets of data show that both codes over-predict the "measured" flow rates by 10% and 17%, respectively. This is slightly non-conservative.

Results for all of the STAT and RELAP computer runs done in this study show that at design powers or greater the wall heat transfer is sub-cooled nucleate boiling. This even holds true for the off-nominal runs – cases near core edges or near the interior of the core where fuel rods are adjacent to relatively larger bodies of water. Both codes illustrate that at reactor design powers all channels operate safely with moderate wall (clad) temperatures (260–290°F). The maximum wall (clad) temperature for a given reactor and conditions are within a few degrees for the two codes, with an average difference of approximately 4°F at design power and 9°F at a 50% higher power.

Each code calculates internally the fuel rod wall friction along the heated and unheated lengths. However, the user must supply inlet and outlet loss coefficients to represent the form losses of the bottom and top fuel rod fixtures. The flow at these two locations is disruptive consisting mostly of contractions and expansions. The calculation of these K losses carries uncertainties. These loss coefficients also depend on the particular fuel rod end fittings and the associated grid plates. These K loss coefficients were re-computed in this study for the particular fuel rod end fixtures illustrated in Fig. 2. This computation is discussed in Appendix A. The effect of the inlet/outlet loss coefficients on several thermal hydraulic parameters is summarized in Section 3. More detailed discussion is given in Section 5.3 and Appendix A. **The K loss coefficients presented are specific to each reactor and with the assumed end fixture geometries. The analyst of any reactor should re-calculate the loss coefficients for that reactor with its specific grid plates and end fixtures.**

*Tables and figures are located at the end of the main body of the report.

An important issue in TRIGA reactor safety is the maximum fuel temperature. As a result of the low clad temperatures with sub-cooled nucleate boiling, the maximum fuel temperature is more dependent on the clad-to-fuel gap and the fuel thermal conductivity rather than the coolant flow rate and the coolant boiling heat transfer coefficient. As a result, either STAT or RELAP may be used for the thermal hydraulics at design reactor powers. RELAP could also be used for the fuel rod temperatures. With STAT one has to calculate the fuel temperatures with some other thermal code.

A second important issue in TRIGA reactor safety is the critical heat flux ratio (CHFR) for the hot rod. The CHFR may be computed, at least, in two ways. The CHFR calculation is performed at the design power; i.e., the flow conditions at design power are used in the CHF correlation. The allowable maximum reactor power is the design reactor power times the CHFR. An alternate computation is to increase continuously the reactor power until the first observance of the ratio of a locally calculated critical heat flux (CHF) divided by its corresponding local wall heat flux equal to 1.0. The CHFR is this power divided by the design power.

The STAT code prints out the minimum CHFR calculated from the Bernath (Ref. 5) and the McAdams (Ref. 4) correlations following the code's thermal hydraulic calculations. Using these printed results, the user selects the results to apply – normally the minimum of the two. RELAP uses the Groeneveld 1986 lookup-table of CHF as a function of mass flux, sub-cooling (negative quality) and pressure (Ref. 6). Through RELAP input commands, the user can have the code print out the CHFR at selected axial locations.

The calculated CHFRs show the largest deviation between the two codes. Computing CHFRs using design power conditions, RELAP predicts, on the average, a CHFR 1.5 times the STAT McAdams prediction and 2.0 times the Bernath prediction.

When the second method is utilized, the sub-cooling becomes small ($<10^{\circ}\text{F}$). STAT limits the sub-cooling to a minimum of 11°F for determining vapor volumes (void fractions). This minimum is usually reached before the Bernath calculated local CHF divided by its corresponding local wall heat flux equals 1.0. RELAP has convergence difficulties before its calculated Groeneveld 1986 CHF divided by its corresponding local wall heat flux equals 1.0. This results because the 1986 Groeneveld correlation predicts a high CHF, which requires a high reactor power for the wall flux to equal the Groeneveld CHF. An alternative technique for this second method of predicting the CHFR is to run RELAP at various reactor powers. Utilizing RELAP's thermal hydraulic conditions at each reactor power, the CHF and CHFR can be calculate with the Bernath correlation. This appears to be a good compromise between the STAT/Bernath CHFR (too low) and the RELAP/Groeneveld CHFR (too high).

Figure 10 shows the STAT and RELAP calculated CHFR versus reactor power for the TAMU and MNRC reactors. The figure also shows the application of RELAP-Bernath approach. The first method of predicting the CHFR, using design reactor conditions, gives the CHFR values at

the left side of the plot. The second method gives the reactor power when the curves cross the line $CHF=1.0$. For this latter technique, both the STAT-McAdams and the RELAP-Groeneveld computer codes fail to achieve a converged solution before the $CHF=1.0$ line. The STAT/Bernath and the RELAP/Bernath achieve reactor powers for $CHF=1.0$ line. However, there is a difference in the results.

2.2 Recommendations

With all of STAT's simplicity, it conservatively predicted TRIGA's safety performance, as evidenced by 40 years of successful TRIGA operation.

Either STAT or RELAP could be used to evaluate the thermal hydraulic conditions at and near design reactor powers. There are small differences in the calculated values of the two codes for the two important variables flow rate and maximum clad temperature. The RELAP code is preferable because of its more sophisticated formulation of the basic conservation equations and constituent equations and correlations.

For the CHF it is recommended to use the method of increasing the reactor power until the first observance of the ratio of a locally calculated CHF divided by its corresponding local wall heat flux equals 1.0. Use RELAP to obtain the hydraulic conditions. The Bernath CHF correlation has been used in the past for TRIGA CHF's with apparent success. It is based on data from several sources, but some of the data is just beyond TRIGA flows and pressure conditions. The use of the Groeneveld 1986 CHF table look-up is not recommended because of its prediction of relatively high CHF's. Near the end of this study, Earl Feldman at ANL noted that a Groeneveld 2006 CHF correlation is available (Ref. 7). This correlation appears promising for application to TRIGA reactors. A critical review of CHF predictions at TRIGA conditions was not an objective of this report, and no review was performed. Reference 9 provides a current review of several CHF correlations, including the Bernath and Groeneveld 2006 correlations. Table 3 shows a comparison between the RELAP/Bernath and RELAP/Groeneveld 2006 CHF predictions.

With CHF correlations presently available, it is recommended to use RELAP for calculating the reactor thermal hydraulics. Then, outside the RELAP code, use the Bernath and the 2006 Groeneveld correlations for a CHF calculation, and select the minimum value. If possible, efforts should be made to examine more closely the basis of both the Bernath and 2006 Groeneveld predictions at TRIGA conditions.

3. SUMMARY OF FINDINGS

All STAT and RELAP runs in this study showed that the wall-to-bulk heat transfer is sub-cooled nucleate boiling, not convective heat transfer. One exception is the 0.25 MW run for the TAMU outlet temperature/flow rate study.

If pool boiling were to occur in low powered rods (very low flow velocities), heat transfer coefficients for sub-cooled pool boiling are equivalent to heat transfer coefficients calculated for sub-cooled nucleate boiling.

For the 1 MW design reactors (WSU, OSU and TAMU), neither STAT nor RELAP show any vapor void at the core outlet for the nominal power and 86°F inlet. For the 2 MW MNRC reactor, both codes show a small outlet void fraction (<1.5%).

For the 1 MW design reactors, hot rod channel Reynolds numbers range from 3500–500 and channel velocities range from 0.55–.65 ft/s. For the 2 MW MNRC reactor, the values are almost twice as much.

The inlet plus outlet K-loss pressure drop relative to the core total pressure drop is approximately 30–0% at design flow rates and 40–0% with inlet/outlet K's equal to two times their nominal values. The lower percentages are for reactors with relatively low K losses (MNRC), and the higher percentages are for reactors with relatively high K losses (TAMU, WSU).

At design power doubling the inlet/outlet K loss coefficients decreases the channel flow rate 10–5% (Fig. 8). Doubling the K loss coefficients decreases the CHF approximately 5–% at design powers (Fig. 11). Note, there is a larger variation of the CHF among correlations than there is with its variation with flow rate or K loss coefficients.

Changes in K's or channel flow rates have little or no effect on the maximum wall temperature (Fig. 9). The subcooled nucleate boiling heat transfer coefficient, h_{nb} , is little effected by flow rate, and h_{nb} is based on $(T_{wall} - T_{sat})$ and not T_{bulk} , i.e., $T_{wall} = Q/A_{wall}/h_{nb} + T_{sat}$.

Fuel rods near reactor edges or large areas of water have low maximum clad temperatures and low CHF's relative to the hot rod. Such rods still have sub-cooled nucleate boiling, and the lower channel flow rates effect little the rod CHF. The hot rod still dominates the safety issue. The hot rod surrounded by other hot rods has slightly lower CHF's as compared to a hot rod surrounded by non-fueled rods.

4. BRIEF DESCRIPTION OF TRIGA REACTOR THERMAL HYDRAULICS

To understand better the selection of the reactors for analyses and to address the thermal hydraulics of TRIGA reactors, it is appropriate to review the overall thermal hydraulic flow behavior of the TRIGA reactors.

The height by span size of the TRIGA core is of the order of 3 ft x 3 ft. The core is located near the bottom of a pool of water at a depth of approximately 25 ft. Typically, there is a 3- ft vertical distance between the core inlet and the bottom of the tank. The water depth to the core inlet gives an operating pressure of approximately 25 psia.

The core is cooled by an overall pool/reactor natural circulation flow loop. The driving pressure difference for this flow circulation is the difference in the density head between the cold pool water outside and adjacent to the core and the warmer flow through the core. In analyzing the thermal hydraulics of the core, one effectively isolates or draws a fluid "control volume" around the core. The flow through the core appears as a forced, low velocity flow (0.5-0 ft/s) with possibly local natural convection effects. The flow is not natural convection/free convection through the core. From an analyses point of view a low-head pump could just as well have produced the core flow.

The low velocity natural-convection-driven flow through the TRIGA reactor core raised some questions by the NRC reviewers during the TAMU SAR review. These questions generally regarded the applicability of the STAT correlations in these flow regimes. The reviewers also asked whether there were other data/correlations which have been developed since the STAT correlations which might be more comprehensive in the low flow regimes. Interest was also expressed regarding a comparison between the STAT code and the industry standard RELAP code.

The STAT code was developed in the mid-1960s specifically for TRIGA thermal hydraulic analyses. The code has simple, but developed from first principles, formulations for the steady state continuity, momentum, and energy equations. It also employs simple correlations for wall friction and heat transfer correlations. The code includes the Bernath and McAdams critical heat flux (CHF) correlations.

The STAT code allows for modeling one or two rods and the portion of the sub-channel communicating with these rods. For the reactor thermal analysis, STAT usually models the highest powered rod (highest rpf) for safety evaluation or an average rod (rpf=1) for overall core performance. Other rod/sub-channels configurations may be analyzed. STAT does not allow for flow mixing between adjacent flow channels, nor does STAT perform the fuel rod thermal performance. Flow channel mixing is usually not important for an average rod analysis, and generally non-conservative for a hot rod analysis.

RELAP has been an industry standard code for the complete analysis of power reactors. Its development and improvements have occurred over at least 25 years. The code performs steady state and transient reactor neutronics, thermal hydraulics and fuel rod thermal analysis. It allows for very general modeling – multiple rod and channel configurations and heat structures for rod thermal performance. The code has sophisticated single and two phase flow modeling both in its continuity, momentum and energy formulations, as well as for wall and interfacial friction and heat transfer correlations. Until recent code versions, the critical heat flux correlation was the 1986 Groeneveld look-up tables (Ref. 6).

RELAP has had considerably comparison with experimental data at high forced convection flow rates, reactor powers and high pressures. Comparison at TRIGA steady state conditions is not known.

5. DISCUSSION OF TASK 1: DEFINE REACTOR PHYSICAL DATA FOR THE TRIGA REACTOR TYPES THAT UTILIZE NATURAL CONVECTION COOLING

5.1 Overall Reactor Core Configurations and Geometries

The four TRIGA reactors selected for study in Ref. 1 generally represent operating TRIGA reactors. TRIGA reactors undergoing, or soon to undergo, the HEU-LEU conversion also influenced the selection of these four reactors. Comparative analyses using STAT and RELAP were performed for these four reactors.

Figure 1 shows the core configuration for the above four representative reactors. Table 1 gives the physical data needed to develop thermal-hydraulic models for the STAT and RELAP5 codes for the above listed reactors. (Table 1 is in British units, Table 1-A is in metric units.) Noted in Table 1 are dimensions for average channels, hot channels and other flow channel configurations deemed important to the study.

The table currently has rod/channel dimensional data primarily for the hot rod, since this is the rod of most interest. Generally when using STAT, a hot rod analysis is performed on a single rod or on a single rod with a second rod representing the average properties of surrounding rods.

With the TRIGA overall natural convection flow circulation, the channel flow rate is a function of rod heat input. A high heat input yields a high flow rate and a lower heat input yields a lower channel flow rate. Hot rods adjacent to cooler rods or adjacent to large flow channels could have lower channel flow rates. Concern here is that these lower flow rates might provide higher coolant temperatures, lower bulk-to-wall heat transfer coefficients and thus higher clad temperatures.

The STAT-RELAP comparison in Section 8.3 includes hot rods adjacent to cooler rods. Such analyses do not require different rod and flow geometries – their geometric input requirements are covered in Table 1.

Table 1 also includes rod configurations near core outer boundaries which have low flow conditions and inner rods adjacent to relatively large flow channels where a rod space has water only. Including the analyses of these "off-nominal" rod configurations allows comparing their thermal results with the often and solely used nominal hot rod configuration.

Sections 5.2 to 5.4 have discussions of several aspects of the Table 1 entries.

5.2 Coolant Flow Area Configurations

The TAMU reactor has two different rod cluster-to-rod cluster gaps: a 0.094 in. small gap (yielding a minimum flow area) and a 0.248 in. large gap (yielding a maximum flow area). The

rod-to-rod gap within a cluster equals 0.119 in. (yielding a nominal flow area). Core edge rods that face the core's straight sides have larger flow areas.

The WSU reactor has the same 0.119 in. rod-to-rod gaps within the cluster as with TAMU. However, the WSU rod cluster-to-rod cluster gaps are the same in both directions. Note the rod/channel dimensions of WSU are similar to the rod/channel dimensions of the TAMU nominal flow channel.

The MNRC (UC Davis) reactor core has a hexagonal rod pattern for each ring. This pattern yields rod/channel cells as isosceles triangles with a uniform pitch. The triangular rod pattern occurs uniformly throughout the entire core. The MNRC hexagonal core has a hexagonal shroud, leaving edge rods with relatively small water flow areas. (The round item in Fig. 1d is the upper grid plate, which hides the hexagonal core shroud. Since six corner rods are missing in the G-ring, the six corner points of the hexagonal shroud are cut. These corners are replaced by short straight sections, minimizing the open water channels at the edges.)

The OSU reactor is a circular core. Each ring of the core has rods arranged in a circle and uniformly spaced. This rod geometry yields some almost regular but mostly irregular rod/channel configurations. The rods in the B and C rings form either an (almost) regular triangular pattern or an (almost) regular square pattern. Rods in the outer rings generally form four sided rectangular cusps. The cusp size varies with location. Table 1 gives rod/channel dimensions for B-C ring rods (hot rods) in a triangular pattern and an E-F ring rectangular cusps (average rod).

5.3 Coolant Flow Inlet and Outlet Pressure Loss Coefficients

Important for model input are the upper and lower grid plate inlet and outlet flow loss coefficients (K values). Figures 2a through 2c show sketches of the reactor rods and rod end fixtures for each of the four reactors. Table 1 includes current inlet and outlet K values for the four reactors. Each inlet K value represents the summation of locally computed K values throughout the lower fixture; e.g., inlet from pool to grid plate hole, expansion from grid plate hole to region below the full rod and contraction into the full rod. Each outlet K similarly represents the summation of local K's within the top fixture. These local K values, and their sums for the total inlet/outlet loss coefficients, are tabulated in Tables A-1 through A-4 in Appendix A. As shown in these tables, uncertainty margin was added to some of the local K values as deemed appropriate.

It is important to note that the resulting K values in Table 1 are referenced to the flow area apportioned to a single rod (via area ratios squared). The local K values computed for flow passages within a fixture are based on the local flow area dictated by the local K correlation.

To compile the list of K values, some K values were reviewed from earlier SAR documents or previous STAT or RELAP analyses. New K values were re-computed for the current study. For

the most part, there is reasonable agreement between the previous K values and the recomputed K values. An exception is with MNRC. Table 1 lists the re-computed K values.

The computation of local K values requires a flow Reynolds number to determine whether the flow regime is laminar or turbulent. Hot channel flow rates and temperatures are used to compute local Reynolds numbers. The grid plates for the reactors WSU, TAMU and MNRC have essentially a uniform geometry across the core. Except for some local Reynolds number dependencies, the K values shown in the tables apply to most rods within the core.

The OSU reactor is an exception. The lower grid plate is not uniform across the core. This grid plate has no holes beneath each rod that feed water to the rods. Instead, in the inner half of the grid plate, circumferential slots and an array of smaller holes feed water to the rods above. The flow through the bottom fixture is two-dimensional. An approximation was made in an attempt to include this 2-D effect. The OSU K values given in Table A-2 apply to a triangular array of rods in the B-C rings; i.e., hot rods.

It appears the previous MNRC K values ($K_{in} = K_{out} = 7.95$) (Ref. 2) were based on a rod geometry that incorporated end fixtures that yield high K values. The end fixtures were comprised of flow regions that had abrupt changes in flow area from one region to the next within the fixture. (Furthermore, $K_{in} = K_{out}$ does not appear likely, and a Sandia MNRC analysis had $K_{in} = 3.58$ and $K_{out} 3.00$.) The current MNRC rods use end fixtures that have smooth flow area changes. Additionally, the MNRC rod flow area is generally less than the local flow areas in the top and bottom fixtures where the K values are originally calculated. Referencing the local K values to the rod channel flow area reduces the K value based on the rod channel flow area. This yields the low MNRC K values reported in Table 1.

The two reactors TAMU and WSU reactors generally have rod channel flow areas less than the local flow areas in the top and bottom fixtures. This geometry yields higher K values based on the rod flow area.

5.4 Axial Power Profiles

STAT frequently uses a chopped cosine axial distribution with tails to describe the rod axial power shape. Reference 8 gives an equation that provides this cosine shape. The equation requires the input parameters z_{extin} , g_e and ak for computing the axial power profile. These STAT input parameters are obtained by curve fitting the cosine and tails equation to a nucleonics derived rod power versus rod axial location. STAT also has the capability of using a series of five second-order polynomials to fit the nucleonics derived rod power profile.

With the RELAP code, the user provides as input a table of rod power at each axial segment of the rod heat structure.

Axial power shapes for the TAMU, WSU and OSU reactors are taken as cosine profiles with tails. Input values for the necessary parameters were obtained from information in previous reactor SAR's. These parameters are:

Reactor	ZEXTIN	GE	AK
WSU	17.5	0.90	45.0
OSU	20.54	0.30	50.1
TAMU	19.82	0.70	45.0

The value of HLIN, equal to the rod heated length, is also required for the profile equation. A previous RELAP model (Ref. 2) of the MNRC reactor used an axial power profile developed from a DIFF3 analysis. This profile is used in the STAT polynomial curve fit and RELAP input tables for MNRC.

Figure 3 shows the axial power shapes used for the four reactors.

The selection of these power shapes for each of the four reactors in this study is sufficient for a comparison study. However, these parameters or rod axial power input depend on the core fuel loading. New values should be computed for the precise fuel loading when an SAR or any reactor specific thermal analysis is performed.

5.5 Reactor Pool Geometry

The remaining input information in Table 1 relates to the reactor pool geometry. This information is use to calculate the pool pressure at the core inlet and to assign a flow area for pool water downflow for the RELAP model.

6. DISCUSSION OF TASK 2: DETERMINE AVAILABLE EXPERIMENTAL DATA

Several TRIGA reactor installations have measured core outlet temperatures under specific operating conditions. A reactor flow rate could be inferred from the predictive computer codes using the measured outlet temperature.

It was thought that temperature outlet data would be available from:

- Torrey Pines
- TAMU
- OSU
- MNRC (UC-Davis)
- Morocco

For core outlet temperature data to be useful, it is necessary that the core inlet temperature and the rod powers at the measured temperature locations are documented along with the outlet temperatures. Outlet temperatures were measured in the Torrey Pines reactor. Unfortunately, local rod powers were not reported. The TAMU reactor has limited but good data. No data was made available from the OSU reactor. No data exists from the MNRC reactor. The Morocco reactor was not operational at the time of this report.

The TAMU data consists of the measured reactor core outlet temperature at four specific locations in the core, Figure 4. Temperature data were taken at four reactor powers — 0.25, 0.5, 0.75, and 1.0 MW. The results of the DIFF3D analysis for the HEU to LEU conversion report were used to determine the average rod power for each of the four measurement temperature locations.

All STAT and RELAP computer runs showed no vapor void in the bulk flow. The local heat transfer regime is sub-cooled nucleate boiling except for the lowest reactor power and near the ends of the rods where the axial power factors are low.

Using the TAMU measured outlet temperatures, channel flow rates at the measured locations were calculated. The flow rate calculation depended on the DIFF3D four rod powers surrounding the flow channel, the measured inlet temperature of 84°F and the assumption that the flow rate could be calculated from $Q=m*cp*\Delta T$.

This latter assumption is supported by recording the outlet temperature as calculated by RELAP for TAMU powers from 1 to 3 MW. Outlet temperatures were then calculated outside of RELAP using MathCad. This calculation used the above simple heat balance equation, the RELAP reported rod powers and the stated inlet temperature. Calculations were performed at reactor powers from 1 to 3 MW. The re-calculated outlet temperatures agreed with the RELAP values within 0.1% at the lower powers and within 0.3% at 3.0 MW. (The RELAP outlet quality at the 3.0 MW run indicates the vapor evaporative heat is only 0.08% of the total rod heat.)

Figure 5 shows the comparison between results for the TAMU data and STAT and RELAP. Plotted are the calculated channel flow rates for the four measurement locations versus reactor power. The first data set shows good agreement between STAT and the data (except at 0.25 MW), and slightly higher flow rate predictions with RELAP. The next two data sets show both STAT and RELAP flow rate predictions higher than the data inferred flow rates (non-conservative). There appears to be something awry with the data measurements for the last data set.

Conclusion

The result of the flow comparison between the STAT and RELAP predicted flow rates and the TAMU flow rates from measured core outlet temperatures shows that the STAT and RELAP flow modeling is reasonable at reactor design powers. Fortunately, variations in the reactor flow rates have almost no effect on the hot rod maximum temperature and a minimal effect on the CHF

7. DISCUSSION OF TASK 3: COMPARE THERMAL-HYDRAULIC CORRELATIONS

7.1 Momentum Equation Formulation

For TRIGA reactors the momentum equation expresses the balance between the driving buoyancy force and the resistive and acceleration forces. The buoyancy force is the difference in the density heads of the external pool and the core. The resistive forces are the channel inlet and outlet form losses (K losses) and the channel wall friction. The acceleration forces occur at the core inlet from the pool and velocity increases in the heated portion of the fuel rod.

STAT employs a single, one dimensional (z-direction) momentum equation to represent both single phase liquid flow and two phase liquid-vapor flow. For two-phase flow STAT computes a local vapor volume and a void fraction. The local mixed specific volume (density) is computed from this void fraction assuming no vapor bubbles that are generated detach from the wall. The STAT user, via input, may include a non-zero vapor detachment fraction. This factor enhances the buoyancy of the bulk flow. Results in Sect. 8.1 show that a non-zero value yields results more in line with RELAP results. A vapor detachment fraction equal to 0.3 has been used in this comparison study; however a value of 1.0 gives flow rate results closer to RELAP flow rates.

The STAT calculation of the local vapor volume, and subsequent void fraction, is a function of sub-cooling and wall heat flux. A table of void volume versus sub-cooling and heat flux was constructed from data by Jordan and Leppert (Ref. 3). This two-dimensional table look-up returns the vapor volume. The table is limited to sub-cooling temperature differences greater than 11°F; i.e., subcooling cannot be less than 11°F. If this limit is encountered, STAT uses the vapor volume at 11°F. The output file prints a warning, and the run continues. This procedure is conservative, since extrapolated vapor volumes, and void fractions, would be larger than values at 11°F. At design reactor powers and slightly higher this limit is not reached.

For setting up the momentum equation formulation in RELAP, the code first determines if vapor generated at the wall leaves into the main stream. This is accomplished by correlations that partition the wall heat flux into a convective portion and a boiling portion. If the wall heat flux is low enough, vapor may form at the wall but not detach into the main stream. At higher heat fluxes vapor enters the main flow stream.

When no vapor exists, RELAP uses a single momentum equation to represent the single phase. If vapor exists, RELAP uses a two-momentum equation model. One equation applies to the liquid phase and one equation applies to the vapor phase. Wall and vapor shear (and heat transfer for the energy equations) are accounted for in both equations.

Conclusion

RELAP has a more sophisticated momentum equation model than STAT. For all of the TRIGA reactor cases run in this study, STAT predicts a lower flow rate as compared to RELAP. This difference has not been resolved. It is relatively easy to verify a STAT flow prediction with an external calculation by examining the STAT output. In RELAP this is not the case. Since RELAP considers two momentum equations with shear interactions between wall and vapor, and comprehensive correlations for void fraction and friction factors, there is not enough output information to replicate the calculation. Although this difference in flow rate exists between the two codes, Sections 7.4 and 8.8 show that a precise calculation of flow rate is not a necessity for a safety evaluation of the TRIGA performance.

7.2 Wall Friction Factor Correlations

The wall friction factor influences the prediction of channel flow rate. Since the channel flow rate results from a balance between the density head and friction forces, the methodology for calculating wall friction is reviewed.

For non-boiling single phase STAT uses the simple turbulent flow correlation $0.079/Re^{0.25}$ (Fanning friction factor). This correlation is valid down to a Reynolds number of about 4000, and possibly lower values, where the transition region exists for a wall roughness appropriate to commercial tubes. The turbulent correlation is not appropriate at Reynolds numbers below 3000. However, its use below 4000 is conservative – higher friction factors (but not below about 1200 when the laminar friction factor is higher). STAT uses no transition to a laminar flow friction correlation.

STAT uses a different friction factor correlation when boiling occurs. STAT utilizes the single phase relationship between the friction factor and the heat transfer coefficient j factor, namely $f/2 = j$ where j is the Stanton number equal to $Nu/Re \cdot Pr$. Rearranged this leads to $f = 2 \cdot h / (\rho \cdot c_p \cdot V)$. The heat transfer coefficient h is the calculated sub-cooled nucleate boiling heat transfer coefficient. Reference 3 presents this relationship between f and j for sub-cooled nucleate boiling.

For single-phase flow RELAP uses a correlation similar to a Colebrook turbulent flow correlation. (The above single phase STAT correlation follows the Colebrook correlation between Reynolds numbers from 3000 to 10^5 .) RELAP uses the simple correlation $f = 64 / (Re \cdot \phi_{sub,s})$ for the laminar flow regime (Moody friction factor). This correlation is for round tubes only – the hydraulic diameter concept does not apply for laminar flow. RELAP also calculates a friction factor in the flow transition region. The code connects the laminar flow friction factor at $Re=2200$ to the turbulent flow friction factor at $Re=3000$ via a straight line.

RELAP uses a very extensive method for calculating the friction factor when boiling occurs. It follows along the lines of the Martinelli two-phase friction factor multipliers. RELAP also uses a partitioning of the wall friction factor between the liquid phase and the gas phase.

Conclusion

The methodology for calculating single-phase friction factors are essentially identical in the two codes. However, for two-phase flow RELAP has a more sophisticated methodology as compared to STAT. The difference in methodology for calculating the two-phase friction factor could be part of the reason for the difference in flow rate predictions. This may be especially true at higher reactor powers where there are larger vapor fractions.

7.3 Wall Heat Transfer Convective Correlations

The convective heat transfer regime is not an important regime for TRIGA reactors. For the hot rod this regime might occur at reactor powers less than about 0.25 MW. For rods with low rpf's it may occur at slightly higher reactor powers. If convective heating is encountered, the wall temperature goes above the saturation temperature ($\approx 235^\circ\text{F}$) and sub-cooled nucleate boiling initiates.

For all cases run for this study with the different reactors, rod-flow geometries and reactor powers both STAT and RELAP show that TRIGA reactors operate in the sub-cooled nucleate boiling regime. The subcooled nucleate boiling heat transfer coefficient supersedes the convective heat transfer coefficient. Forced convection or natural convection heat transfer regimes are not encountered in TRIGA reactors.

The comparison between the TAMU measured outlet temperatures and the predicted temperatures produced the only exception to the above statement. The data at the group of the lowest powered rods and at 0.25 MW reactor power had convective heating only for a short distance at the beginning of the heated rod.

A brief description of the convective wall heat transfer correlations given in STAT and RELAP follows.

Typical Reynolds numbers for the TRIGA reactors at 1 MW are 3500–8500 for the hot rods. Flow channels at the reactor outer boundaries where rod powers are lower and flow areas are larger can have flow Reynolds number in the 2500–3000 range.

The STAT and RELAP codes both use the Dittus-Boelter correlation for calculating the forced convection turbulent flow heat transfer if this convective condition were to occur in a core flow channel. The Dittus-Boelter correlation is generally applicable down to a Reynolds number of about 4000. Below this Reynolds number the typical transition region occurs. However, turbulence at the inlet to the fuel rod (lower reflector section) from the region between the rod and the lower grid plate could lower the applicability of the correlation to as low as 3000.

For convective heat transfer, local natural convection along the heated walls could effect the forced convection heat transfer coefficient. The ratio of Grashof number to Reynolds number squared is indicative of the local natural convection effect. The Gr/Re^2 ratio for TRIGA reactors is in the range of 0.3–0.8. These ratios suggest local natural convection could occur when convective cooling occurs. With subcooled nucleate boiling the question is mute.

Conclusion

Convective cooling of fuel rods in TRIGA reactors is not sufficient to keep the rod wall temperature below the saturation temperature ($\approx 235^\circ\text{F}$). Subcooled nucleate boiling is the predominant mode of rod cooling in TRIGA reactors.

7.4 Wall Heat Transfer Flow Boiling Correlations

At design powers, and even as low as 25% of design powers, TRIGA reactors operate with the wall heat transfer regime as sub-cooled nucleate boiling. Since the wall heat flux is fixed locally, forced or natural convective heat transfer correlations predict wall temperatures significantly greater than the bulk flow saturation temperature. Both the STAT and RELAP show that local sub-cooled nucleate boiling then occurs, producing very moderate wall temperatures.

STAT uses a correlation by McAdams (Ref. 4, pg. 392, Fig. 14-22) for its evaluation of a sub-cooled nucleate boiling heat transfer coefficient. The McAdams correlation is based on sub-cooled data at low pressures (30–90 psia) and low water velocities (1–12 ft/s). The TRIGA reactor operates at pressures and flow velocities at the low end and slightly below the low ranges of the correlation. When necessary, extrapolation beyond the range of the McAdams data is minimal. Use of the correlation should be appropriate. The McAdams correlation applies to sub-cooled nucleate boiling, but not to saturated (bulk) boiling.

RELAP uses the Chen correlation, which covers a wide range of boiling conditions. It has fair applicability at low pressures and low water velocities. If the subcooling diminishes to zero, RELAP switches from a sub-cooled boiling correlation to a saturated pool boiling correlation.

For flow in core regions where large cross-sectional flow areas exist (edge of cores) low cooling water velocities may exist. These are regions typically of low rod power and sufficient water availability for high degrees of subcooling and low outlet temperatures. (See Table 2 for the OSU G-Ring and TAMU side rod runs.) Pool boiling correlations may be more appropriate than the forced convection sub-cooled nucleate boiling correlations used. For these conditions, separate calculations show that wall-minus-saturation temperature differences calculated for sub-cooled pool boiling are comparable to wall-minus-saturation temperature differences for sub-cooled nucleate boiling.

Conclusion

The flow boiling heat transfer correlation is important in determining the clad wall temperature (with a locally fixed wall heat flux). Results in Section 8.2 show that the predicted wall

temperature by STAT and RELAP are quite close, and of the order of 50°F higher than the cooling water saturation temperature (of the order of 230°F). Either correlation appears appropriate for TRIGA reactors at design powers, below design powers and above design powers that are comfortably below burnout where the heat transfer is still to saturated conditions.

7.5 Critical Heat Flux Correlations

The calculation of the critical heat flux (CHF) in each code is performed after the thermal hydraulics analysis. These correlations utilize several of the thermal hydraulic results, such as velocity or mass flux, system pressure or saturation temperature, bulk flow temperature or quality, and flow channel geometry.

Appreciable CHF data reside in the literature; however, most of the data apply to power reactors – high pressures and high flow velocities. STAT uses both a McAdams and a Bernath correlation for evaluating the critical heat flux, and thus the critical heat flux ratio (CHFR). The McAdams correlation (Ref. 4, pg 392, eq. 14-6) is based on limited data with water at low pressures, mostly 60 psia, and relatively low velocities: 1, 4 and 12 ft/s. The data show a diminishing critical heat flux with decreasing velocity from 4 ft/s to 1 ft/s. McAdams' correlation fits his data well. In constructing the correlation, McAdams assumed, and used, a zero heat flux at zero velocity. (Before zero velocity is attained, pool boiling would occur, and the CHF would not be zero.)

The Bernath correlation (Ref. 5) uses several independent databases. These databases include the McAdams data and low pressure Columbia University data (1956), as well as other data with water and other coolants. Most of the other data is at higher pressures (some low mixed within) and low-to-high velocities. The Columbia data are at 15–30 psia and 6–25 ft/s. The Bernath correlation agrees reasonably well with the McAdams data (except for the low critical heat fluxes at 1 ft/s), the Columbia data, and some of the other water data at high pressure and low velocity. Bernath looked at a 36 point data set by Gunther (1951) with pressures 14.7–115 psia and velocities 5–12 ft/s. Bernath's correlation agreed reasonably well ($\pm 20\%$) with approximately 35% of the data. Bernath quotes that the remaining data exhibited much scatter, and chose not to use any data.

RELAP utilizes a large look-up table of critical heat flux as a function of system pressure, channel mass flux (lbm/s-ft^2) and vapor quality (negative values for sub-cooled liquid). Groeneveld compiled the table in 1986 (Ref. 6), and then with an update in 1995. The table is very extensive, covering pressures and mass fluxes typical to light water reactors. The table does extend to low pressures and mass fluxes found in TRIGA reactors; however, the estimate of the data accuracy at these conditions is suggested uncertain (Groeneveld 1995). Several correlations, and not direct data, were used to construct the table in this low pressure, low velocity region.

After extracting a CHF value from the Groeneveld table, the value is modified by several factors (K values) appropriate to the specific applications; e.g., rod channel flow, hydraulic diameter, void fraction and channel orientation. For TRIGA reactors these k values are either 1.0 or slightly less. The multiplicative product of the factors is around 0.7 (RELAP output), reducing the table critical heat flux value.

The Groeneveld correlation generally yields an appreciably higher CHF (approximately 60% higher) than the Bernath correlation.

It is instructive to examine the applicability of the Bernath and McAdams correlations at TRIGA velocities; i.e., at and below 1.0 ft/s. Figure 6 shows a plot of the critical heat flux versus flow velocity for subcooling values of 80°F and 100°F (typical TRIGA sub-cooling at design power CFHR calculation). The plot shows that the McAdams correlation decreases continually with decreasing velocity, and then quite rapidly at velocities below 0.5 ft/s. TRIGA velocities are in the range of 0.55–0.65 ft/s at design power and 0.75–1.0 ft/s when the reactor power is increased to achieve CHFR=1.0. In these TRIGA velocity ranges, the Bernath correlation predicts lower CHFs than the McAdams correlation, which is conservative. Only below a velocity of 0.3 ft/s does the McAdams correlation dip below the Bernath correlation.

In the comparison of TAMU measured outlet temperatures with STAT and RELAP predictions (Section 6), the data were taken at low reactor powers (0.25–1.0 MW) and in core regions with lower rpfs relative to peak rpfs. Channel flow velocities were in the range of 0.25–0.5 ft/s. In all STAT runs in this comparison, the McAdams CHF was lower than the Bernath CHF.

Near the end of this study, Earl Feldman of ANL indicated a 2006 Groeneveld CHF correlation is available (Ref 7). Reference 9 provides a current review of several CHF correlations, including the Bernath and Groeneveld 2006 correlations. Earl Feldman of ANL provided CHFRs for the four study reactors using the Groeneveld 2006 correlation and the method of increasing reactor power until the CHFR=1.0 (Ref. 10). These values are given in Table 3 along with the corresponding RELAP/Bernath CHFRs.

Conclusion

Lacking other CHF data or reliable correlations for TRIGA conditions at this time, it may be prudent to calculate the CHF for the Bernath and 2006 Groeneveld correlations and use the minimum value. The method of increasing the reactor power until the local wall heat flux equals the calculated CHF is recommended.

8. DISCUSSION OF TASK 4: PERFORM CALCULATIONS AND COMPARE RESULTS

8.1 STAT and RELAP Analyses Configurations

STAT and RELAP models were constructed to represent the geometry and thermal conditions of the entries in Table 1. Table 2 summarizes the results of the total cases run for the four study reactors. Most cases apply to a single hot rod and associated flow channel, since a hot rod usually produces the limiting thermal conditions. For WSU, OSU and TAMU the cases are at the design reactor power (1 MW) and a higher power (1.5 MW). For MNRC the design power is 2 MW, and the higher power was chosen as 2.5 MW. Cases were also run for the WSU, TAMU and MNRC hot rods with adjacent rod(s) having a 10% lower rpf.

A few cases of "off-nominal" cold rods were run. One case for the OSU reactor models a rod in the G-ring having a low power factor and adjacent to a graphite rod and the core barrel – assumed zero power for both. This configuration is a low powered rod adjacent to a relatively large water channel and relatively high unheated wall area, contributing to low buoyancy and low flow rate. Two cases for the TAMU reactor model rods adjacent to the graphite side reflector forming the side of the core. One case looks at the highest powered rod along the reactor side (5F3) and surrounded by significant water. This rod is also adjacent to the next highest powered rod along the reactor side (5F2). The second TAMU case looks at a very low powered rod (2F3), which is in the corner of the core and adjacent to water. A TAMU case was also run for interior rods adjacent to the large water column at core location 3D. This last case represents medium-to-high powered rods adjacent to a very large water flow area.

STAT models are limited to one flow channel and two rods. If more rods of different powers are involved, the rod powers of several rods are averaged into a geometry with only two rods. Typically, the rod of interest is selected as one of the STAT rods, and the remaining rods are averaged into the second STAT rod.

RELAP has the capability to model many separate rods and flow channels. However, the RELAP model developed contained only two separate rods, but allowed each rod to have only one coolant channel. When necessary, a similar averaging of rod powers is done as with STAT.

8.2 STAT and RELAP Thermal Hydraulics General Results

Table 2 summarizes the output from the runs performed using STAT and RELAP. The table shows the agreement and disagreement between the two codes. In general, the agreement is good. STAT tends to predict a lower channel flow rate (conservative). The average of the flow differences for all of the runs at design power is 12% and 18% at 1.5 times the design power.

Maximum wall temperatures at these conditions are within a few degrees for the two codes, with an average difference of approximately 4°F at design power and 9°F at the higher power. The CHF Rs show the largest deviation. On the average RELAP predicts a CHF R 1.5 times the

STAT McAdams prediction and 2.0 times the Bernath prediction. (The RELAP CHFRRs are from the built-in Groeneveld 1986 correlation.)

Conclusion

STAT predicts lower channel flow rates relative to RELAP. The associated channel outlet temperature, flow velocities and flow Reynolds numbers reflect this trend.

Results for all of the computer runs at design power or greater show that the wall heat transfer is sub-cooled nucleate boiling. This even holds true for the off-nominal runs. Both codes illustrate that at reactor design powers all channels operate safely with moderate clad temperatures (260–290°F).

8.3 STAT and RELAP Thermal Hydraulics Off-Nominal Rod Results

The first set off-nominal cases in Table 2 are with low powered rods and larger flow channel areas. The OSU reactor has a G-Ring rod facing the core shroud.

The TAMU reactor has a side rod, a corner rod, and a group of interior rods with moderate powers facing a large water column.

The flows in these channels are in the laminar-turbulent transition region and in the fully turbulent region ($2500 < Re < 10000$) and with low velocities (0.2–0.3 ft/s). If a convective, versus sub-cooled boiling, flow were to exist in these low flow regions, local wall natural convection would occur. Either the low transition region or natural convection would yield relatively low wall heat transfer coefficients. These low wall heat transfer coefficients would then produce high rod wall temperatures (700–1000°F) since the rod heat flux is fixed. When the wall temperature rises a few degrees above the flow saturation temperature, subcooled nucleate boiling occurs. A high heat transfer coefficient and a low wall temperature would then result.

Interestingly, even though the maximum heat flux of an off-nominal rods may be one-half of the maximum heat flux of the hot rod, the maximum clad temperature of the off-nominal rod is only 5-10°F less than the hot rod. This is because with sub-cooled nucleate boiling, the wall heat flux is related to $(T_{wall} - T_{sat})^n$ where the exponent n is between 3-4. (Note, T_{wall} is referenced to T_{sat} not T_{bulk} .) Inverting the Q/A vs $(T_{wall} - T_{sat})$ equation gives $(T_{wall} - T_{sat})$ proportional to $(Q/A)^m$, where m is between 0.25–0.33. Changes in Q/A are muted for the corresponding change in $(T_{wall} - T_{sat})$.

In spite of the low flows, or velocities, Table 2 shows that these off-nominal cases have moderate clad temperatures and high CHFRRs.

The TAMU case of the rods at core location 3D and adjacent to the large water column exhibits the same conditions as above. The flow Reynolds number is larger (≈ 9000) due to the large hydraulic diameter ($Re = G \cdot dh / \mu$), but the flow velocities are still less than 0.3 ft/s.

In these above channel configurations with large flow areas and low water velocities, the subcooled nucleate boiling may be closer to pool boiling and not flow boiling. Surprisingly, subcooled pool boiling produces heat transfer coefficients, and wall temperatures, not far from the subcooled flow boiling results. Saturated pool boiling heat transfer coefficients may be on the low side. However, a sub-cooling of 50°F doubles the saturated heat transfer coefficient and a subcooling of 100°F triples the saturated heat transfer coefficient. This multiplying gives good heat transfer coefficients for subcooled pool boiling. The subcooling in the low flow channels analyzed above is considerable (>100°F).

In this group of off-nominal runs, hot rod configurations where adjacent rods have slightly lower critical heat flux ratios have also been included. These cases posed some concern that lower rpf rods adjacent to the hot rod might reduce the channel flow rate and cause higher clad temperatures and lower CHF_Rs. Runs were done for WSU, TAMU and MNRC to investigate this condition.

Adjacent rod rpf's were reduced by 10% from the hot rod rpf – typical rpf difference between hot rod and adjacent rods. The results in Table 2 show that indeed the channel flow rate is diminished, but only slightly. Additionally, the CHF_Rs are increased by a minute amount.

Conclusion

Off-nominal rods provide more safety margin than hot rods. The maximum clad temperature is below the maximum clad temperature of the hot rod, albeit by only 5–10°F. The CHF_Rs are considerably higher than the hot rod CHF_Rs. Slightly lower powered rods adjacent to hot rods almost insignificantly effect the maximum clad temperatures and CHF_Rs – and the results are in a favorable direction.

8.4 STAT and RELAP Hot Rod Flow Rate versus Reactor Power

Figure 7 shows the STAT and RELAP predictions of hot rod flow rates versus reactor power for the TAMU and MNRC reactors (cluster and hexagonal rod configurations). As indicated in Section 7.1, STAT input may include a non-zero vapor detachment fraction (vdf), which enhances the buoyancy of the bulk flow. Figure 7 contains three curves for STAT with different values of the vapor detachment fraction – 0.0, 0.3 and 1.0. The RELAP hot rod flow rate increases monotonically with reactor power. The STAT curves in Fig. 7 show that a non-zero value of vdf yields results more in line with RELAP results. A vdf value of 0.3 has been used for the STAT runs in this study. (A vdf value equal to 1.0 might be justified according to RELAP flow rates.)

RELAP shows no net vapor generation for the hot rod until a reactor power of 1.5 MW for the TAMU reactor. RELAP output indicates the MNRC reactor initiates vapor at 2.0 MW (outlet void fraction equal to 0.0015). STAT shows vapor generation for the hot rod for TAMU at 1.0 MW and for MNRC at 2.0 MW.

As the reactor power increases, the predicted flow rates of the two codes further diverge. This divergence may be due to the significant differences in the momentum equation modeling and/or wall friction between the two codes (Sections 7.1 and 7.2).

Conclusion

Figure 7 shows that the STAT predicted flow rates are more conservative than the RELAP predictions. Is STAT too conservative and is RELAP reasonable? TRIGA measured output temperature data possibly would be helpful in resolving this issue. Fortunately, a precise calculation of the flow rate is not a necessity for an accurate safety evaluation of the TRIGA performance. With subcooled nucleate boiling, the calculated clad temperature is little affected by the channel flow rate. The channel flow rate does affect the CHF, but it is not a strong effect as indicated in Section 8.8. There is a larger variation of the CHF among correlations than there is with its variation with flow rate.

8.5 STAT and RELAP Hot Rod Flow Rate versus Inlet/Outlet Loss Coefficient

As indicated in Section 5.3, the specification of the inlet and outlet loss coefficients has some uncertainty. The values of the loss coefficients can directly affect the channel flow rate. Figure 8 shows a plot of the hot channel flow rate as a function of loss coefficient for each of the reactors at their design powers (TAMU, WSU and OSU 1MW and MNRC 2 MW). The plot actually shows a normalized flow rate (flow rate at increased loss coefficients divided by flow rate at nominal loss coefficients) versus a normalized loss coefficients ($K_i + K_o$ divided by the sum of the nominal $K_i + K_o$). A normalized loss coefficient of two means the inlet and outlet loss coefficients are each twice their nominal values.

For the WSU and TAMU reactors with relatively large loss coefficients ($K_i + K_o = 3.40$ and 2.94 , respectively), doubling the loss coefficients decreases the flow rate by 13%. For the MNRC reactor with relatively small loss coefficients ($K_i + K_o = 1.13$), doubling the loss coefficients decreases the flow rate by 8%.

The plot in Fig. 8 was generated using the STAT code. Similar results would be expected using the RELAP code, since the flow rates refer to design powers where the two codes predict similar flow rates.

Conclusion

In view of the relatively small effect of K losses on the flow rate, it appears reasonable to add margin to the K loss coefficients. Some margin was added to the loss coefficients used in this report, as shown in Appendix A. More importantly, the analyst who performs a TRIGA reactor thermal analysis should verify the geometry of the bottom and top grid plates and end fixtures, and perform their own calculation of the reactor's inlet and outlet loss coefficients.

8.6 STAT and RELAP Hot Rod Maximum Wall Temperature versus Hot Rod Flow Rate

As previously discussed, two important items determining reactor safety are the maximum fuel temperature and the CHF. The maximum fuel temperature is dependent on the wall maximum

heat flux, the clad temperature, the fuel-to-clad gap thermal conductance, and the fuel thermal conductivity. It is pointed out in Section 8.2 that the maximum wall (clad) temperature varies little as thermal hydraulic parameters change because the wall-to-fluid heat transfer is via sub-cooled nucleate boiling. With the sub-cooled nucleate boiling, the wall-to-saturation temperature differences are small.

Figure 9 shows the effect of the hot rod flow rate on the maximum wall temperature for the TAMU (design 1 MW) and MNRC (design 2 MW) reactors. The abscissa shows normalized flow rates – an actual flow rate divided by the reactor design (nominal) flow rate. The range of the normalized flow rate is approximately plus 50%/minus 30%. This range of flow rates was obtained by varying only the inlet and outlet K losses. Thus, Fig. 9 represents the effect of wall temperature with other independent parameters, such as axial heat rate, inlet temperature and pressure held constant.

Figure 9 shows results for both STAT and RELAP. The sub-cooled nucleate boiling correlation used in STAT is not a function of channel flow rate. Thus, the clad maximum temperature curves for STAT are straight lines. The RELAP curves show a less than 1°F change over the flow rate range. (The reason for the maxima in the RELAP curves was not pursued because the RELAP wall heat transfer correlation is quite complex – see Section 5.4.)

Conclusion

Figure 9 results emphasize that the wall heat flux and sub-cooled nucleate boiling heat transfer coefficient essentially set the maximum wall temperature. The boiling heat transfer coefficient is sufficiently large so that the wall temperature is of the order of 50°F above the saturation temperature, and varies little from this value. The maximum fuel temperature is more dependent on the fuel-to-clad gap and the fuel thermal conductivity.

8.7 STAT and RELAP CHF versus Reactor Power

The critical heat flux ratio, CHF_R, indicates the margin of safety between the reactor design power and the reactor power for which the departure of nucleate boiling (DNB) occurs. The wall heat flux at DNB is the critical heat flux (CHF). The critical heat flux ratio, CHF_R, is the ratio of this DNB (equally the CHF) divided by the wall heat flux at the reactor design power.

The calculation of the CHF_R is performed after the thermal hydraulics calculations are completed. It is a locally axial calculation. The CHF calculation typically uses at least several of the following thermal hydraulic parameters at the specified axial location:

- Mass flux G - or velocity
- Water bulk temperature
- Water saturation temperature - or saturation pressure
- Water subcooling – ($T_{sat} - T_{bulk}$) or quality
- Water pressure

Additionally, the CHF may use channel geometric parameters; e.g., rod bundle geometry, hydraulic diameter and/or heated length to the specified axial location.

Using the built-in CHF correlations of each code (STAT – Bernath and McAdams, RELAP – Groeneveld 1986), each code calculates the critical heat flux (CHF) at axial locations using the channel thermal hydraulic conditions at that axial location. Each code then calculates a local CHF as the ratio of the local CHF divided by the local wall heat flux. STAT calculates this CHF for Bernath and McAdams at every axial position. STAT then scans for the minimum CHF for each correlation and prints both values. In RELAP, the user specifies several axial locations for performing the CHF calculation. As a guide, the minimum CHF usually occurs at or shortly after the axial location where the wall heat flux peaks. RELAP prints the minimum of its calculated CHF values.

The CHF may be computed, at least, in two ways. The first way, and easier way, is to calculate the CHF using the thermal hydraulic conditions at the reactor design power. That is, at a design power run, use the printed CHF value for that run. An alternate computation is to increase continuously the reactor power until the first observance of the ratio of a locally calculated critical heat flux (CHF) divided by its corresponding local wall heat flux equals 1.0. The "reactor CHF" is this reactor power divided by the design reactor power. This second method usually gives a lower (more conservative) CHF value as compared to the first method.

The curves in the Figure 10 illustrate the two methods of calculating the CHF. The plot shows CHF versus reactor power for the TAMU and MNRC reactors.

The first method applied to TAMU shows that STAT/Bernath and RELAP/Groeneveld 1986 give CHF values equal to 3.62 and 6.14 at the design powers, respectively (also Table 2 values). For the second method applied to the TAMU reactor, the reactor power for which a minimum of the local CHF/local wall flux ratio equals 1.0 is 2.25 MW for STAT/Bernath (curve crosses CHF=1.0). The RELAP code showed instabilities before the curve decreased to CHF=1.0. The TAMU reactor CHF is then 2.25, which is lower than the first method CHF of 3.62.

For the MNRC reactor, the first CHF method gives CHF values of 1.80 for STAT/Bernath and 3.59 for RELAP at their design conditions (also Table 2 values). For the second CHF method, the reactor power for the curve crossing CHF=1 is 3.03 MW for STAT/Bernath. Again, RELAP shows instabilities as reactor powers approached 4 MW. Using an exponential extrapolation, one estimates that the RELAP reactor power at the CHF=1 curve crossing is 5.4 MW. The reactor CHF's are then 1.51 (3.03 MW/2.0 MW design) according to STAT/Bernath and 2.7 (5.4 MW/2.0 MW design) for RELAP. Both of these CHF values are lower than calculated for the first method.

Any other CHF correlation can be used with either of the codes for calculating the CHFR since the CHFR calculation follows the thermal hydraulic calculation. The necessary CHF thermal hydraulic variables for any selected CHF correlation can be extracted from the code. The CHFR can then be calculated. This is easy using the first method of the CHFR calculation, since the needed thermal hydraulic parameters are at the reactor design power. The second method becomes a trial and error procedure. A relatively high reactor power is selected, or reactor powers can be continuously increased from the design power. Either STAT or RELAP is run to obtain the thermal hydraulic conditions at that power. The necessary CHF parameters are extracted from the code output. Using the selected CHF correlation, the CHF is calculated at all, or several selected, axial locations. The wall heat flux is also noted at these axial locations. The minimum ratio of calculated local CHF divided by its corresponding local heat flux is noted. If this ratio is not equal to 1.0, a new reactor power is selected, and the process is repeated until the ratio equals 1.0. This power is called the DNB reactor power. The CHFR is then this DNB power divided by the design power.

Figure 10 shows the results of this CHFR method using RELAP for the reactor thermal hydraulics and the Bernath correlation for the CHF. For the TAMU reactor the generated curve crosses the CHFR=1 line slightly below 3.0 MW (2.87 MW from the actual calculation). The TAMU CHFR is then 2.87. This value is lower than the STAT/Bernath CHFR value. For the MNRC reactor the generated curve crosses the CHFR=1 line at 3.5 MW. The MNRC CHFR is then 1.75 (3.5 MW/2.0 MW).

Near the end of this study, Earl Feldman at ANL noted that a 2006 Groeneveld CHF correlation is currently available (Ref 7). Earl Feldman used this correlation with the RELAP thermal hydraulics to compute CHFR's (Ref. 10). These results are given in Table 3, along with the RELAP/Bernath CHFR values. The RELAP/Bernath values are still lower than the RELAP/Groeneveld 2006 values.

Conclusions

It appears that the application of the Bernath correlation for TRIGA reactors in the past has been conservative relative to the Groeneveld 1986 correlation. Lacking an alternate proven CHF correlation, the continued use of the Bernath correlation is recommended. The 1986 Groeneveld table look-up appears to yield too high CHFR for TRIGA conditions. The McAdams CHF correlation yields CHFR values larger than the Bernath correlation. This is especially true when increasing the reactor power to achieve a CHFR. The McAdams correlation is also based on very limited data. Its use is optional.

The 2006 Groeneveld table look-up has been reviewed by ANL and should also be utilized. D.D. Hall and I Mudawar of Purdue University have also done extensive investigations for CHF correlations of water in tubes. Unfortunately, much of their data is private. It is recommended to use RELAP for calculating the thermal hydraulics. Outside the RELAP code use the Bernath and the 2006 Groeneveld correlations for a CHFR calculation, and select the minimum value..

Efforts should be made to examine more closely the basis of the 2006 Groeneveld predictions at TRIGA conditions.

8.8 STAT and RELAP Hot Rod CHFR versus Inlet/Outlet Loss Coefficient

Because of the uncertainty in calculating the inlet and outlet loss coefficients, it is useful to show the effect of the loss coefficients on the CHFR.

Figure 11 shows CHFRs versus inlet/outlet loss coefficients for the three 1 MW reactors (WSU, OSU and TAMU) and the 2 MW design MNRC reactor. The abscissa shows normalized loss coefficients (K_i+K_o divided by the sum of the nominal K_i+K_o). As previously stated, a normalized loss coefficient of two means that the inlet and outlet loss coefficients are each twice their nominal values. The plot in Fig. 11 is generated using the STAT code.

The figure shows that doubling the K loss coefficients decreases the CHFR approximately 5–8% at design powers. The effect could be larger if the method of increasing the reactor power to achieve a CHFR=1.0 is used. It is noted, that when comparing Figs. 11 and 12, that there is a larger variation of the CHFR among correlations (at least 50%) than there is with its variation with the K loss coefficients (5–8%).

8.9 STAT and RELAP Hot Rod CHFR versus Hot Rod Flow Rate

Figure 12 shows the TAMU (1 MW design) and MNRC (2 MW design) hot rod CHFRs versus hot rod channel flow rate. The plots show CHFRs calculated by the STAT/Bernath combination and the RELAP/Groeneveld 1986 combination. The abscissa in Fig. 12 shows normalized flow rates – an actual flow divided by the reactor design (nominal) flow rate. The range of the normalized flow rate is approximately plus 25-50%/minus 30%. This range of flow rates was obtained by varying the inlet and outlet K losses and wall friction coefficient. Thus, Fig. 12 represents the effect of flow rate with other independent parameters, such as axial heat rate, inlet temperature and pressure held constant. Over the flow rate range shown, the CHFR varies approximately 30% total for STAT and 25% total for RELAP.

To achieve the 30% minus normalized flow rates, the K loss coefficients were increased 4-6 times. To achieve the 40% plus flow rates, the loss coefficients were set equal to zero and the rod friction factor was reduced. Flow variations within a code would not be expected to vary by this much. Only code-to-code results would show such a flow variation. The Fig. 12 plot can be used to gauge the effect of realistic variations of channel flow rate within a code on the CHFR. However, these results were obtained using the thermal hydraulic conditions at the design powers, the first CHFR method. Caution should be used interpreting the results when the second CHFR method is utilized.

9. REFERENCES

1. ANL SOW for Work Order No.2 Under BOA 63-00003, Appendix B, "TRIGA REACTOR THERMAL-HYDRAULICS STUDY", Sect. 3.0, Technical Tasks, Phase 1: STAT-RELAP Comparison, September 5, 2006
2. Ross Jensen's MNRC RELAP analysis and associated RELAP input and output computer files.
3. Jordan, D.P. and G. Leppert, "Pressure Drop and Vapor Volume with Sub-cooled Nucleate Boiling", International Journal of Heat and Mass Transfer, Vol. 5, pp 751-761, January, 1962.
4. McAdams, W.H., "Heat Transmission", McGraw-Hill, 1954; also McAdams, W.H. et al, "Heat Transfer at High Rates to Water with Surface Boiling", Indust. and Engrg. Chemistry, Vol. 41, No. 9, pp 1945-1953, 1949.
5. Bernath, L.B., "A Theory of Local Boiling Burnout and Its Application to Existing Data", Chem. Eng. Progress Symposium Series No. 30, Vol. 56, pp 95-116.
6. Groeneveld D.C. et al, "1986 AECL-UO Critical Heat Flux Lookup Table", Heat Transfer Eng., Vol. 7, Nos. 1-2, pp 48-62, 1986.
7. Groeneveld D.C. et al, "The 2006 CHF look-up table", Nuclear Engineering and Design, 237, pp 1909-1922, 2007.
8. "STAT – A Fortran Program for Calculating the Natural Convection Heat Transfer – Fluid Flow in an Array of Heated Cylinders", General Atomics Rept. GEN-44, July, 1989.
9. Feldman, Earl E., "Fundamental Approach to TRIGA Steady-State Thermal-Hydraulic Analysis, Argonne National Laboratory, ANL/RERTR/TM07-01, Sept. 2007.
10. Personal communication: Earl Feldman, Argonne National Laboratory and J.V. Del Bene, General Atomics, December, 2007.

Table 1. TRIGA Reactor Core Physical Data

Reactor/ Channel Type	No. Rods	Rod Dia. (in.)	Rod-Rod Pitch (in.)	Channel Flow Area (in. ²)	Wet'd Perim. (in.)	Hyd. Dia. (in.)	Un-htd Rod Bot. (in.)	Un-htd Rod Top (in.)	Un-htd Fixture At Top (in.)	$K_{inlet}^{(1)}$	$K_{outlet}^{(1)}$	rpf	apf
WSU – Square Cluster	100	1.411					4.055	4.055	1.60	2.02	1.38		
Av. And hot rod area			1.530	0.7772	4.433	0.7014						1.75	1.36
OSU – Circular	90	1.475					3.77	3.77	1.15	2.26	0.63		
Av. Rod, Cusp area				0.8683	4.634	0.7496						1.00	1.25
Hot rod, Triangle area			1.645	0.6335	4.634	0.5468						1.60	1.25
Ring G				1.0893	4.152	1.0494						0.819	1.25
TAMU – Rect. Cluster	90	1.411					4.055	4.055	1.60	1.64	1.30		
Av. Rod, Nom. Area			1.530	0.7772	4.433	0.7014						1.00	1.26
Hot rod, Min. area				0.7390	4.433	0.6668						1.565	1.26
Side rods 5F3,5F2				1.4450	3.746	1.5428						1.065	1.26
Corner rod 2F3				0.7225	2.638	1.0954						0.503	1.26
Interior rods+water				13.334	21.591	2.4703						1.447	1.26
MNRC – Hexagonal	101	1.475					3.77	3.77	2.70	0.59	0.54		
Unif. Tri., av. And hot			1.714	0.8355	4.634	0.7212						1.68	1.34

	Depth to Top of Top Grid Plate (ft)	Tank Dia. (ft)	Tank Ax (ft ²)
WSU – Square Cluster	22.0		180
OSU – Circular	16.0	6.50	33.18
TAMU – Rect. Cluster	23.5		424
MNRC – Triangular/hex	20.3	7.00	24.5

⁽¹⁾ K_{loss} coefficients are specific to the assumed lower and upper grid plate and fixture geometries

Table 1-A. TRIGA Reactor Core Physical Data – Metric Units

Reactor/ Channel Type	No. Rods	Rod Dia. (cm)	Rod-Rod Pitch (cm)	Channel Flow Area (cm ²)	Wet'd Perim. (cm)	Hyd. Dia. (cm)	Un-htd Rod Bot. (cm)	Un-htd Rod Top (cm)	Un-htd Fixture Top (cm)	$K_{inlet}^{(1)}$	$K_{outlet}^{(1)}$	rpf	apf
WSU - Square Cluster	100	3.584					10.30	10.30	4.064	2.02	1.38		
Av. and hot rod area			3.886	5.014	11.26	1.782						1.75	1.36
OSU - Circular	90	3.746					9.576	9.576	2.921	2.26	0.63		
Av. rod, Cusp area				5.602	11.77	1.904						1.00	1.25
Hot rod, Triangle area			4.178	4.087	11.77	1.389						1.60	1.25
Ring G				7.028	10.55	2.665						0.819	1.25
TAMU - Rect. Cluster	90	3.584					10.30	10.30	4.064	1.64	1.30		
Av. rod, Nom. area			3.886	5.014	11.26	1.782						1.00	1.26
Hot rod, Min. area				4.768	11.26	1.694						1.565	1.26
Side rods 5F3,5F2				9.323	9.515	3.919						1.065	1.26
Corner rod 2F3				4.661	6.701	2.782						0.503	1.26
Interior rods+water				86.026	54.84	6.275						1.447	1.26
MNRC - Hexagonal	101	3.746					9.576	9.576	6.8m	0.74	0.64		
Unif. tri., av. and hot			4.354	5.014	11.77	1.832						1.68	1.34

	Depth to Top of Top Grid Plate (ft)	Tank Dia. (m)	Tank Ax (m ²)
WSU - Square Cluster	6.71		16.7
OSU - Circular	4.88	1.98	3.08
TAMU - Rect. Cluster	7.16		39.4
MNRC - Triangular/hex	6.19	2.13	2.78

⁽¹⁾ K_{loss} coefficients are specific to the assumed lower and upper grid plate and fixture geometries

Table 2. STAT-RELAP Comparison Results

Reactor/ Code	Rod Type	Total Power (MW)	Rod Power (MW)	Rod Flow (lbm/hr)	Max Void Frac.	Q/A max (Btu/s*ft ²)	T liq/T vap Out (°F)	T wall max (°F)	Vel. In/Out (ft/s)	Re In/Out	chfr ⁽⁶⁾ McAd/Bern Groen-1986
WSU	Av. rod	1.0	0.010000								
STAT	Hot	1.0	0.017504	627.1	0.0	48.7	181.2	274.1	0.52/0.53	3650/8050	4.03/3.41
RELAP	Hot	1.0	0.017500	690.7	0.0	48.7	172.5	277.0	0.57/0.58	4115/8595	5.68
STAT	Adj. rod lower rpf ⁽⁴⁾	1.0	0.016629	616.7	0.0	48.7	178.0	274.1	0.51/0.52	3585/7740	4.05/3.45
STAT	Hot	1.5	0.026257	725.2	0.023	73.2	209.5	278.0	0.60/0.63	4240/10800	2.55/2.00
RELAP	Hot	1.5	0.026250	835.0	0.004	73.0	193/238	286.6	0.69/0.72	5045/11950	3.60
OSU	Av. rod	1.0	0.011111								
STAT	Hot	1.0	0.017784	561.2	0.0	43.6	194.1	266.9	0.57/0.59	3150/7440	4.25/2.77
RELAP	Hot	1.0	0.017780	632.8	0.0	43.5	181.9	269.9	0.64/0.66	3680/8040	6.40
STAT	Hot	1.5	0.026676	653.7	0.10	65.4	225.2	270.6	0.66/0.78	3690/10460	2.59/1.51
RELAP	Hot	1.5	0.026669	774.2	0.011	65.3	203/233	278.7	0.79/0.83	4585/11295	4.07
STAT	G-ring rod w/Gr	1.0	0.002276 ⁽³⁾	418.0	0.0	22.3	104.6	261.5	0.26/0.26	2560/3050	8.28/11.2
RELAP	G-ring rod w/Gr	1.0	0.002275 ⁽³⁾	436.2	0.0	22.3	103.8	256.8	0.26/0.26	2655/3195	12.8
TAMU	Av. rod	1.0	0.011111								
STAT	Hot	1.0	0.017394	616.8	0.0	44.9	182.2	274.8	0.54/0.55	3610/7930	4.43/3.62
RELAP	Hot	1.0	0.017389	681.5	0.0	44.8	173.1	277.0	0.59/0.61	4120/8520	6.14
STAT	Adj. rod lower rpf ⁽⁴⁾	1.0	0.016526	606.7	0.0	44.9	179.0	274.8	0.53/0.54	3550/7630	4.46/3.66
STAT	Hot	1.5	0.026090	706.5	0.048	67.4	212.0	278.6	0.61/0.67	4170/10900	2.75/2.09
RELAP	Hot	1.5	0.026083	806.9	0.0015	67.3	196/240	285.8	0.70/0.73	4970/11770	3.86
STAT	Side rods 5F3,5F2	1.0	0.005932 ⁽¹⁾	680.3 ⁽¹⁾	0.0	28.2	115.7	271.5	0.30/0.30	4640/6080	6.50/10.4
STAT	Corner rod 2F3	1.0	0.001398 ⁽⁵⁾	260.5 ⁽⁵⁾	0.0	14.4	104.3	266.0	0.23/0.23	2515/3000	13.0/19.1
STAT	Interior rods+water	1.0	0.046684 ⁽²⁾	5990	0.0	41.6	112.6	274.1	0.27/0.27	7620/9730	4.76/9.68
MNRC	Av. rod	2.0	0.019802								
STAT	Hot	2.0	0.033218	985.9	0.014	87.6	201.0	279.2	0.76/0.78	5580/13725	2.45/1.80
RELAP	Hot	2.0	0.033190	1211.2	0.005	86.4	180/238	291.5	0.93/0.96	7260/15150	3.59
STAT	Adj. rod lower rpf ⁽⁴⁾	2.0	0.030985	963.2	0.008	87.6	195.8	279.2	0.74/0.76	5445/13000	2.47/1.84
STAT	Hot	2.5	0.041498	1067.5	0.048	109.5	218.7	281.6	0.82/0.87	6080/16550	1.88/1.33
RELAP	Hot	2.5	0.041488	1405.8	0.016	108.0	187/238	297.6	1.08/1.14	8500/18450	2.88

(1) Power/flow for two ¼ rods, (2) Total power of eight rod fractions, rod fractions sum to 3.5 full rods, (3) Power from ¼ of rod facing water channel, (4) Rod adjacent to hot rod has 10% lower rpf, (5) Power/flow for ¼ of rod facing corner, (6) CHF's calculated within respective codes at design power conditions. Two values per line refer to STAT's built-in McAdams and Bernath. Single value per line refers to RELAP's built-in Groeneveld 1986.

Table 2-A. STAT-RELAP Comparison Results – Metric Units

Reactor/ Code	Rod Type	Total Power (MW)	Rod Power (MW)	Rod Flow (kg/hr)	Max Void Frac.	Q/A max (W/cm ²)	T liq/T vap Out (°C)	T wall max (°C)	Vel. In/Out (m/s)	Re In/Out	chfr ⁽⁶⁾ McAd/Bern Groen-1986
WSU	Av. rod	1.0	0.010000								
STAT	Hot	1.0	0.017504	284.4	0.0	55.3	82.9	134.5	0.16/0.16	3650/8050	4.03/3.41
RELAP	Hot	1.0	0.017500	313.3	0.0	55.3	78.1	136.1	0.17/0.18	4115/8595	5.68
STAT	Adj. rod lower rpf ⁽⁴⁾	1.0	0.016629	279.7	0.0	55.3	81.1	134.5	0.16/0.16	3585/7740	4.05/3.45
STAT	Hot	1.5	0.026257	328.9	0.023	83.1	98.6/114	136.7	0.18/0.19	4240/10800	2.55/2.00
RELAP	Hot	1.5	0.026250	378.7	0.004	82.9	89.4/114	141.4	0.21/0.22	5045/11950	3.60
OSU	Av. rod	1.0	0.011111								
STAT	Hot	1.0	0.017784	254.6	0.0	49.5	90.1	130.5	0.17/0.18	3150/7440	4.25/2.77
RELAP	Hot	1.0	0.017780	287.0	0.0	49.4	83.3	132.2	0.20/0.20	3680/8040	6.40
STAT	Hot	1.5	0.026676	296.5	0.10	74.3	107.3	132.6	0.20/0.24	3690/10460	2.59/1.51
RELAP	Hot	1.5	0.026669	351.2	0.011	74.2	95.0/112	137.1	0.24/0.25	4585/11295	4.07
STAT	G-ring rod w/Gr	1.0	0.002276 ⁽³⁾	189.6	0.0	25.3	40.3	127.5	0.08/0.08	2560/3050	8.28/11.2
RELAP	G-ring rod w/Gr	1.0	0.002275 ⁽³⁾	197.9	0.0	25.3	39.9	124.9	0.08/0.08	2655/3195	12.8
TAMU	Av. rod	1.0	0.011111								
STAT	Hot	1.0	0.017394	279.8	0.0	51.0	83.4	134.9	0.16/0.17	3610/7930	4.43/3.62
RELAP	Hot	1.0	0.017389	309.1	0.0	50.9	78.4	136.1	0.18/0.19	4120/8520	6.14
STAT	Adj. rod lower rpf ⁽⁴⁾	1.0	0.016526	275.2	0.0	51.0	81.7	134.9	0.16/0.16	3550/7630	4.46/3.66
STAT	Hot	1.5	0.026090	320.5	0.048	76.5	100.0	137.0	0.19/0.20	4170/10900	2.75/2.09
RELAP	Hot	1.5	0.026083	366.0	0.0015	76.4	91.1/116	141.0	0.21/0.22	4970/11770	3.86
STAT	Side rods 5F3,5F2	1.0	0.023662 ⁽¹⁾	308.6 ⁽¹⁾	0.0	32.0	46.5	133.1	0.09/0.09	4640/6080	6.50/10.4
STAT	Corner rod 2F3	1.0	0.001398 ⁽⁵⁾	118.2 ⁽⁵⁾	0.0	16.4	40.2	130.0	0.07/0.07	2515/3000	13.0/19.1
STAT	Interior rods+water	1.0	0.046684 ⁽²⁾	2717	0.0	47.2	44.8	134.5	0.08/0.08	7620/9730	4.76/9.68
MNRC	Av. rod	2.0	0.019802								
STAT	Hot	2.0	0.033218	447.2	0.014	99.5	93.9	137.3	0.236/0.24	5580/13725	2.45/1.80
RELAP	Hot	2.0	0.033190	549.4	0.005	98.1	82.2/114	144.2	0.28/0.29	7260/15150	3.59
STAT	Adj. rod lower rpf ⁽⁴⁾	2.0	0.030985	436.9	0.008	99.5	91.0	137.3	0.23/0.23	5445/13000	2.47/1.84
STAT	Hot	2.5	0.041498	484.2	0.048	124.4	103.7	138.7	0.25/0.27	6080/16550	1.88/1.33
RELAP	Hot	2.5	0.041488	637.7	0.016	122.7	86.1/114	147.6	0.33/0.35	8500/18450	2.88

(1) Power/flow for two ¼ rods, (2) Total power of eight rod fractions, rod fractions sum to 3.5 full rods, (3) Power from ¼ of rod facing water channel, (4) Rod adjacent to hot rod has 10% lower rpf, (5) Power/flow for ¼ of rod facing corner, (6) CHFR's calculated within respective codes at design power conditions. Two values per line refer to STAT's built-in McAdams and Bernath. Single value per line refers to RELAP's built-in Groeneveld 1986.

Table 3. Comparison of Bernath and Groeneveld 2006 CHFR Predictions

	WSU	OSU	TAMU	MNRC
RELAP/Bernath	2.76	2.36	2.87	1.75
RELAP/Groeneveld 2006	3.50	3.70	3.59	1.97
Ratio: Row 2/Row 1	1.27	1.57	1.25	1.13

Figure 1a. WSU Core Configuration

GA-C26016

Figure 1b. TAMU Core Configuration

Figure 1c. OSU Top Grid Plate Showing the Core Configuration



Figure 1d. MNRC (UC Davis) Bottom Grid Plate Showing the Core Configuration

Figure 2a: TAMU and WSU Rods and End Fittings



Figure 2b. OSU Rod and End Fittings

Figure 2c. MNRC Rod and End Fittings

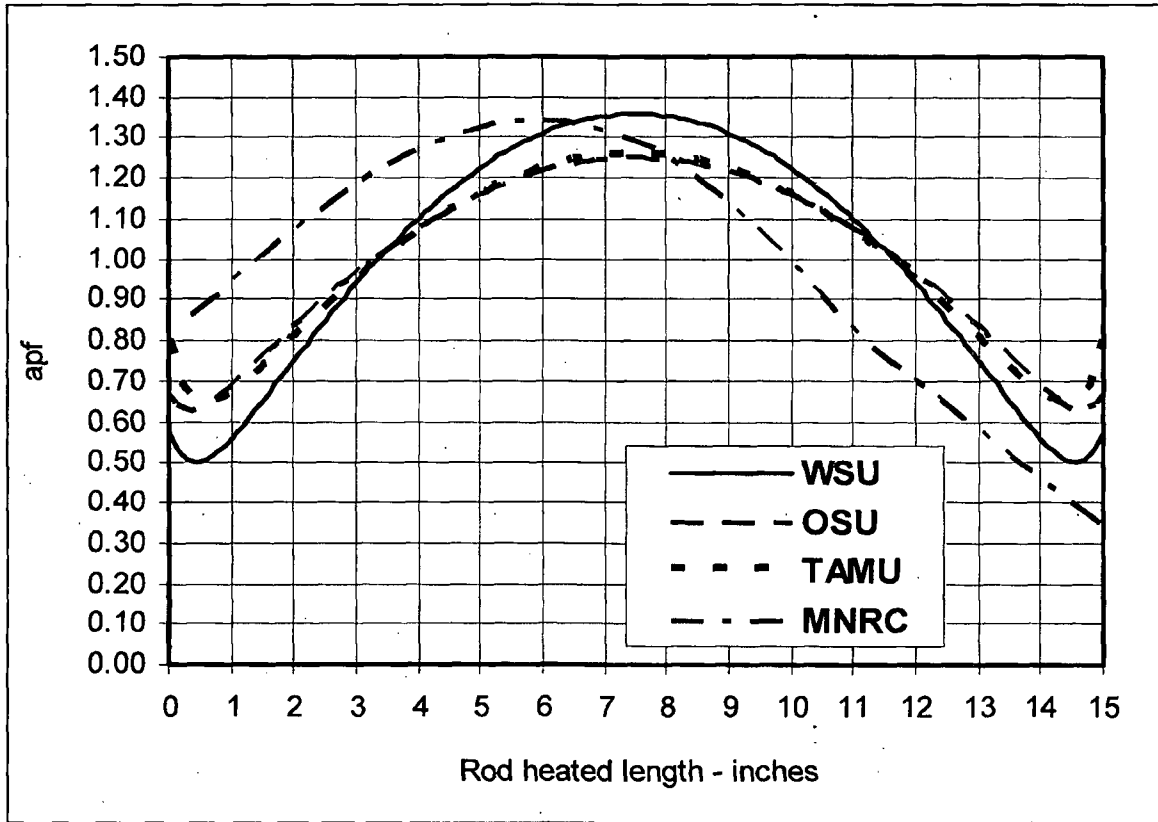


Figure 3. Reactor Rod Axial Peaking Factors

Figure 4. TAMU Core Configuration Showing Measured Outlet Temperature Locations

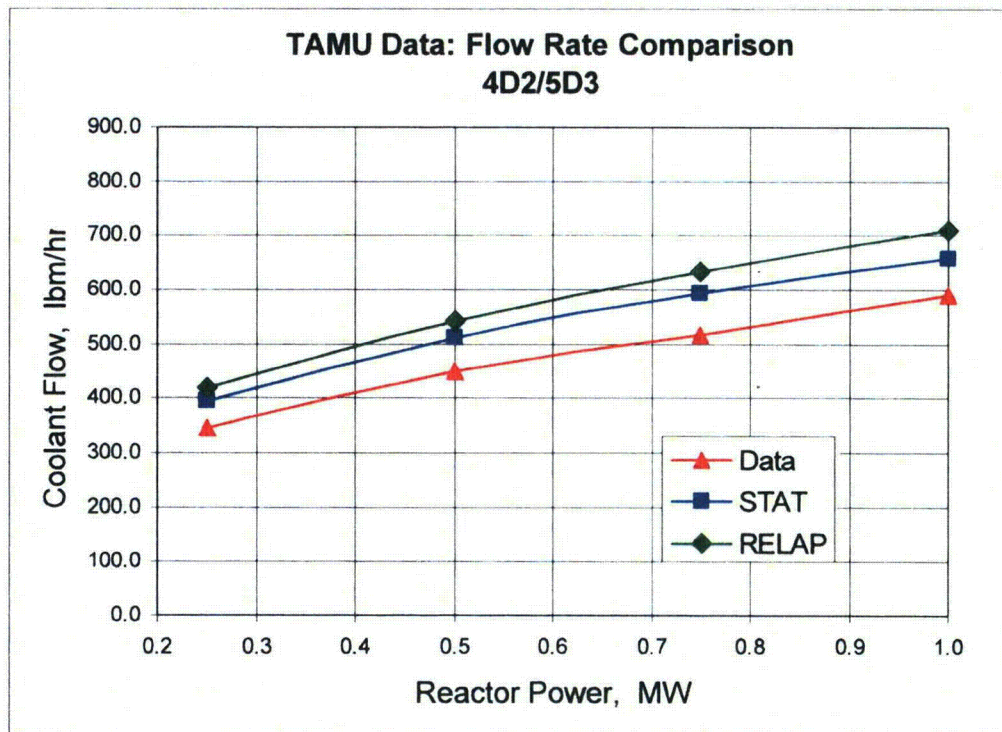
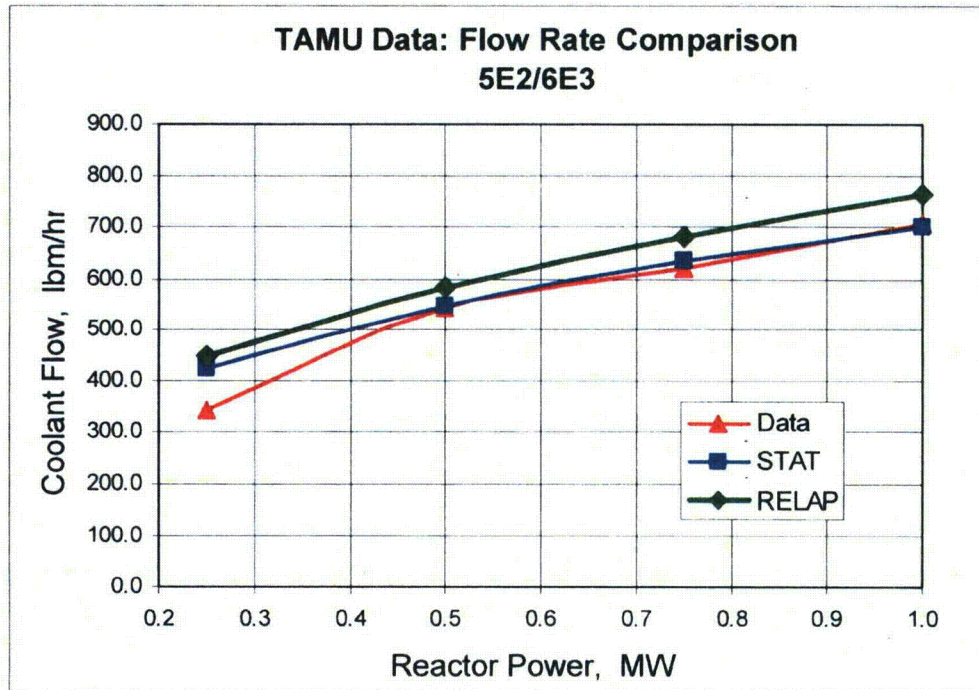


Figure 5. Flow Rate Comparison

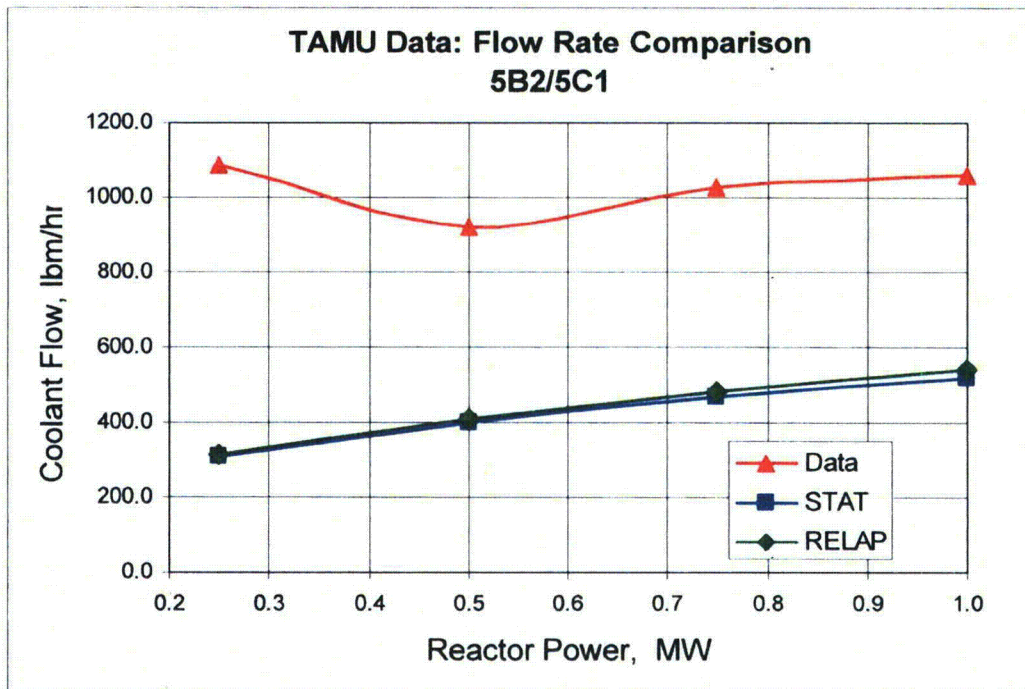
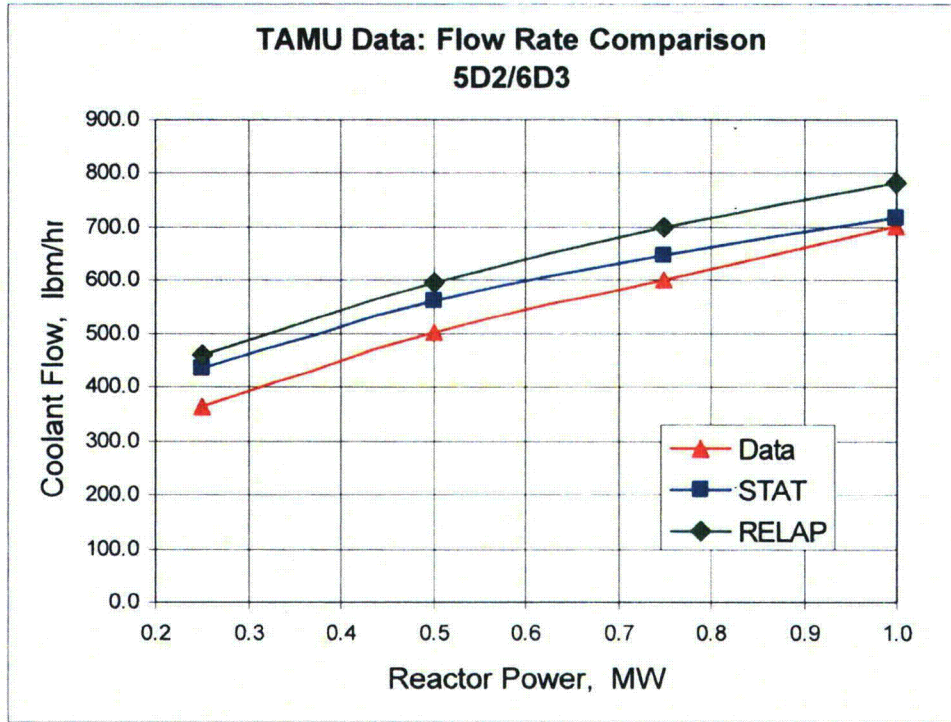
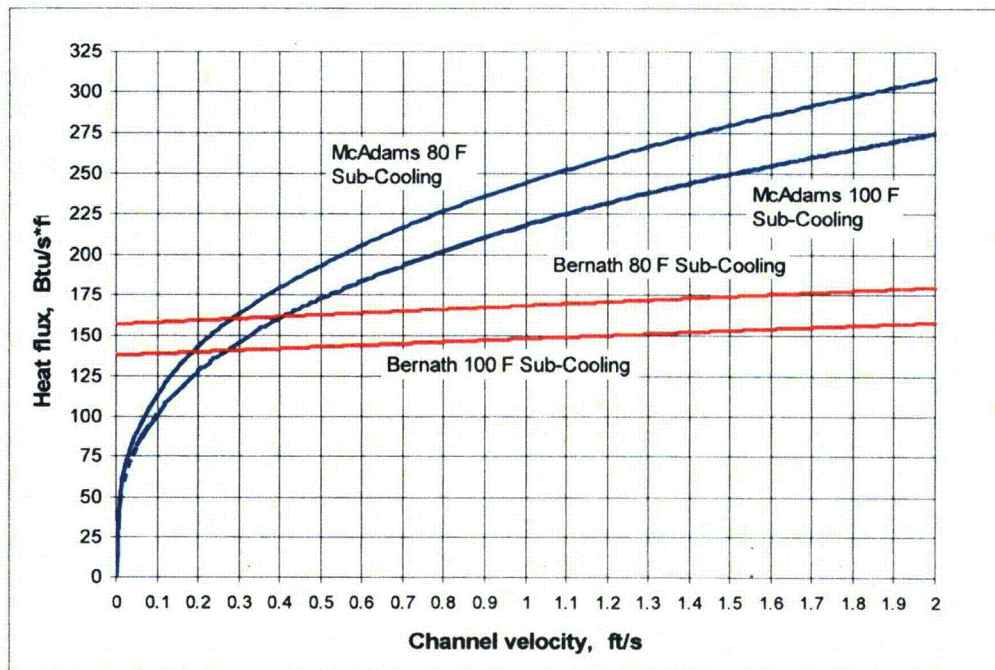


Figure 5. Flow Rate Comparison (Continued)



For 80°F and 100°F Subcooling

Figure 6. Bernath and McAdams Critical Heat Fluxes vs. Channel Velocity

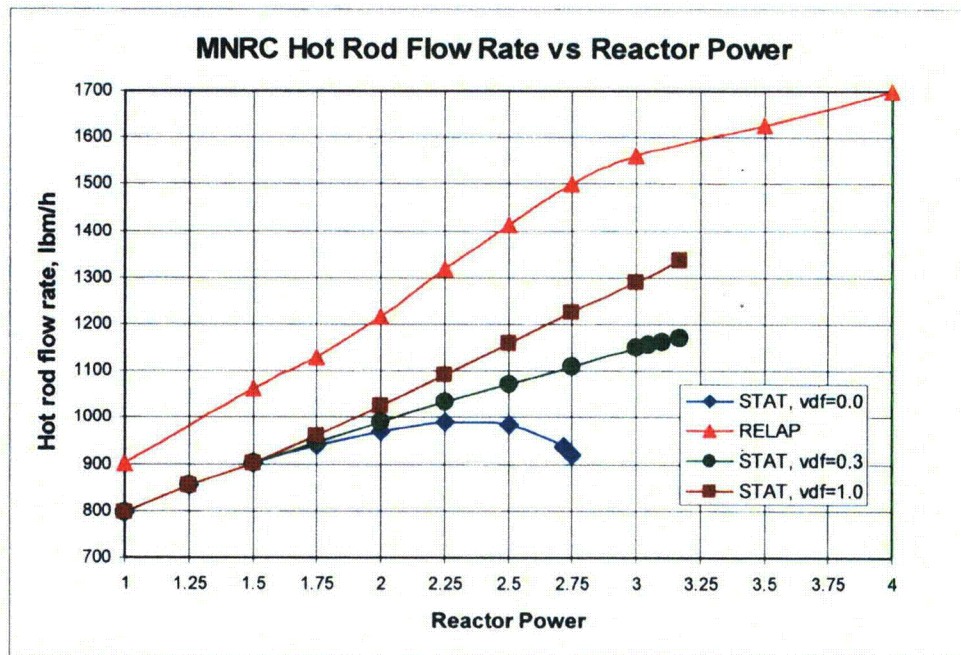
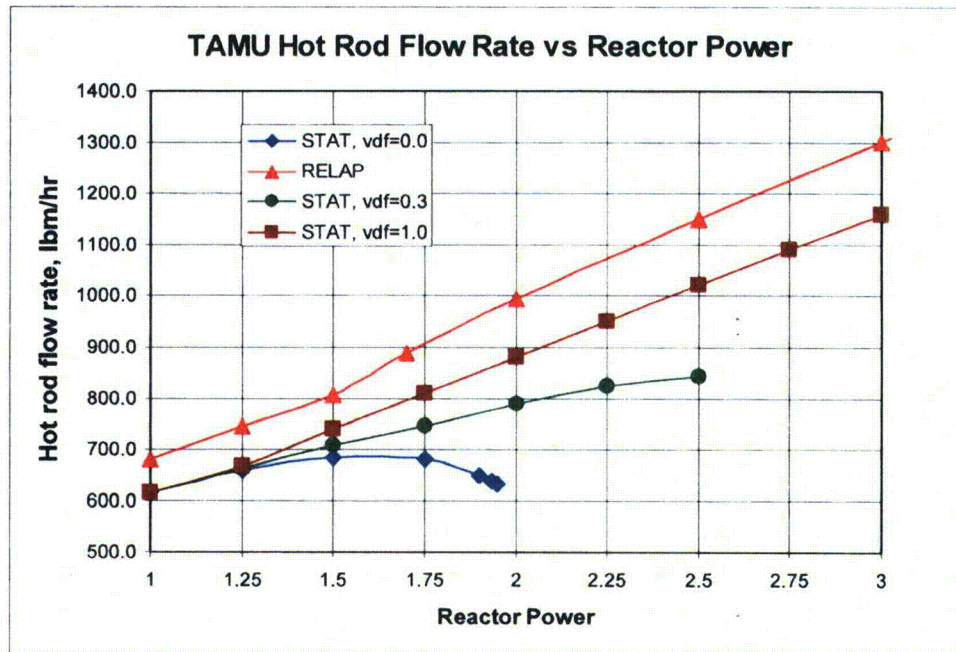


Figure 7. Hot Rod Flow Rate vs. Reactor Power

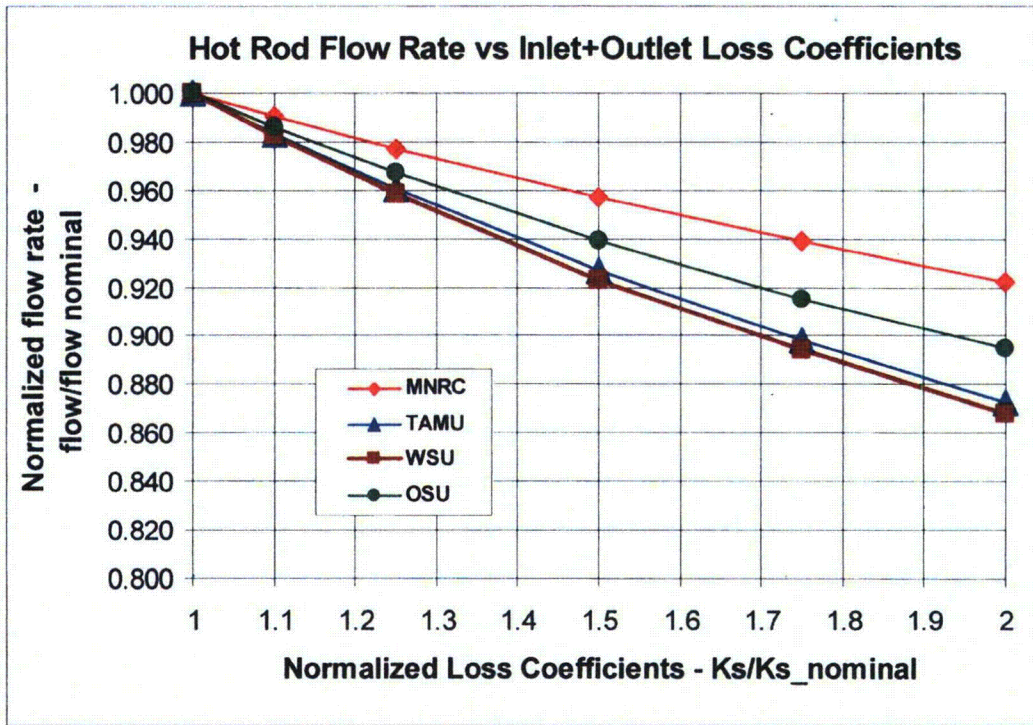


Figure 8. Hot Rod Flor Rate vs. Inlet + Outlet Loss Coefficients

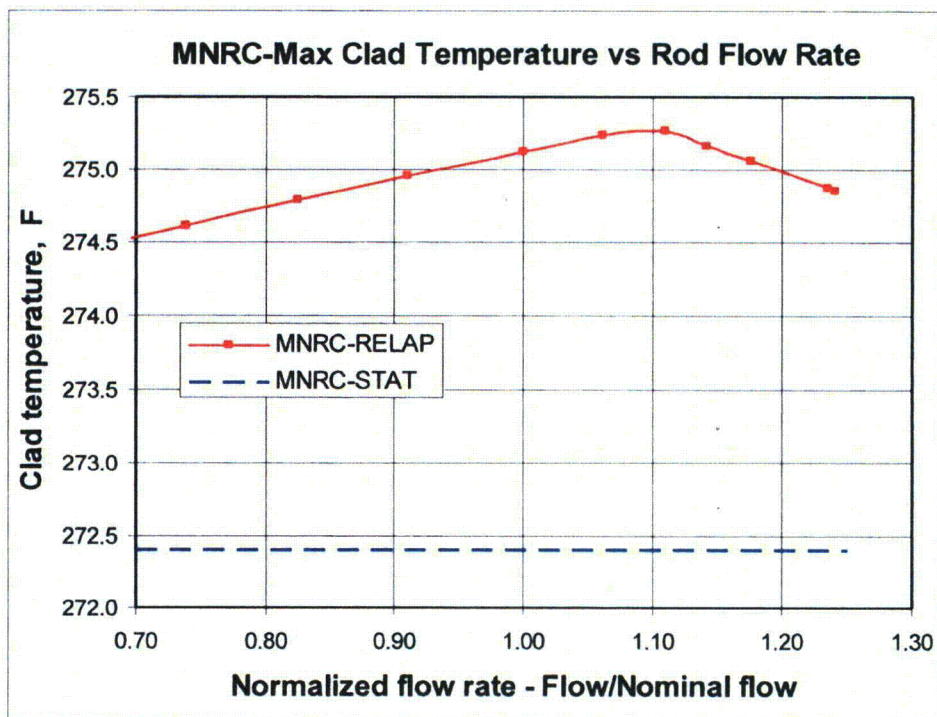
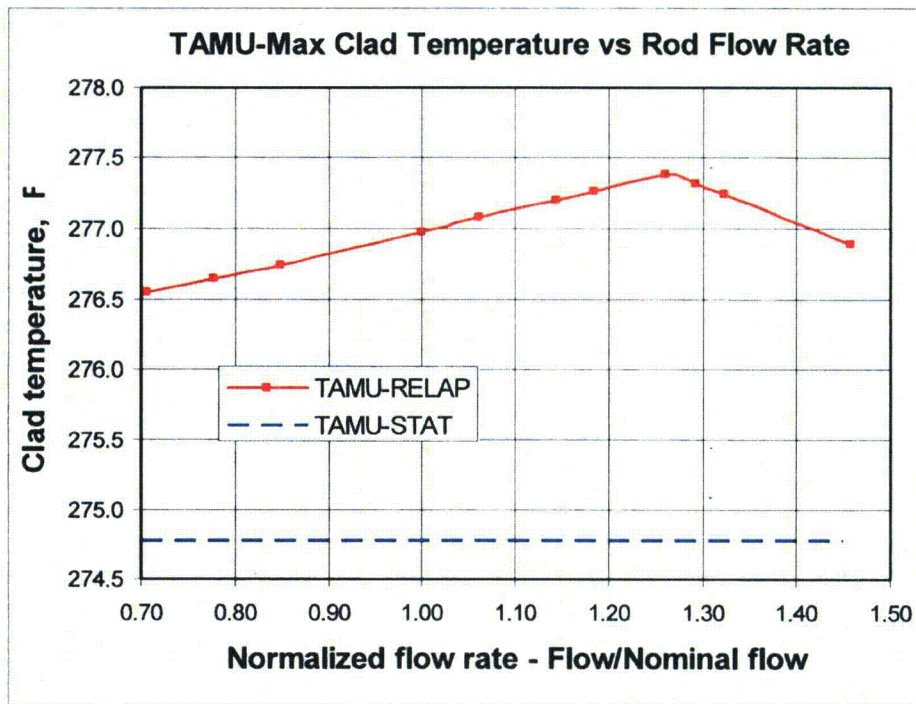


Figure 9. Max. Clad Temperature vs. Rod Flow Rate

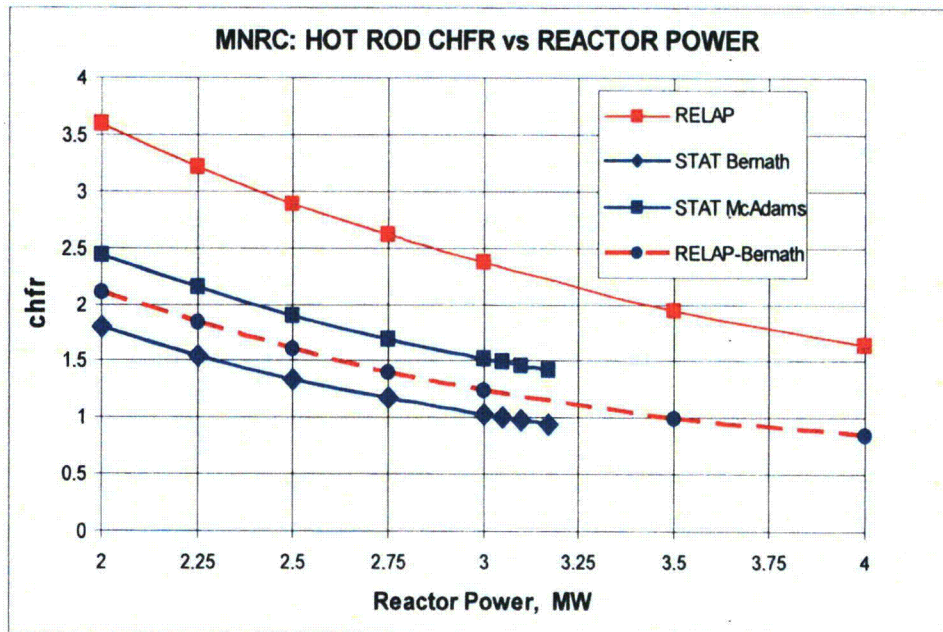
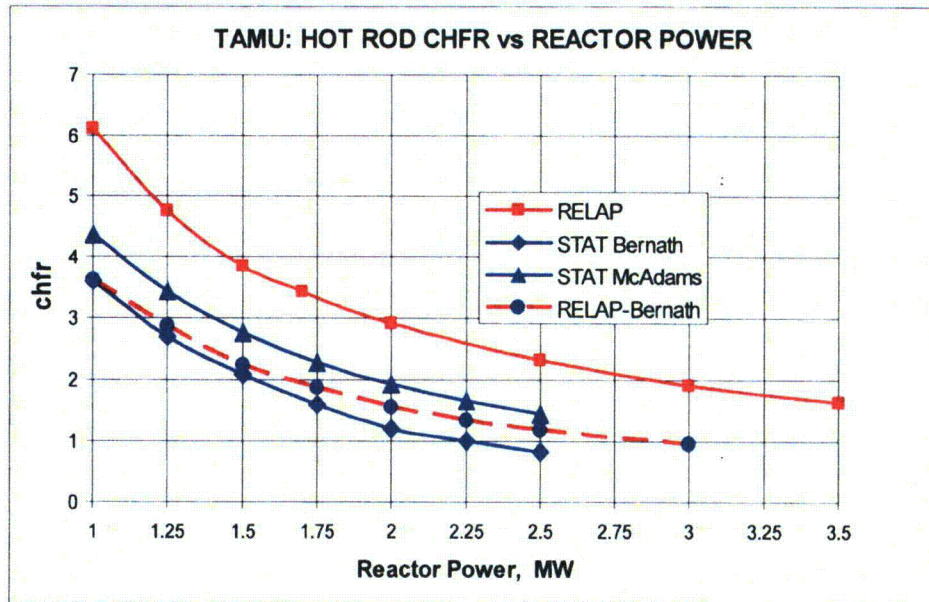


Figure 10. Hot Rod CHFR vs. Reactor Power

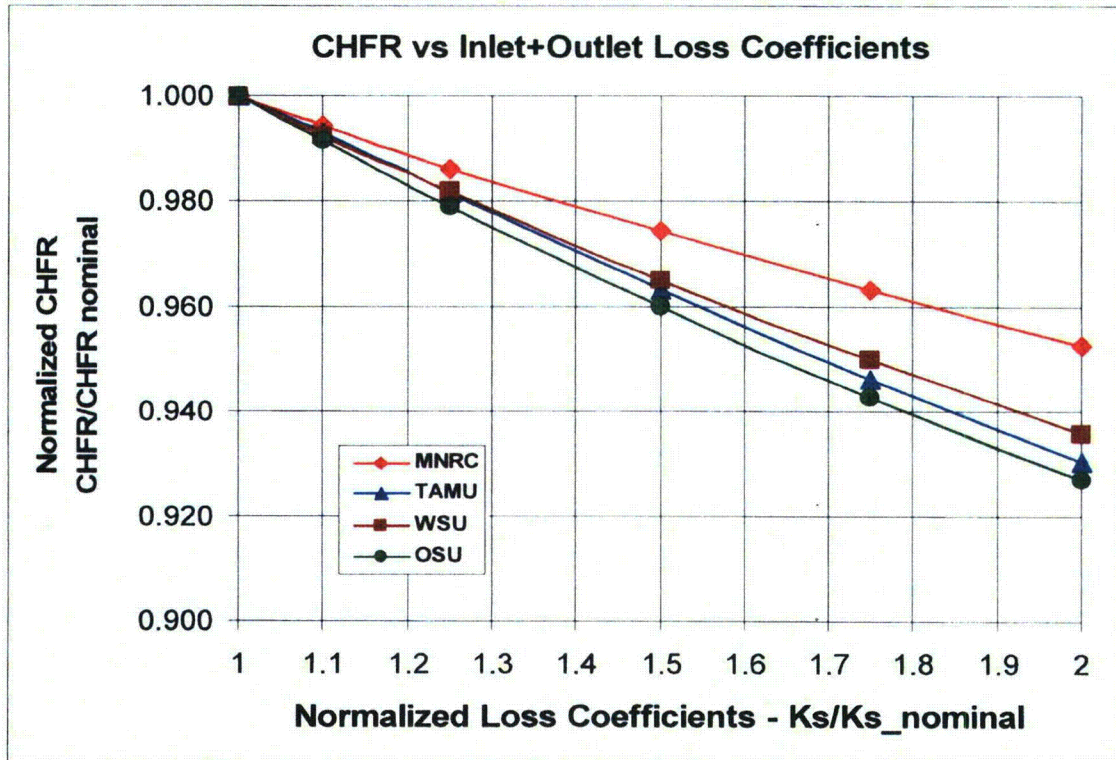


Figure 11. CHFR vs. Inlet/Outlet Loss Coefficients

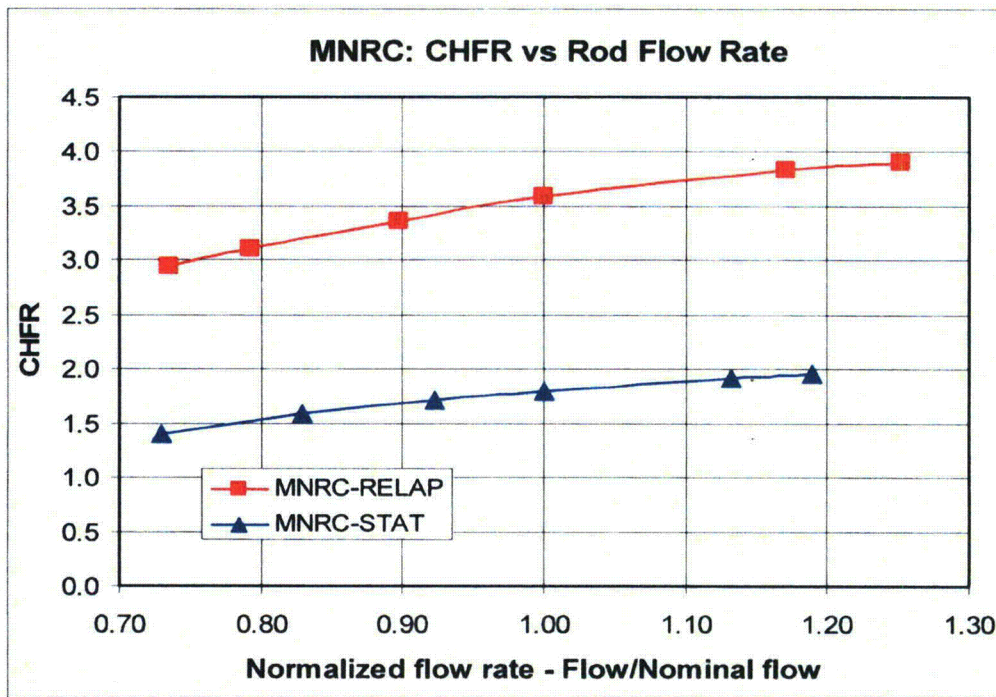
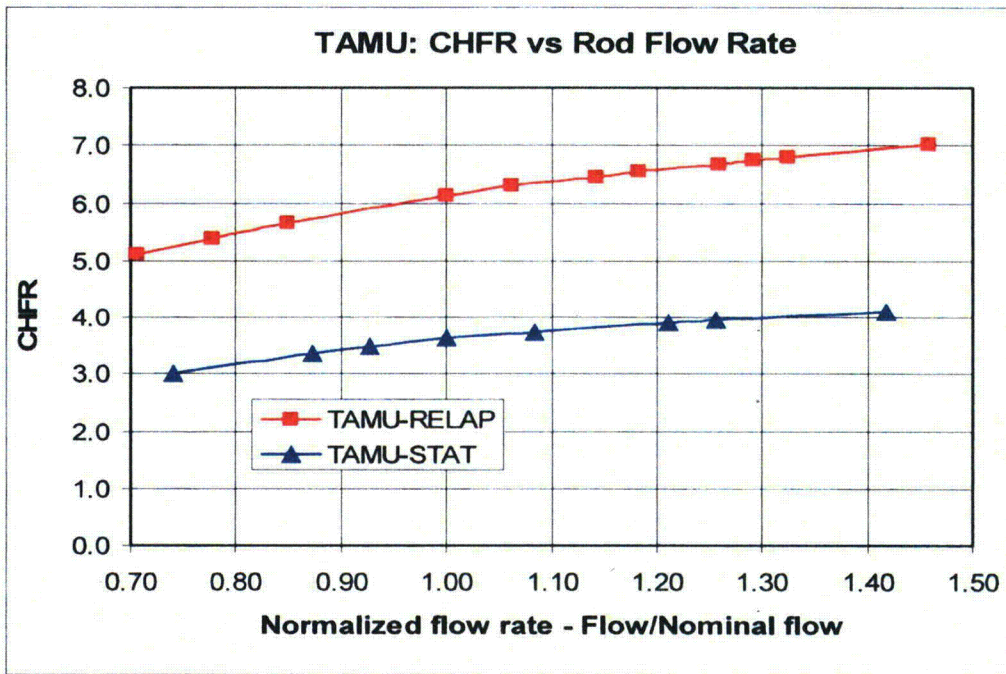


Figure 12. CHFR vs. Rod Flow Rate

APPENDIX A: EVALUATION OF INLET/OUTLET LOSS COEFFICIENTS

Rod channel inlet and outlet loss coefficients express the form losses of the rod bottom and upper rod fixtures. Figures A1-A3 below illustrate the geometry of these inlet and outlet fixtures. Generally, the inlet/outlet loss coefficients consist of a series of abrupt contractions and expansions. Rather than model the geometry of each of these expansions or contractions, a single loss coefficient for each of the core inlet and outlet locations is used to represent the total of the individual local loss coefficients. (The STAT code only takes a single inlet and a single loss coefficient referenced to the rod flow area.)

Since the detailed geometry of the inlet/outlet fixtures is not included in the models, the total loss coefficients are usually referenced to the rod channel flow area. The numerical value of a local loss coefficient could increase or decrease when referenced to the rod channel flow area. The correction of a local loss coefficient based on the local area to an effective loss coefficient based on the rod channel flow area is given by: $K_{\text{eff, rod channel}} = K_{\text{local}} * (\text{Area}_{\text{rod channel}} / \text{Area}_{\text{local}})^2$. Most often the rod channel area is less than the local area. The effective loss coefficient based on the rod channel area may then appear unrealistically low. When used with the smaller flow area and channel flow rate (and higher velocity), the pressure loss in the fixture is computed correctly.

Before proceeding with any TRIGA thermal analysis, it is strongly recommended that the geometry of the fuel rod end fixtures and grid plates be verified. The user should check the K loss coefficients in this report for applicability to their reactor.

Tables A-1 through A-4* give the local loss coefficients used in this study for the inlet and outlet end fixtures for the four reactors. Local loss coefficients are calculated for the axial locations specified in Figs. A-1 through A-3*. Callouts in these figures show the locations where local K values are calculated. For each local loss coefficient the table gives from left to right the following:

- Location of the loss
- Type of loss
- "From"/"to" areas
- Numerical value of the "from" area
- Numerical value of the "to" area
- Area for which the local coefficient is based
- Reynolds number at this area
- Local K loss coefficient
- Ratio of rod channel-to-local area
- Local K loss coefficient based on the rod channel flow area
- Sum of these latter loss coefficients, which is given in Table 1 of the main report

For this report the calculation of the above local expansion and contraction K losses are generally based on Ref. A.1. An exception is the calculation of the contraction loss from the pool to the bottom grid plate and the expansion loss from the top grid plate to the pool above.

*Tables and figures are located at the end of Appendix A.

At these locations it is assumed that the pool does not act as a large reservoir with flow to a single inlet or a single outlet. Rather the pool supplies multiple parallel inlets at the bottom grid plate and receives flow from multiple parallel outlets at the top grid plate. Inlet and outlet loss coefficients are obtained from Ref. A.2.

Further description is given for several specific items in reactors OSU, TAMU and MNRC. WSU calculations are similar to the TAMU calculations except for some of the flow areas.

The calculation of the inlet losses for the OSU reactor is difficult. As shown in Figure 1c of the main report, each ring has uniformly spaced rods 360° around the ring. This leads to an irregular rod pattern throughout the core. Following this, the bottom grid plate does not have flow holes in a regular pattern. Instead, for the inner one-half of the core there are 24.5 in. diameter holes located in the B, C and D rings, and then circumferential slots between the B and C rings and between the C and D rings. Each slot provides flow to several adjacent rod channels. The bottom grid plate has very few cooling holes for rods in the E through G rings. Instead, the core shroud has large openings near its bottom to provide for a radial inflow to the rods in the E to G rings. The upper grid plate has 1.505 in. diameter holes to accept the top fixture for each rod in the core. Typical loss coefficients are calculated for rods in the B-C rings. The bottom grid plate does not have a regular pattern of a grid plate hole associated with each fuel rod. Thus, the total flow area in the bottom grid plate out to half way between the C and D rings was computed. This total flow area was assigned evenly to the 16 rods in the B and C rings for the computation of bottom grid plate K loss coefficients. The OSU loss coefficients given in Table A-2 apply only to the hot rod. They were also used for the G-ring fuel/graphite rod analysis.

The TAMU reactor has an essentially rectangular core (see Figure 1b of the main report) with uniformly spaced four-rod clusters. A large port in the lower grid plate centered beneath the cluster feeds cooling water to the four rods of the cluster. The WSU grid plate is similar. However, the TAMU lower grid plate has 0.75 in. diameter holes at each corner of a cluster. These holes provide an additional cooling path parallel to the main grid port. Table A-3 illustrates this condition for the local inlet loss coefficients. The upper grid plate has no such parallel flow path.

Unlike the preceding three reactors with abrupt area changes in the rod fixtures, the MNRC reactor has end fixtures with mostly smooth changes in the flow areas. The losses in the MNRC bottom and top rod fixtures include wall friction losses {Moody type, $f = \text{function}(Re)$ } along these smooth surfaces. Table A-4 shows lines with "Fin surface friction" which give the equivalent loss coefficient for the smooth wall friction.

The specification of the outlet condition and losses merits further discussion. At some local elevation, either at the core exit or further up towards the pool surface, it is implicitly assumed that the local static pressure in the upflow core plume equals the local static pressure in the pool water downflow. That is, at some axial elevation the lateral pressure is uniform. This allows one to equate the core friction pressure drop plus the hot leg density head equal to the adjacent pool water friction pressure drop plus the cold leg density head (assuming the correct +/- signs are applied). Generally, the flow velocity of the downflow is quite small, and the downflow

friction pressure drop can be neglected. Additionally, the downflow is essentially at a constant temperature.

If the selected elevation is far upward from the core outlet, the upflow velocity can be considered zero. However, there is a warm density head of the upflow plume adjacent to the cold density head of the downflow. This "chimney effect" adds to the overall cold-minus-hot density head driving the natural convection flow through the core. A difficulty here is that the warm upflow mixes with the cold downflow, and the temperature of the upflow diminishes. Calculation of the upflow axial temperature profile, which is necessary in order to calculate the hot density head, is difficult.

An alternate choice is to select the elevation where $P_{\text{upflow}} = P_{\text{downflow}}$ immediately after the core outlet; for example, see Fig. A-4. Analyses of jets or hot plumes entering an open environment usually make the assumption that the lateral pressure difference is zero between the jet or plume and the ambient at the same lateral point (Refs A.1 and A.3 for example). In fact, Ref. A.3, pg. 108, eq. 5-56 gives an approximate expression for this lateral pressure difference. Using typical TRIGA core outlet conditions, this pressure difference is of the order of three magnitudes smaller than the core outlet K loss.

In construction of a STAT or RELAP model, consideration should be given to the core exit flow/pressure conditions. Figure A5 shows the RELAP model used in this study. The "sngvol" diffuser block just above the core outlet provides a common pressure location where the pressure drops of the core average pipe and the hot pipe are equated to the density head of the tank portion adjacent to the core.

If a diffuser region has a shroud separating the core outlet/diffuser flows from the pool water (Morocco reactor), the RELAP model of Fig. 5A can be slightly modified to replicate this diffuser configuration. The junction in Fig. 5A joining the top of the pool region adjacent to the core to the bottom of the diffuser block can be changed to bypass the diffuser block and to connect to the bottom of the upper tank block. This axial location then becomes the plane uniform lateral pressure between core and reactor pool.

The K loss coefficients presented are specific to each reactor and with the assumed end fixture geometries. The analyst of any reactor should recalculate the loss coefficients for that reactor with its specific grid plates and end fixtures.

Appendix A References

- A.1 Blevins, Robert D., "Applied Fluid Dynamics Handbook", Van Nostrand Reinhold Co., 1984, pg. 76, Frame 11 and pg. 78 Frame 17.
- A.2 Kays, W.M. and A.L. London, "Compact Heat Exchangers", McGraw-Hill, 1964, Figs. 5-2 and 5-3.
- A.3 Pai, Shih-I, "Fluid Dynamics of Jets", Van Nostrand Reinhold Co., 1954.

Table A-1. WSU Inlet/Outlet K Loss Coefficients

Rod channel area⁽¹⁾, $A_D = 3.109 \text{ in.}^2$ **Inlet Loss Coefficient:**

Location	Type	Area-to-Area	Area 1 (in. ²)	Area 2 (in. ²)	Area K Based On	Area Rey. No.	Local K	$A_D/A_$	K Based On A_D
Pool to grid plug	Contraction	P-A	9.364	3.976	A	8950	0.40	0.782	0.245
Grid plug to cruciform	Contraction	A-B	3.976	2.178	B	7725	0.287	1.427	0.585
Cruciform to 4 pin support	Expansion	B-C	2.178	6.222	B	7725	0.422	1.427	0.861
4 pin support to rod cluster	Contraction	C-D	6.222	3.109	D	5730	0.328	1.0	0.328
Sum local K's for total inlet loss coefficient K_i									2.018

Outlet Loss Coefficient:

Location	Type	Area-to-Area	Area 1 (in. ²)	Area 2 (in. ²)	Area K Based On	Area Rey. No.	Local K	$A_D/A_$	K Based On A_D
Rod cluster to 4 pin support	Expansion	D-E	3.109	6.303	D	5730	0.257	1.0	0.257
4 pin support to top fitting	Contraction	E-F	6.303	2.680	F	3382	0.386	1.160	0.520
Top fitting to pool	Expansion	F-P	2.680	9.364	F	3382	0.45	1.160	0.606
Sum local K's for total outlet loss coefficient K_o									1.382

(1) All channel areas are for a four rod cluster. STAT/RELAP flow area is a one rod cusp area within the four cluster rods.

Table A-2. OSU Inlet/Outlet K Loss Coefficients

Rod channel area⁽¹⁾, $A_D = 0.6335 \text{ in.}^2$ **Inlet Loss Coefficient:**

Location	Type	Area-to-Area	Area 1 (in. ²)	Area 2 (in. ²)	Area K Based On	Area Rey. No.	Local K	A_D/A	K Based On A_D
Pool to slots/holes	Contraction	P-A	3.111	0.551	A	5390	0.45	1.150	0.595
Slots/holes to fins	Expansion	A-B	0.551	1.841	A	5350	0.47	1.150	0.844 ⁽²⁾
Slots/holes to fin turns	Flow turning	A-B	0.551	1.841	A/B av	6380	1.0	0.530	0.365 ⁽²⁾
Fins to nub	Expansion	B-C	1.841	2.035	B	7360	0.009	0.344	0.001
Nub to rod	Contraction	C-D	2.035	0.633	D	3120	0.458	1.0	0.458
Sum local K's									2.263

Outlet Loss Coefficient:

Location	Type	Area-to-Area	Area 1 (in. ²)	Area 2 (in. ²)	Area K Based On	Area Rey. No.	Local K	A_D/A	K Based On A_D
Rod to nub	Expansion	D-E	0.633	2.035	D	7830	0.474	1.0	0.474
Nub to fins	Contraction	E-F	2.035	1.136	F	4890	0.278	0.557	0.086
Fins to top nub	Expansion	F-G	1.136	2.035	F	4890	0.195	0.557	0.061
Top nub to pool	Expansion	G-P	2.035	3.111	G	18500	0.120	0.311	0.012
Sum local K's for total outlet loss coefficient K_o									0.633

(1) All channel areas are for a single rod. (2) Includes a 30% increase for uncertainties.

Table A-3. TAMU Inlet/Outlet K Loss Coefficients

Rod channel area⁽¹⁾, A_D 3.424 in.²**Inlet Loss Coefficient:**

Location	Type	Area-to-Area	Area 1 (in. ²)	Area 2 (in. ²)	Area K Based On	Area Rey. No.	Local K	A_D/A_*	K Based On A_D
Pool to grid plug	Contraction	P-A	9.679	3.142	A	6310	0.40	1.090	0.475
Grid plug to cruciform	Contraction	A-B	3.142	2.178	B	8507	0.161	1.572	0.379
Cruciform to 4 pin support	Expansion	B-C	2.178	6.537	B	8507	0.445	1.572	1.099
Sum local K's									1.953
K _{in} + K _{out} for the 0.75" dia. Hole ($A_x=0.442$ in. ²) in the bottom grid plate and associated with a cluster									60
K _{eff} for the two above parallel flow paths and all K's based on A_D ($1/\sqrt{K_{eff}} = 1/\sqrt{K_{sum}} + 1/\sqrt{K_{hole}}$)									1.402
4 pin support to rod cluster	Contraction	C-D	6.537	3.424	D	6310	0.238	1.0	0.238
Sum local K's for total inlet loss coefficient K_i									1.640

Outlet Loss Coefficient:

Location	Type	Area-to-Area	Area 1 (in. ²)	Area 2 (in. ²)	Area K Based On	Area Rey. No.	Local K	A_D/A_*	K Based On A_D
Rod cluster to 4 pin support	Expansion	D-E	3.424	6.618	D	6310	0.233	1.0	0.233
4 pin support to top fitting	Contraction	E-F	6.618	2.995	F	3333	0.366	1.143	0.478
Top fitting to pool	Expansion	F-P	2.995	9.679	F	3333	0.45	1.143	0.588
Sum local K's for total outlet loss coefficient K_o									1.299

(1) All channel areas are for a four rod cluster. STAT/RELAP flow area is a one rod cusp area within the four cluster rods.

Table A-4. MNRC Inlet/Outlet K Loss Coefficients

Rod channel area⁽¹⁾, A_c 0.8355 in.²

Inlet Loss Coefficient:

Location	Type	Area-to-Area	Area 1 (in. ²)	Area 2 (in. ²)	Area K Based On	Area Rey. No.	Local K	$A_c/A_$	K Based On A_D
Pool to grid hole	Contraction	P-A	2.544	1.178	A	4750	0.60	0.709	0.302
Grid hole to above grid hole	Expansion	A-B	1.178	2.531	A	4750	0.143	0.709	0.143
Fin surface friction		A-C	1.178	0.8355	C	10000	0.142 ⁽²⁾	1.0	0.142
Sum local K's									0.587

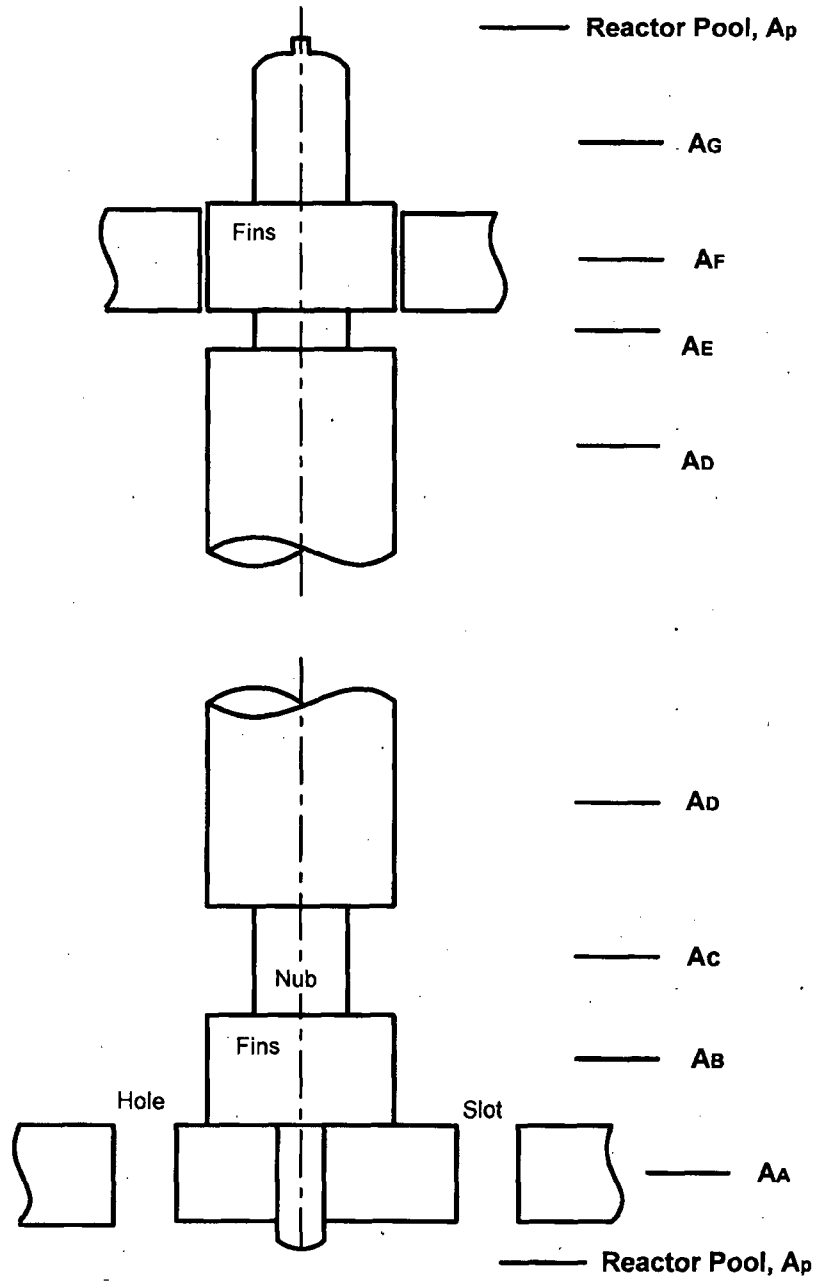
Outlet Loss Coefficient:

Location	Type	Area-to-Area	Area 1 (in. ²)	Area 2 (in. ²)	Area K Based On	Area Rey. No.	Local K	$A_c/A_$	K Based On A_D
Rod channel to top grid	Expansion	C-D	0.8355	1.388	C	8000	0.158	1.0	0.158
Fin surface friction		C-E	1.187	2.235	C	15000	0.327 ⁽²⁾	1.0	0.327
Top grid to top fixture	Expansion	D-E	1.388	2.235	D	4000	0.144	0.602	0.052
Top fixture to pool	Expansion	E-P	2.235	2.544	E	18000	0.015	0.374	0.002
Sum local K's									0.539

(1) All channel areas are for a single rod.

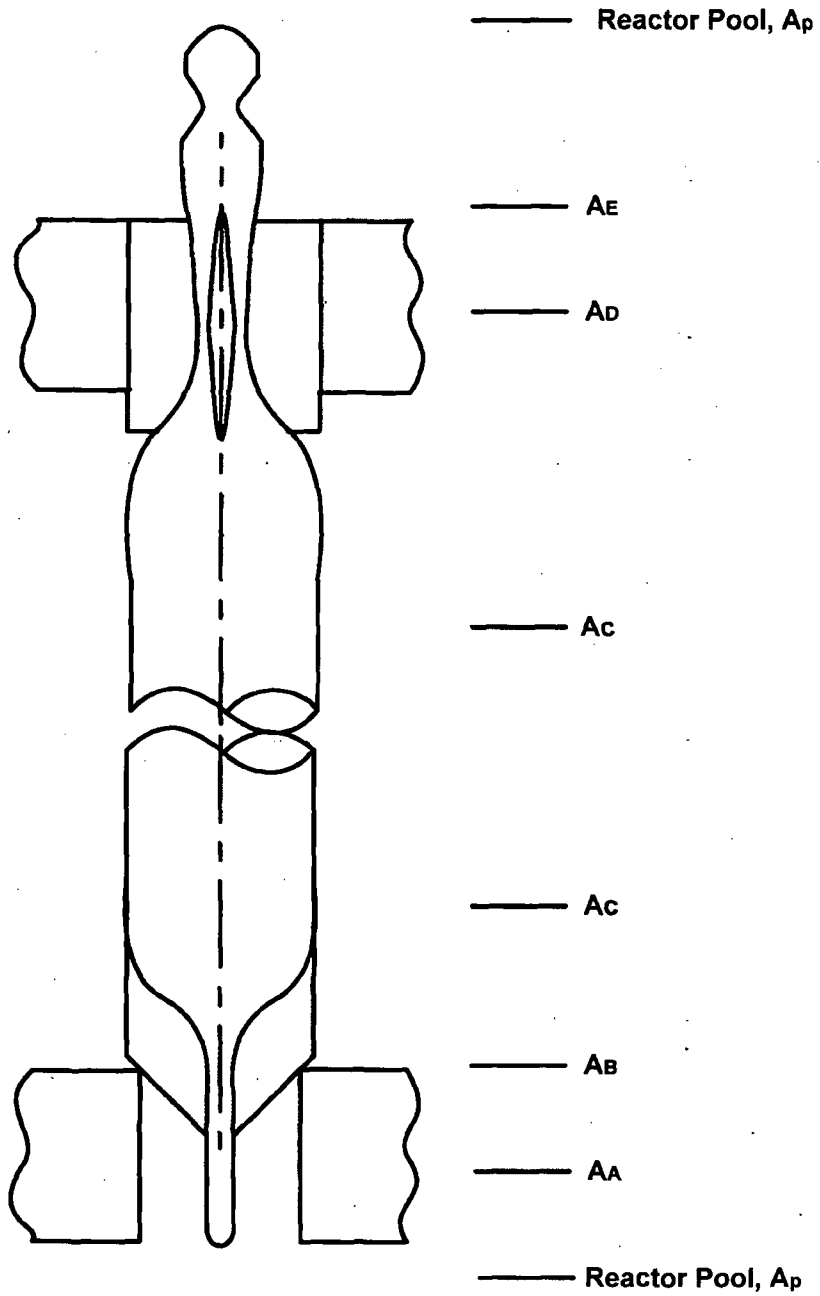
(2) Includes a 1.50 multiplying factor for uncertainty

Figure A-1. TAMU and WSU Rod and End Fixtures



(Sketch -- not to scale)

Figure A2. OSU Rod and End Fittings



(Sketch – not to scale)

Figure A-3. MNRC Rod and End Fixtures

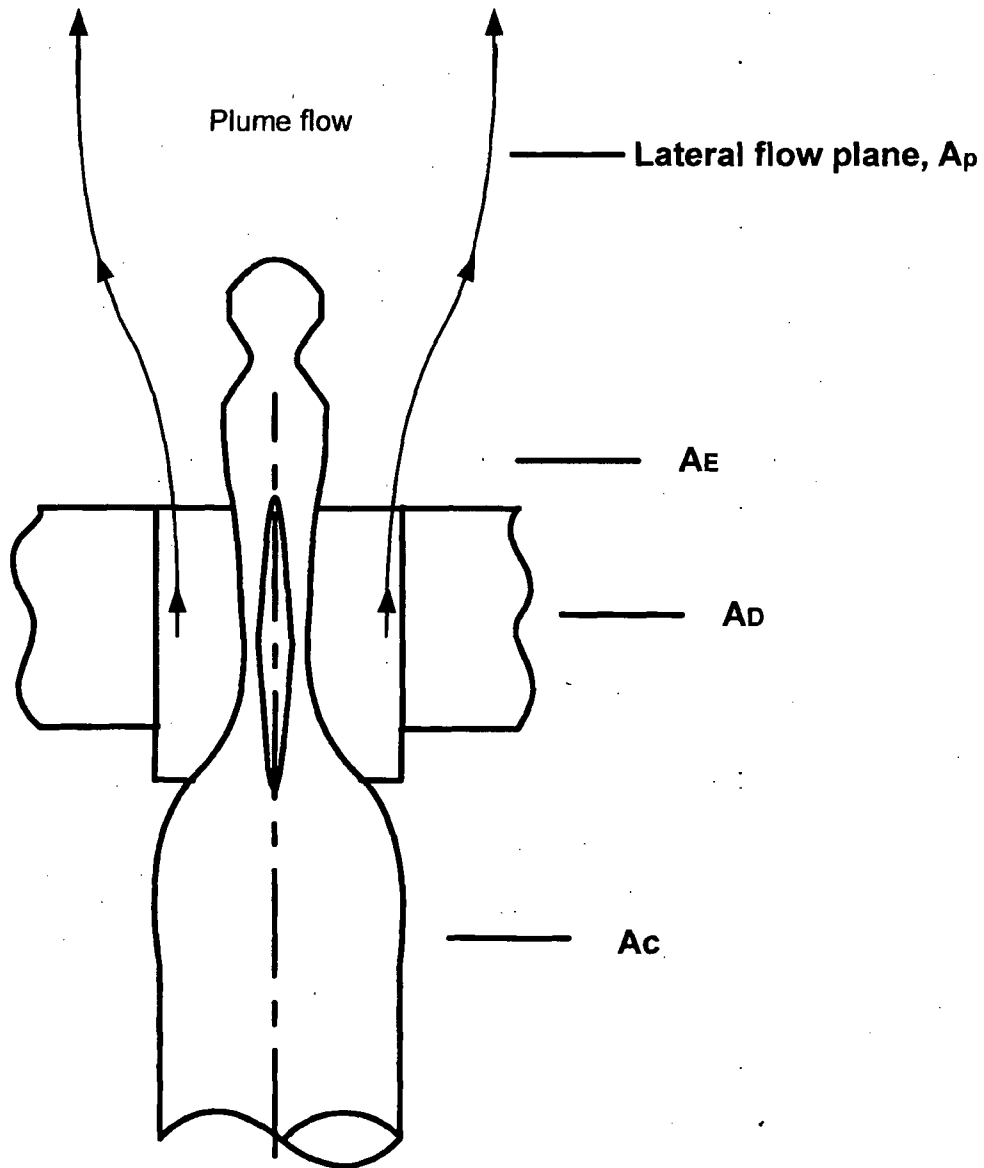


Figure A-4. Illustration of Uniform Lateral Pressure Plane at Core Outlet

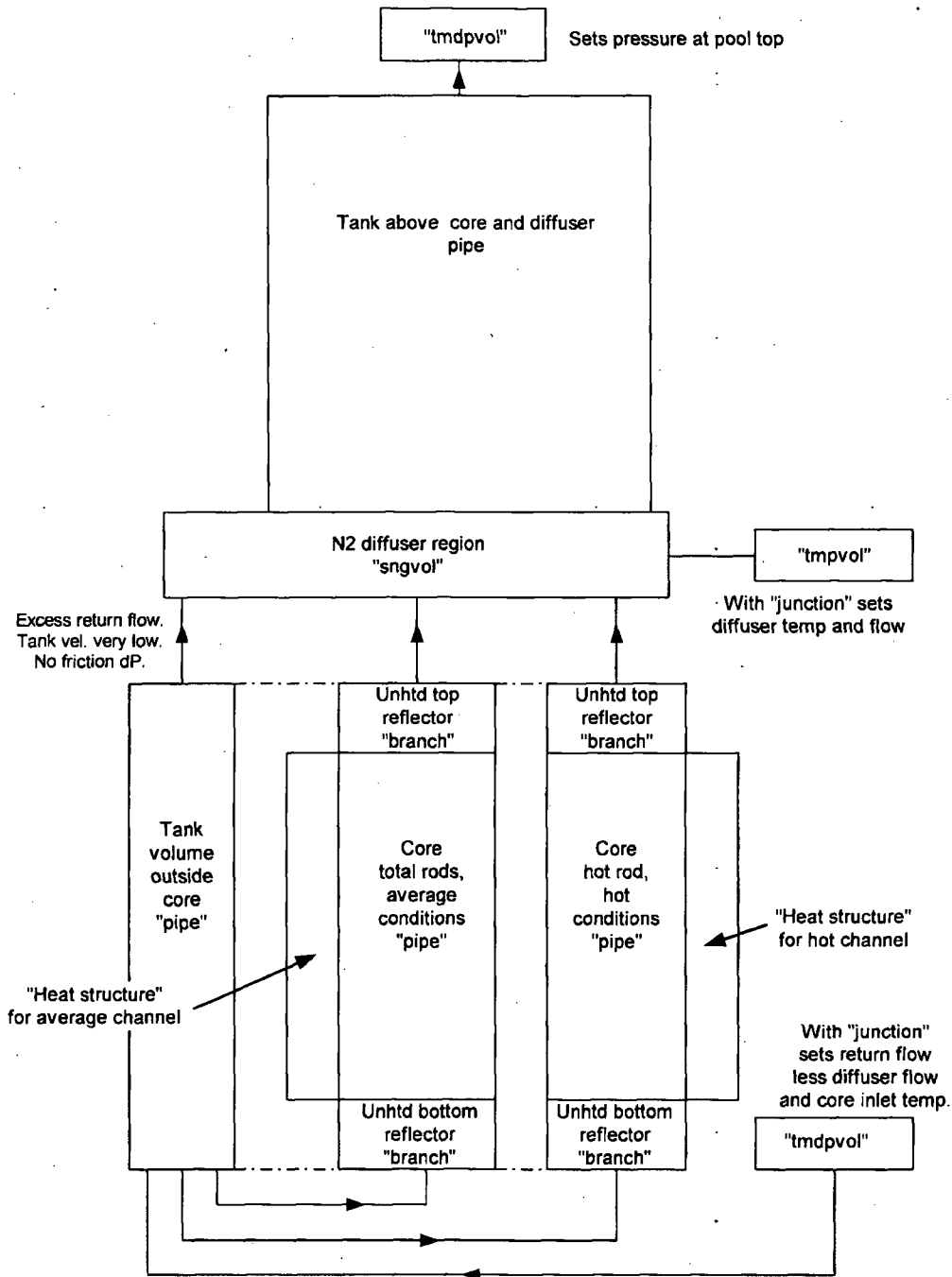


Figure A-5. RELAP Model for Current Study



GENERAL ATOMICS

P.O. BOX 85608 SAN DIEGO, CA 92186-5608 (858) 455-3000